THE APPLICATION OF DYNAMIC NUCLEAR POLARIZATION ENHANCED NMR TO NON-EQUILIBRIUM SYSTEMS

A Dissertation

by

SEAN MICHAEL BOWEN

Submitted to the Office of Graduate Studies of
Texas A&M University
in partial fulfillment of the requirements for the degree of

DOCTOR OF PHILOSOPHY

December 2011

Major Subject: Chemistry

The Application of Dynamic Nuclear Polarization Enhanced

NMR to Non-Equilibrium Systems

THE APPLICATION OF DYNAMIC NUCLEAR POLARIZATION ENHANCED NMR TO NON-EQUILIBRIUM SYSTEMS

A Dissertation

by

SEAN MICHAEL BOWEN

Submitted to the Office of Graduate Studies of
Texas A&M University
in partial fulfillment of the requirements for the degree of

DOCTOR OF PHILOSOPHY

Approved by:

Chair of Committee,	Christian Hilty
Committee Members,	David Barondeau
	Gyula Vigh
	Steven Wright
Head of Department,	David Russell

December 2011

Major Subject: Chemistry

ABSTRACT

The Application of Dynamic Nuclear Polarization Enhanced

NMR to Non-Equilibrium Systems. (December 2011)

Sean Michael Bowen, B.S., Purdue University

Chair of Advisory Committee: Dr. Christian Hilty

Nuclear magnetic resonance (NMR) yields remarkably detailed structural information about virtually any molecule. However, its application to non-equilibrium systems is hampered by a lack of sensitivity. To increase the amount of signal that can be obtained from an NMR experiment, hyperpolarization schemes such as dynamic nuclear polarization (DNP) have been previously introduced. The work detailed here focuses on the development of methods utilizing DNP to study non-equilibrium systems such as chemical and biochemical reactions in real-time.

To work with hyperpolarized samples, we have designed and constructed a rapid injection and mixing system. This system permits the use of samples with short spin-lattice relaxation times. For the study of reactions under non-equilibrium conditions, the system provides the capability for samples to be mixed with a second reagent.

A chromogenic trypsin catalyzed ester hydrolysis reaction was used to validate the DNP-NMR technique as a tool for kinetic analysis. It is shown that the DNP-NMR method agrees with the conventional UV method within the uncertainty of the measurement. In addition to the determination of kinetics, DNP-NMR is amenable to

mechanistic analysis of a reaction. We have developed a technique based on selective inversion of spin-polarization, which allows for mapping of atoms between reactant and product. This scheme was applied to a Grignard reaction, demonstrating applicability to organic reactions. For the rapid measurement of heteronuclear correlation spectra, we have developed a technique utilizing the differential scaling of scalar coupling under off-resonance irradiation.

Although DNP-NMR yields outstanding spectra with even small quantities of sample, peak intensities are not quantitative. It is nevertheless possible to compare peak multiplets obtained from fractionally isotope labeled samples. Using biosynthetically labeled lipids from *E. Coli* cells, we showed that the resulting labeling patterns reflect their biosynthetic pathways.

As a final case-study employing several of these new methods, the uronate isomerase catalyzed isomerization of glucuronate into fructuronate was studied. The ability to follow the reaction in real-time while directly observing all anomeric forms of the reactant and product permits the independent determination of kinetics for each anomeric form of substrate and product. This study revealed the anomeric specificity of the enzyme.

DEDICATION

To my mother

ACKNOWLEDGEMENTS

First and foremost, I would like to thank my advisor, Christian Hilty, for his guidance, support and patience throughout my graduate career. None of my accomplishments would have been possible without Christian's helpful suggestions and tireless leadership. As one of Christian's first students, I was privileged to have the ability to work closely with him in the process of setting up the lab. Christian has always involved me in all aspects of the lab, and made me feel that my input is welcomed and appreciated.

I would also like to thank my committee members Dr. Barondeau, Dr. Vigh, and Dr. Wright for their support throughout the course of this work. Furthermore, I wish to thank Dr. Raushel and Dr. Soriaga for their willingness to act as substitute committee members. Additionally, I would like to thank the members of the Hilty research group for making my time in lab enjoyable. Looking back over the last 5 years, I could not dream of better friends or coworkers.

I also wish to thank my past instructors for their encouragement to pursue my dreams. Foremost, I would like to acknowledge my past scientific mentors. These include Dr. Dale Margerum, my undergraduate research advisor and Dr. Beatriz Cisneros, my undergraduate academic advisor. Additionally, I cannot forget my high school science teachers Mrs. Cyndi Levin, Mr. Glenn Mauger, and Mr. Bob Seal. Without them, I would not have developed my love of science which continues to drive me. Last but certainly not least, I would like to thank my mother and the rest of my family for being there for me in both good times and bad.

TABLE OF CONTENTS

Page

CHAPTER Page

CHAPTER Page

LIST OF FIGURES

Page

Page

Page

Page

LIST OF TABLES

Page

CHAPTER I

INTRODUCTION

The study of the kinetics and mechanisms of chemical reactions is an area of fundamental importance to all areas of chemistry. However, detailed information is often difficult to obtain in real-time as many reactions are not amenable to study with commonly used techniques. Additionally, commonly used techniques such as UV/Visible spectrophotometry cannot deliver detailed structural information about reaction intermediates and products. In order to gather this information, it is necessary to resort to other techniques. One such technique is Nuclear magnetic resonance (NMR), which can deliver unparalleled structural information about virtually any molecule of interest. However, NMR is insensitive, often requiring signal averaging to build adequate signal to noise and consequently cannot measure in real-time during the course of a reaction. Because of the limitations imposed, a variety of techniques have been devised to improve NMR sensitivity. The focus of this dissertation is the application of NMR for the measurement of fast reaction kinetics and mechanisms by overcoming the inherent sensitivity limitations of NMR.

We have utilized dynamic nuclear polarization (DNP) as a means of increasing the NMR signal. DNP delivers signal enhancements of several orders of magnitude and obviates the need for signal averaging. DNP is an ideal technique for this application since it is compatible with virtually any small molecule and yields a solution-state sample that is readily mixed with other reagents. The high levels of signal enhancement,

This dissertation follows the style of *Analytical Chemistry*.

enable the use of DNP enhanced NMR (DNP-NMR) for measurement of fast chemical and biochemical reactions on the timescale of a few seconds.

An interesting challenge posed by a technique such as DNP is the need to modify some of the NMR concepts that we hold near and dear. First and foremost, the fact that spin-lattice relaxation is no longer a friend enabling faster repetition rates; but instead a signal robbing foe. Once in the liquid state, samples need to be transferred quickly to the NMR spectrometer for measurement; otherwise the enhanced signal will decay back to the equilibrium polarization.

The work in this dissertation was made possible by a rapid sample injector detailed in Chapter III. The system was designed and fabricated within our lab. The rapid sample injector allows for hyperpolarized samples to be rapidly transported into the NMR spectrometer for measurement. Its reliable function permits the acquisition of high quality NMR spectra. Additionally, it permits the mixing of a second reagent which enables the measurement of the kinetics and mechanisms of chemical reactions.

For working with this type of hyperpolarization, an NMR concept that has to be altered is the best approach for measuring multiple scans. Conventionally, multiple scans are acquired by waiting for spin-lattice relaxation to return the spins to equilibrium before commencing the next scan. In the case of the present DNP-NMR experiments, this is not possible and it is necessary to use a different scheme to enable multiple scans to be measured from a single sample.

Our approach for measuring reaction kinetics is detailed in Chapter IV, where we have analyzed the kinetics of trypsin catalyzed ester hydrolysis and compared them to

traditional UV spectrophotometric assay measurements. In this proof of concept experiment we demonstrate the applicability of DNP-NMR to enzyme catalyzed reactions and show that the results obtained from the DNP-NMR method compare favorably to those from the traditional UV assay. While, the DNP-NMR technique requires only NMR active atoms to be present, the UV assay demands that the reaction be chromogenic.

At some point while measuring reaction kinetics, it is likely that there will be a need to measure heteronuclear correlations, which are invaluable in the structural elucidation process. Just like before, conventional techniques are not applicable to DNP-NMR. Therefore we introduce an off-resonance decoupling based scheme for obtaining heteronuclear correlations in Chapter V. Conventional two-dimensional techniques yield both correlations as well as additional dispersion by virtue of the second dimension. The off-resonance decoupling scheme delivers just correlations. As we show, this is adequate for many systems. This is especially true when observing ^{13}C which has a large chemical shift range and good peak dispersion. Furthermore, the fast nature of the technique means that correlations could in principle be obtained during the course of a chemical reaction. This may be of utility for characterizing transient species, for example.

Chapter VI describes an application not typically considered in conventional NMR, the mapping of atoms between reactant and product in a chemical reaction. These temporal correlations are particularly valuable because acquiring them in the traditional way would be both costly and time-consuming. In this approach, we show that we can

site-specifically label a resonance through application of a selective RF pulse. This is in contrast to the traditional use of selectively isotope labeled reactant molecules. In the hyperpolarized experiment, the initially prepared spin state can be followed throughout the course of the reaction.

The work in Chapter VII makes use of the ability of DNP-NMR to measure high-resolution spectra with high signal to noise, enabling quantitative integration of peak multiplet patterns. We show that we can use the signal enhancement to determine isotope correlation patterns. Through the use of fractional isotope labeling, we probe the labeling patterns in *E. Coli* membrane lipids. Then we compare the observations to known lipid biosynthesis pathways. Due to the enhanced signal, it is possible for us to obtain good quality spectra from small quantities of cell culture. Since the amount of required isotopically labeled reagent is small, it is possible to examine many different combinations.

Lastly, the work in Chapter VIII has been done in collaboration with Prof. Frank Raushel and his research group at Texas A&M. It details the application of the DNP-NMR techniques developed in the previous chapters to the uronate isomerase catalyzed isomerization of D-glucuronate into D-fructuronate. Unlike typical coupled assays, it is possible to observe the reaction with the equilibrium shifted to any arbitrary point - not just strongly shifted towards product as is often the case. Additionally, the NMR technique can observe all anomeric forms of reactant and product and determine how their concentrations vary with time. This direct, real-time measurement of the concentration of anomeric forms is not readily possible with other techniques.

CHAPTER II

BACKGROUND AND THEORY

This chapter provides background on NMR and its inherent sensitivity limitations due to low signal. The origins of these limitations are discussed as well as approaches to cope with the low signal. After this, a variety of techniques are introduced that directly attack the inherent problem of low signal, instead of attempting to cope with it. The advantages and disadvantages of each technique are then mentioned. A detailed introduction to our chosen technique, dynamic nuclear polarization is provided. Finally, the use of NMR for monitoring fast reaction kinetics is introduced and connected to our work.

2.1 Nuclear Magnetic Resonance and Sensitivity

High-resolution nuclear magnetic resonance (NMR) spectroscopy provides unparalleled structural information. NMR is a powerful analytical technique for the elucidation of molecular structure and has become an indispensable tool to analyze products of organic syntheses,[1-3] to identify natural products,[4-6] and to determine biochemical processes.[7-8] Because of chemical shift, NMR is able to provide detailed site specific information. Additionally NMR is unique in its ability to provide correlations between nuclei linked through bonds or space through the acquisition of multidimensional spectra.

While NMR is able to provide structural information of unrivalled richness, it is limited by its lack of sensitivity. In some cases this insensitivity is overcome by simply increasing the size of the sample. However in many cases this is not possible. This is

especially true for natural products and the products of organic synthesis, where the available quantity of sample may be exceedingly small. These mass constraints limit the applicability of NMR by removing the most convenient way of increasing the sensitivity.

As shown in Figure 2.1, a spin ½ system has two possible energy levels. This is analogous to optical spectroscopy where a ground state and an excited state are present. Unlike optical spectroscopy, the energy gap between ground and excited states is so small that population of the β state is considerable. The large population of the β state drastically reduces the sensitivity of the experiment.

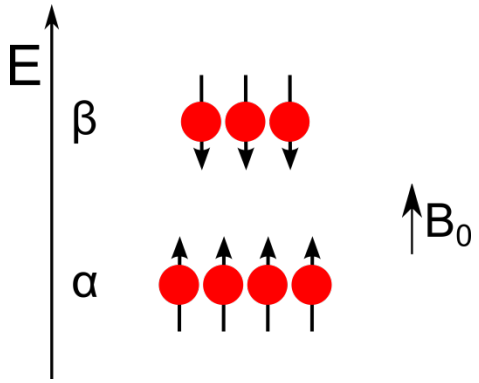

Figure 2.1. Spin ½ energy levels in the presence of an externally applied magnetic field (B_0). Two states exist: a low-energy state (α) where spins are aligned parallel to B_0 and a high-energy state (β) where spins are aligned anti-parallel to B_0. The illustrated orientations are correct for spins with positive gyromagnetic ratios; spins with negative gyromagnetic ratios will be reversed.

The alignment of spins with respect to the magnetic field is determined by Boltzmann statistics. The ratio of populations of the two states is expressed by

$$\frac{N_\beta}{N_\alpha} = e^{-\frac{\Delta E}{kT}} \tag{2.1}$$

where ΔE is the energy difference between states, k is Boltzmann's constant, and T the temperature in Kelvin. For the magnetic resonance specific case

$$\Delta E = h\gamma B_0 \tag{2.2}$$

where h is Planck's constant, γ the gyromagnetic ratio, and B_0 the applied magnetic field.

In practice it is much more relevant to consider not the ratio of populations of the two states, but the normalized difference in populations between the two states. This term known as the polarization, P, is defined as

$$P = \frac{N_\alpha - N_\beta}{N_\alpha + N_\beta} \tag{2.3}$$

Combination of equations 2.1, 2.2, and 2.3 yields

$$P_{eq} = \frac{e^{-\frac{h\gamma B_0}{kT}} - 1}{e^{-\frac{h\gamma B_0}{kT}} + 1} = \tanh\left(\frac{h\gamma B_0}{2kT}\right) \tag{2.4}$$

Table 2.1. Gyromagnetic ratios for selected spin ½ species.

Species	Gyromagnetic Ratio (MHz/T)
^{1}H	42.576
^{13}C	10.705
^{15}N	-4.3156
^{19}F	40.059
electron	-2.8025 x 10^{4}

The gyromagnetic ratios for selected species are shown in Table 2.1[9-10].

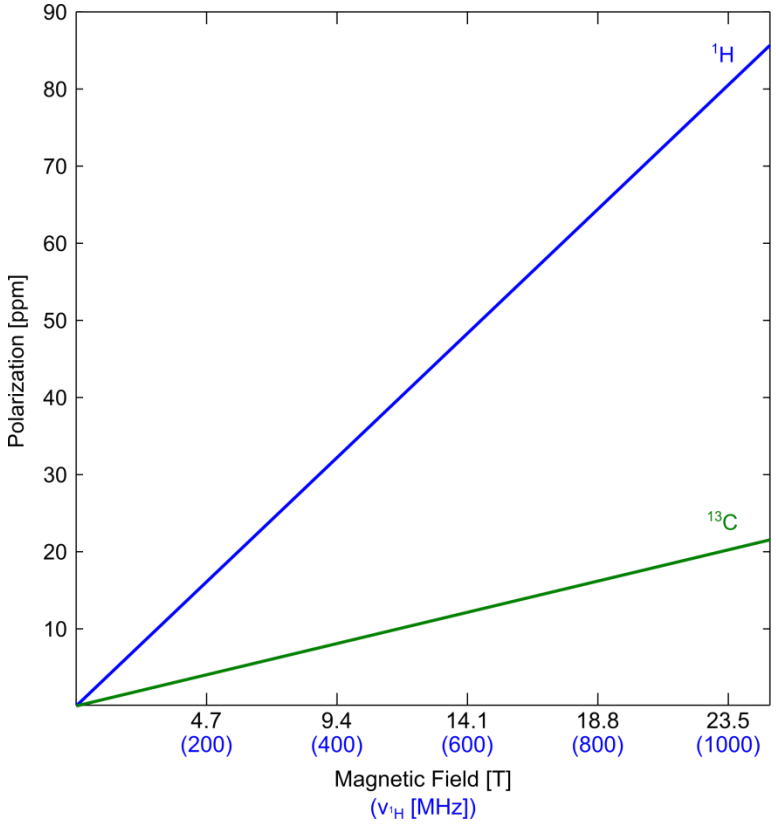

Figure 2.2. Plot of polarization of ^{1}H and ^{13}C as a function of magnetic field at ambient temperature (298 K) as calculated by equation 2.4. For reference, proton Larmor frequencies are also shown.

As shown in Figure 2.2, the polarization for two of the most common NMR nuclei, ^{1}H and ^{13}C, is less than 100 ppm throughout the typical range of magnetic fields applied in magnetic resonance experiments. The increase in polarization with increasing magnetic field is essentially linear, and the overall sensitivity scales with scales with $B_0^{3/2}$.[11-12] However, the cost of NMR magnets tends to increase exponentially with respect to magnetic field. Additionally, current superconductor technology is already at the upper limit of its achievable magnetic field strength.[13]

Because of the expense and difficulty in constructing ultra-high field magnets as well as the modest return on investment, increasing magnetic field is not currently a reasonable means for dramatically increasing the sensitivity.

One common scheme for sensitivity enhancement is the use of signal averaging. While signal averaging does indeed improve the signal to noise ratio (SNR) of the NMR experiment, it does so at the expense of increased experiment time. When signal averaging, the SNR is proportional to $t^{1/2}$. This means that improving the SNR by a factor of 10 will increase the duration of the experiment by a factor of 100. This can easily cause the duration of an experiment to become unreasonably long. Nonetheless its simplicity and ease of implementation have given it near universal application in modern NMR experiments.

While signal averaging is a valuable tool, it also renders NMR unsuitable for the kinetic measurement of non-equilibrium processes occurring on short timescales. If the timescale of the process is shorter than the duration of signal averaging, the desired kinetics would be averaged together and the results would be hidden.

One means of improving the sensitivity of NMR is to decrease the noise. As the effect of a decrease in noise is akin to an increase in signal with respect to the SNR, this is a valid approach. Indeed, significant advances in NMR instrumentation have been made in recent years, including better probe design, cold-probe technology, and the use of microcoils.[14] Nonetheless, the key issue with the most room for improvement is the low polarization of nuclear spins. Increasing the signal by virtue of increasing the

polarization of nuclear spins would dispense with the need for signal averaging and enable rapid measurement of NMR spectra using minute quantities of sample.

2.2 Hyperpolarization

Increasing the polarization of the spin system will proportionally increase the signal and therefore the sensitivity of the experiment. Since it is not feasible to significantly increase polarization by increasing the magnetic field, it is necessary to resort to alternative means. Through the process of hyperpolarization, a spin system is artificially prepared in a highly polarized non-equilibrium state prior to the NMR experiment. With hyperpolarization, it is possible to generate polarization levels of more than 10%. This corresponds to a direct enhancement in SNR of more than 10^4 times.

There are a variety of hyperpolarization techniques, each having benefits and drawbacks. Some techniques enjoy more widespread applicability while others benefit from being easy to implement. In this section a variety of competing techniques are briefly discussed, leading up to a more comprehensive discussion of the more relevant solid-state DNP technique.

2.2.1 "Brute Force" Polarization

Conceptually, the "brute force" scheme is the simplest and most obvious means of achieving high levels of polarization.[15] As evident from equation 2.4, there are two parameters that are not fixed and are therefore available for manipulation. They are the magnetic field which has already been mentioned and the temperature. Since

significantly increasing the magnetic field has been ruled out, the remaining option is to decrease the temperature.

As shown in Figure 2.3, subjecting a sample to even moderate magnetic fields and low temperature, the spin polarization does indeed increase as compared to values at ambient temperature. However, attaining polarization levels close to 100% requires temperatures in the millikelvin range which are extremely difficult to achieve. Even if these temperatures were easily attained, the nuclear T_1 relaxation times become extremely long (weeks).[16] Additionally, the applications shown for the "brute force" approach involve noble gases in which no transition to ambient conditions has been attempted.[17]

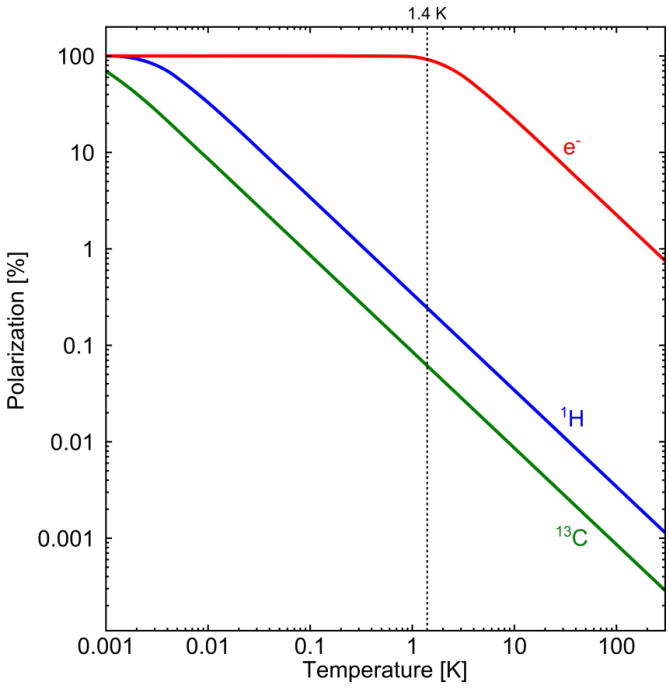

Figure 2.3. Polarization of ^1H, ^{13}C and e^- as a function of temperature with B_0 of 3.35 T corresponding to 94 GHz e^- frequency (W-band) as calculated from equation 2.4.

Compared to the nuclear case, the electron shows much more favorable results. As shown in Table 2.1, the electron gyromagnetic ratio is 658 times larger than ^{1}H and 2,618 times larger than ^{13}C. Owing to its high gyromagnetic ratio, electron spins are highly polarized compared to nuclear spins. At even modest temperatures attainable with liquid helium, the electron spin polarization exceeds 90%. Even at low temperature, the electronic relaxation time is short. This means that polarization builds quickly. Indeed, low temperature electron paramagnetic resonance (EPR) experiments are common.

2.2.2 Optical Pumping

Optical pumping involves the use of light to excite electronic transitions.[18] In a popular embodiment, rubidium vapor is pumped with circularly polarized laser light tuned to its S → P transition line. This generates electronic spin polarization on the rubidium. Through collisional mixing between rubidium and the noble gas as well as nitrogen quenching collisions, it is possible to attain high levels of polarization of the nuclear spin system.

Optical pumping is applicable only to NMR-active noble gases such as ^{3}He and ^{129}Xe. Polarized noble gases are useful as they can be targeted to specific molecular sites, for example xenon biosensors[19] have been developed to detect polarized xenon in magnetic resonance imaging.[20] However, this technique cannot give chemical information about arbitrary molecules.

2.2.3 Para Hydrogen Induced Polarization (PHIP)

PHIP relies on the use of para-hydrogen, the nuclear spin singlet of the H_2 molecule.[21] In para-hydrogen the two proton spins are anti-parallel, while in the triplet ortho-hydrogen they are parallel. Para-hydrogen is the lower energy isomer and is favored at low temperature, but the interconversion between states is slow unless a paramagnetic catalyst is introduced. Once formed, the catalyst is removed and para-hydrogen can be returned to room temperature where the equilibrium ratio of ortho/para will slowly reestablish itself.

By itself, para-hydrogen is not suited for NMR measurement. Instead, it is used to hydrogenate a substrate by a chemical reaction. Once this occurs the spin correlation between the atoms is initially retained but the symmetry is broken, resulting in a highly enhanced proton spectrum.[22] Alternatively, polarization may be transferred to heteronuclei via INEPT based schemes. This also allows the polarization to be "stored" on heteronuclei with substantially longer T_1 as compared to protons. The key disadvantage of PHIP is the need to perform a hydrogenation reaction as it limits application to unsaturated compounds.

2.3 Dynamic Nuclear Polarization

Dynamic Nuclear Polarization (DNP) provides a scheme for hyperpolarization of essentially any spin ½ nucleus. There are DNP schemes applicable to both solid samples and solution state samples. DNP does not require any special features of molecules nor does it require a chemical reaction to occur.

As discussed, electron spin polarization is significantly greater than nuclear spin polarization. DNP serves as a means of transferring polarization from electron spins to nuclear spins. In the ideal case it is capable of increasing nuclear spin polarization to match that of electron spin polarization.

All forms of DNP rely on the application of RF irradiation to transfer polarization between electron spins and nuclear spins. This irradiation is delivered close to the electron Larmor frequency at the magnetic field utilized for the experiment.

2.3.1 Overhauser Effect

Since the DNP process requires the presence of unpaired electrons, it was first predicted by Overhauser for use with metals.[23] Initial work involved the use of finely divided metal powders, subsequent work shifted to alkali metals dissolved in liquid ammonia.[24-25] Today, the focus has shifted to solutions containing dissolved stable free radicals.[26] In this realization, now known as Overhauser effect DNP, continuous saturation of electron spin transitions is applied and nuclear polarization is generated through time-dependent stochastic interactions between nuclear spins and electron spins in the presence of microwave irradiation. This reliance on stochastic interactions limits Overhauser DNP to liquids or metals.

In order to utilize Overhauser DNP with aqueous solutions, it is necessary to work at low frequency or to use samples small enough to not pose serious problems with absorption of the applied microwave radiation. As absorption of microwaves by water leads only to heating, it reduces DNP efficiency and is best avoided. At a modest magnetic field of 0.35 T, the electron Larmor frequency is 9.8 GHz and the optimal

sample volume is a mere 4 μL for one experimental setup.[27] The need to compromise magnetic field strength and sample size mean that Overhauser DNP is often unable to reach its full potential.

2.3.2 Motivation for Solid State DNP

As previously stated, the "brute-force" scheme is not a viable means of generating hyperpolarized nuclear spins on its own. However, owing to the high gyromagnetic ratio of electron spins, it is a viable means of generating highly polarized electron spins. The polarization from the electron spins can then be transferred to nuclear spins. As the "brute-force" scheme requires low temperatures, this necessitates the use of solid samples. Note that these schemes are distinct from Overhauser DNP as they require solid, insulating samples as opposed to the requirement for liquid and/or conducting samples in the Overhauser case.

Performing DNP with non-paramagnetic substances requires the addition of a free-radical to provide the unpaired electron spins. While it is possible to generate free radicals by exposing a solid sample to ionizing radiation, it is most common to add a stable free-radical to the sample. A few stable free radicals popular in DNP are shown in Figure 2.4. These radicals are selected because they are stable and unreactive under most ordinary conditions. They also possess desirable features, such as narrow lines in their EPR spectra that improve the DNP process.

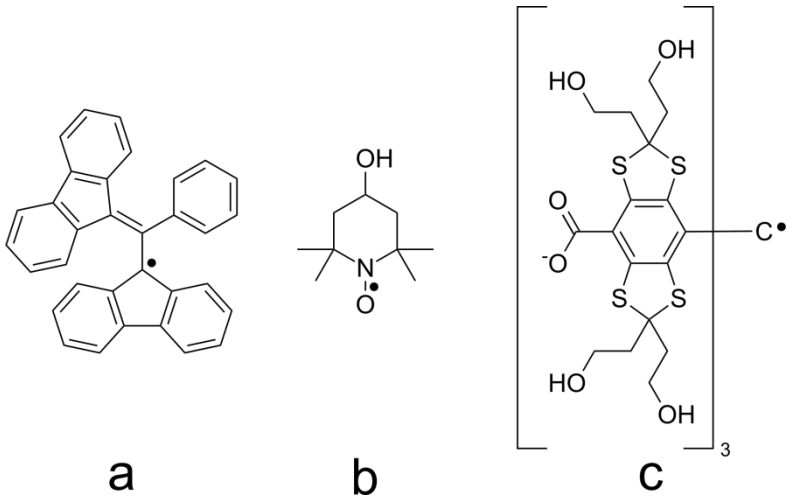

Figure 2.4. Stable free radicals utilized in DNP. (a) *α,γ*-Bisdiphenylene-β-phenylallyl (BDPA) a resonance stabilized radical with a narrow EPR line. (b) 1-Oxyl-2,2,6,6-tetramethyl-4-hydroxypiperidine (TEMPOL), a member of the nitroxide family. TEMPOL is stabilized by stearic hinderance and has an inhomogeneously broadened EPR lineshape that is also split by couplings to ^{14}N. (c) Tris{8-carboxyl-2,2,6,6-tetra[2-(1-hydroxymethyl)]-benzo(1,2-d:4,5-d')bis(1,3)dithiole-4-yl}methyl (OX63), a member of the trityl family. It is stabilized by stearic hindrance and has a narrow EPR lineshape due to the absence of NMR-active nuclei near the radical site.

Another requirement for the DNP sample is that the electron spins are uniformly dispersed among the nuclear spins. Since the sample is polarized in the solid state this means that it needs to be an amorphous glass instead of a crystalline solid. While some solvents naturally form an amorphous solid upon freezing, often it is necessary to add an auxiliary glassing solvent. The most common need for glassing solvents is with aqueous samples. Aqueous compatible glassing solvents include polyols such as ethylene glycol, glycerol, and even glucose. Additional glassing solvents include mixtures of water with dimethyl sulfoxide (DMSO) and/or methanol. Organic solvents such as toluene often freeze in an amorphous fashion without additional glassing agents. A comprehensive

study of glassing solvents as applied to EPR spectroscopy has been published by Drago.[28]

Before beginning a discussion of solid state DNP techniques, it is prudent to introduce the concept of spin temperature. While the concept of spin temperature has been rigorously explained by Abragam, a cursory description will be provided here.[29] In a simple sense, the spin temperature is simply the thermodynamic temperature of the spin system. As the polarization of a spin system increases, the magnitude of its spin temperature decreases. This is to say that the spin system "feels" colder than the actual temperature by virtue of its hyperpolarization. The key point necessitating the use of spin temperature is the ability of DNP to generate a spin system with an excess of spins in the upper energy level. Based upon equation 2.4, the only way for this situation to occur based upon temperature is for the temperature to be negative. Despite the appearance, a spin system with negative system is not colder than absolute zero, but is instead hotter than infinite temperature. Thus the range of spin temperatures increases with + 0 K being the coldest temperature and - 0 K being the hottest temperature.[30] The concept of spin temperature is useful both for ease of explanation as well as for interesting applications of samples with negative spin temperature.[31]

2.3.3 Solid Effect DNP

The aptly named solid effect is applicable to solid state, non-metallic samples. It relies upon microwave irradiation at the electron Larmor frequency plus or minus the nuclear Larmor frequency as illustrated in Figure 2.5. This irradiation causes classically forbidden simultaneous electron and nuclear spin transitions. These simultaneous

transitions occur because of the presence of a hyperfine interaction between the electron and nuclear spins. The hyperfine interaction allows for a small but finite probability of the mutual spin transition occurring.[17] Because the probability of the transition is low, the process is slow compared to electron relaxation, but faster than nuclear T_1 relaxation. This is important as the nuclear T_1 relaxation process causes the spins to return to thermal equilibrium, destroying hyperpolarization. As the electron spins attain a much higher level of polarization much faster than the nuclear spins, the DNP process yields higher polarization than the nuclear "brute-force" approach and achieves the maximum polarization faster.

2.3.4 Thermal Mixing DNP

Thermal mixing is an alternative mechanism for solid state DNP. It is similar to the solid effect except that it involves the electron spin ensemble instead of a single electron spin. The electron spin ensemble arises because electron-electron interactions are considerably stronger than electron-nuclear interactions. Hyperpolarization is achieved in a two-step process involving an electron-electron flip-flop followed by excitation of the nuclear spin transition.[32] The thermal mixing process is most easily viewed as a strong coupling between the spin temperature of the electron spin ensemble and the nuclear spin system. RF irradiation near the electron Larmor frequency leads to a reduction in the magnitude of the spin temperature. As the systems are coupled they will achieve a common spin temperature leading to highly polarized nuclear spins.[33-34] Because thermal mixing does not depend on the occurrence of a largely forbidden transition, it is more efficient than the solid effect.

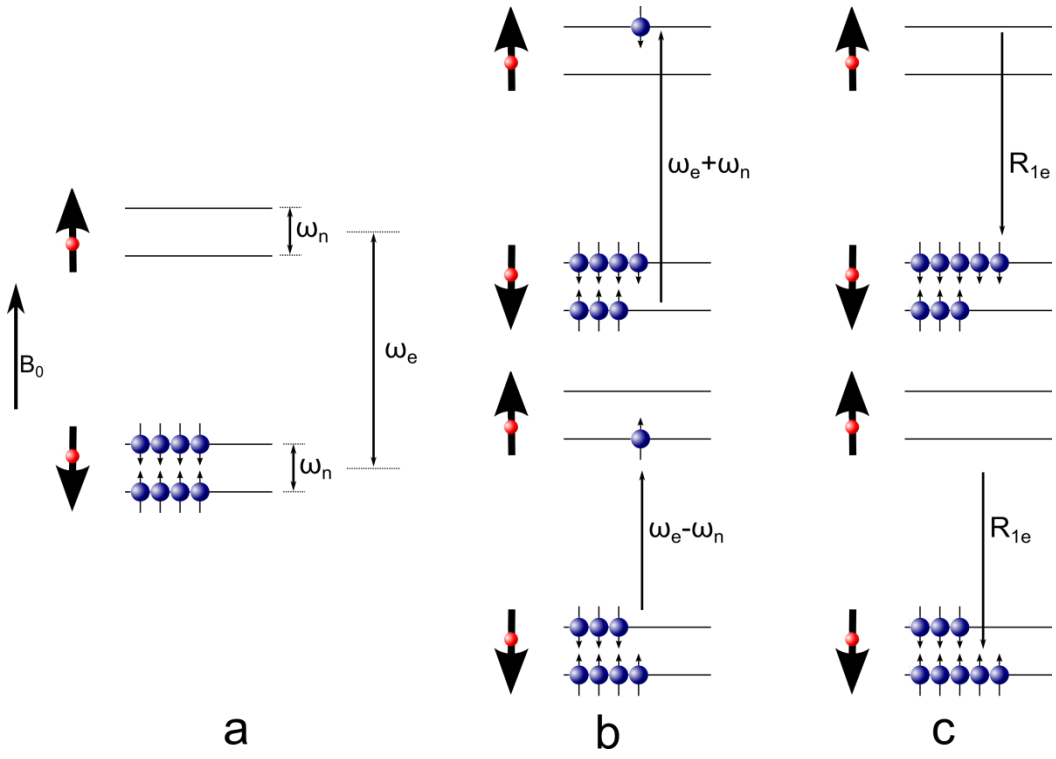

Figure 2.5. The solid effect. Nuclear spins are shown in blue and electron spins in red. (a) In the beginning nuclear spins are unpolarized, while electron spins are fully polarized. (b) When the system is irradiated with microwaves at $\omega_e + \omega_n$ a "flip-flip" transition occurs, while irradiation at $\omega_e + \omega_n$ results in a "flip-flop" transition. (c) Electronic spin-lattice relaxation occurs, restoring the electron spin to thermal equilibrium while enhancing the population of one of the nuclear spin states. The cycle is now free to repeat itself until the nuclear spins are fully polarized. Note that the lower case produces a spin system with positive spin temperature, while the upper case produces a spin system with negative spin temperature.

2.3.5 Cross Effect DNP

The cross effect is the last of the three solid-state DNP mechanisms. Unlike the previous mechanisms, the cross effect requires two discrete electron spins to polarize one nuclear spin. In order for the solid effect to occur, it is necessary for two electron spins to be separated by the correct distance and have the correct orientation such that their frequencies differ by the nuclear Larmor frequency. This means that the cross

effect is dependent on radical species with inhomogeneously broadened EPR spectra. Nitroxyl based biradicals, containing two or more radical sites tend to be best suited to the cross effect.[35-36]

2.3.6 Comparison of Mechanisms

The dominant DNP mechanism in any experiment is dependent upon several parameters. These include the homogeneity and width of the EPR line(s), and the nuclear Larmor frequency. The exact mechanisms at play are dependent upon the experimental conditions.

For solid state DNP, it is common to use a higher magnetic field strength (> 9.4 T) in order to improve NMR resolution and temperatures are typically in the 10 – 90 K range. Additionally, the most common scheme is to hyperpolarize ^{1}H with subsequent transfer to other nuclei as desired. At the high magnetic fields utilized in these studies, the Larmor frequency of ^{1}H is relatively large. Under these conditions, the solid effect dominates with radicals of narrow linewidth, while the cross effect dominates with inhomogeneously broadened radicals.

At the lower temperatures and more modest magnetic fields favored in the dissolution DNP technique, the predominant effect depends on the radical supplying unpaired electron spins and the nucleus being polarized. The thermal mixing mechanism is applicable to a wide range of nuclei from ^{1}H down to those with ultra-low gyromagnetic ratio such as ^{89}Y.[37] Increased contributions from the solid effect and cross effect are also possible with different radicals and/or nuclei.

2.3.7 Solid State DNP Enhanced NMR

Since samples polarized using solid state DNP are already in the solid state, it makes sense to measure them in the solid state. High resolution solid state NMR spectra are easily obtained through the use of magic angle spinning (MAS). DNP combined with high resolution MAS has grown from its early roots and solid state DNP-NMR systems are commercially available.[38] Working at higher temperatures (> 77 K) common in solid state DNP-NMR means that electronic spin-lattice relaxation is faster and therefore high power microwave sources are required. These high power microwave sources are typically gyrotron based and designed to operate at high magnetic fields common in NMR.[39] Solid state systems operating at lower temperature are also possible and are capable of utilizing cheaper and more common solid-state microwave sources.[36] Through the use of DNP, enhancements of more than 200 fold are possible, corresponding to 40,000 fold time savings.[35]

2.4 Solid-to-liquid State DNP

In order to observe dynamic processes such as chemical reactions, it is necessary to measure in the liquid state. However, optimal hyperpolarization conditions occur at low temperature in the solid state. Thus it is necessary to shift the sample from a solid at low temperature to a solid at high temperature. Accomplishing this task requires the sample to be rapidly heated so that NMR experiments may be performed in the liquid state.

Two ways to accomplish this temperature jump have been described. One of those techniques has been performed by the Griffin group and involves the rapid heating

of a solid sample with high intensity infrared radiation.[40] Another one was pioneered by Ardenkjaer-Larsen et al and involves the use of hot, pressurized solvent to rapidly dissolve the hyperpolarized sample and transport it to a separate high-resolution NMR magnet.[41] Alternatively, a dual-center magnet has been designed that possesses 3.35 T and 9.4 T isocenters for DNP and solution NMR measurements respectively.[42] While the former method permits a sample to be reused indefinitely, it does not allow for many applications of the hyperpolarized sample. The latter method permits many applications of the hyperpolarized sample both in spectroscopy as well as imaging.

The dissolution DNP process is the method used in the work described in this dissertation. While MAS systems are restricted to temperatures where the coolant remains in gaseous form, dissolution DNP systems are free to operate at lower temperatures. Because of this, dissolution DNP systems operate at temperatures where electron spins are more than 90% polarized and therefore able to deliver high levels of nuclear polarization. Additionally, low temperature means that low-power solid-state microwave sources may be used.

While the highest polarization levels occur at the lowest temperatures, a compromise is made between polarization level and the difficulty of maintaining low temperatures. In the commercial Hypersense system used in this work, a temperature of 1.4 K is readily maintained by a pumped liquid helium bath. This simple cooling method is robust and the operating cost is reasonably low. DNP systems operating at temperatures down to 0.9 K have been described and operate with closed cycle sorption

cooling systems.[43] Lower temperatures would require more complicated cooling systems such as dilution refrigerators or ^{3}He.[41]

The magnetic field used in dissolution DNP systems needs only to be strong enough to ensure high electron polarization at the operating temperature. Also, it has been reported that maximum attainable polarization levels decrease at high magnetic fields (> 5 T).[26] Because of these points and the ease of locating solid-state microwave sources, 3.35 T, corresponding to W band or 94 GHz electron Larmor frequency has become the de facto standard for dissolution DNP systems. Results obtained at 4.6 T or 130 GHz electron Larmor frequency show increased levels of polarization at the expense of increase polarization buildup time.[44] With inhomogeneously broadened radicals such as TEMPOL, benefits have been reported when operating at 5 T or 140 GHz electron Larmor frequency.[45]

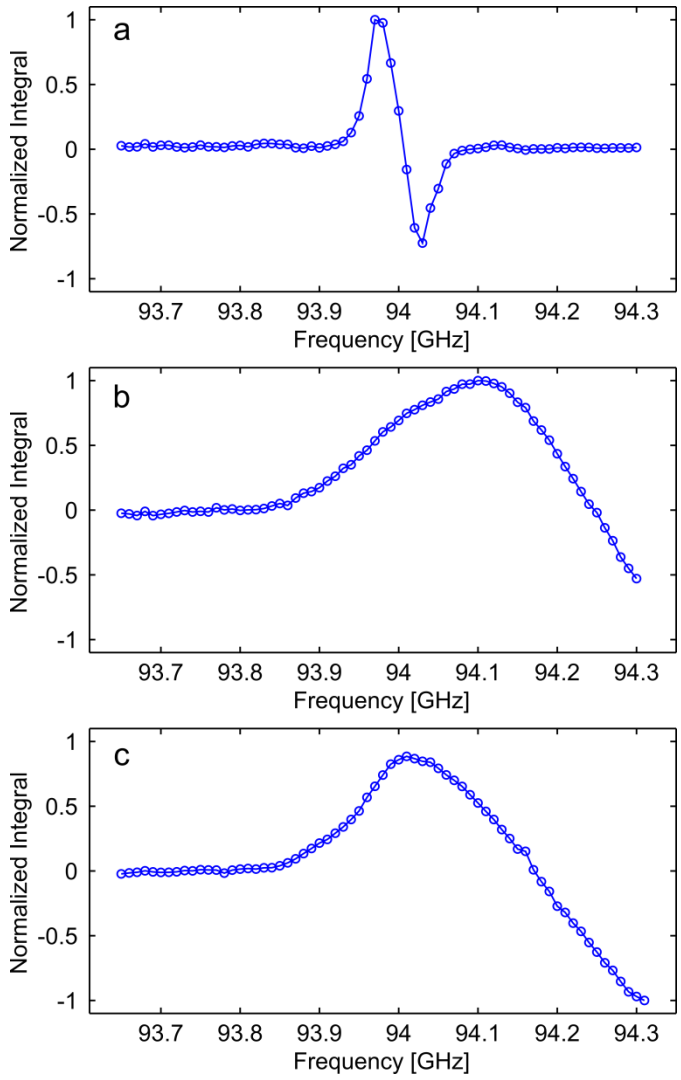

Figure 2.6. Microwave sweeps for (a) ^{13}C and OX63 radical, (b) ^{13}C and TEMPOL radical, and (c) ^{19}F and TEMPOL radical. The lack of a negative peak in (b) and (c) is due to a limited tuning range of the microwave source.

Since the irradiation frequency for maximum polarization under any given set of conditions is not predictable, it is necessary to measure the polarization as a function of frequency. This process is known as a microwave sweep and allows for the determination of the optimal microwave irradiation frequency for a given sample.

Examples of microwave sweeps performed with different samples are shown in Figure 2.6. In (a) it is possible to clearly see peaks for both positive and negative polarization.

Once the optimum microwave frequency is known, it is possible to determine the level of hyperpolarization achieved in a sample. This is readily determined through comparison of the hyperpolarized signal with the thermal signal as shown in Figure 2.7. It is apparent that the DNP polarization buildup is faster and attains significantly higher levels of polarization. Due to the reduction in signal caused by the application of RF pulses, the exponential fit shown in Figure 2.7 is modified. Equation 2.5 shows the modified equation which corrects for the signal lost through application of RF pulses of small flip angle α and repetition time T_R. The spin-lattice relaxation time T_1 and the maximum intensity I_M are determined by non-linear curve fitting to the measured data.

$$I_M\left(1-e^{-\frac{T_R}{T_1}}\right)\left(\frac{1-\cos^n(\alpha)e^{-\frac{nT_R}{T_1}}}{1-\cos(\alpha)e^{-\frac{T_R}{T_1}}}\right) \tag{2.5}$$

For hyperpolarized sample

$$I_M\left(1-e^{-\frac{T_R}{T_b}}\right)\left(\frac{1-\cos^n(\alpha)e^{-\frac{nT_R}{T_b}}}{1-\cos(\alpha)e^{-\frac{T_R}{T_b}}}\right) \tag{2.6}$$

Equation 2.6 differs only by the replacement of the spin-lattice relaxation time T_1 with the DNP buildup time constant T_b.

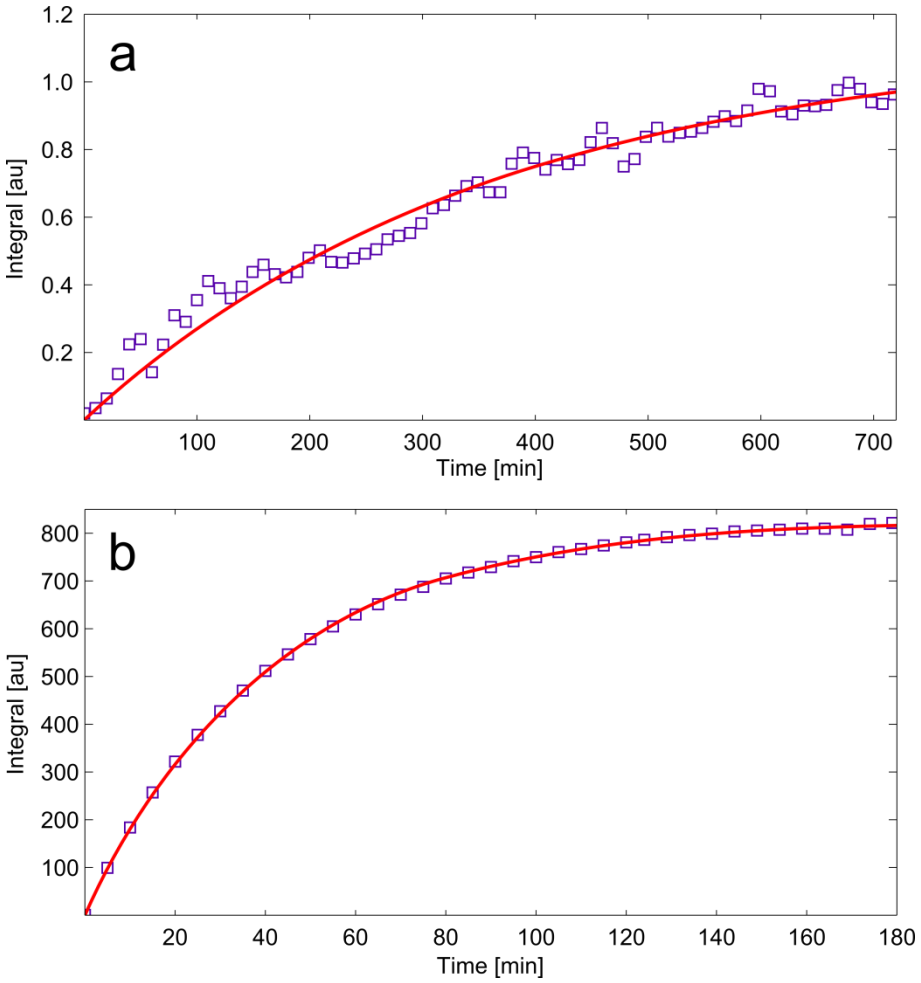

Figure 2.7. Polarization buildup curves for a sample of ^{13}C-Urea with OX63 radical. (a) Thermal buildup with curve fit by equation 2.5 and (b) DNP buildup with curve fit by equation 2.6. The DNP buildup indicates an enhancement of 642 times compared to the thermal buildup. Based upon equilibrium polarization calculated with equation 2.4, the polarization is 39%.

After the sample has achieved maximum polarization at low temperature in the DNP system, it is necessary to dissolve it in heated solvent to generate a solution at approximately room temperature for measurement. Furthermore, it is desirable to transfer it to a higher magnetic field to improve the resolution of the NMR spectrum.

Figure 2.8 shows the DNP system and the 9.4 T NMR magnet used for high-resolution NMR measurement.

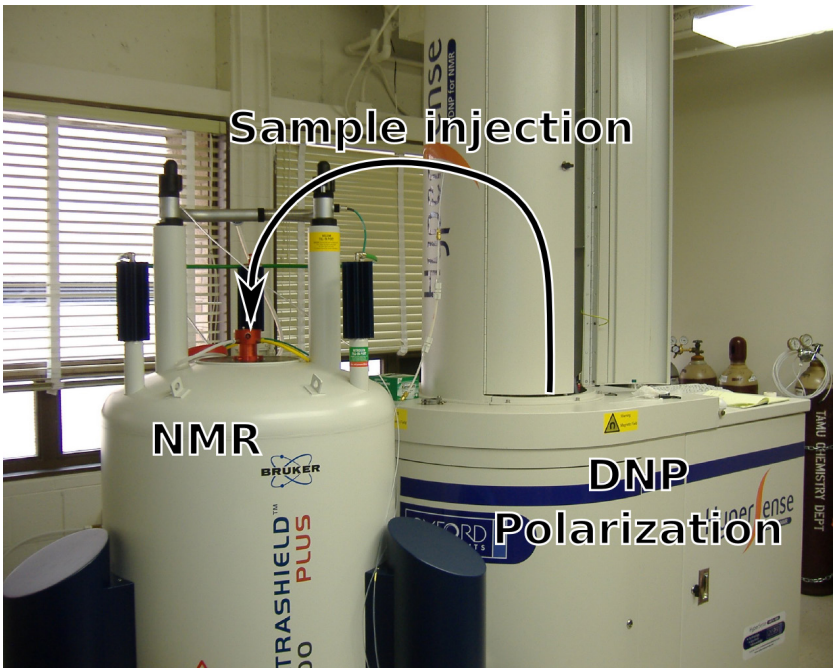

Figure 2.8. Layout of DNP system and NMR magnet.

In the liquid state, the 39% polarization described earlier represents an enhancement of nearly 50,000-fold as compared to thermal polarization at 9.4 T and 298 K. With signal enhancements of this magnitude, NMR spectra are readily measured in a single scan. Since no signal averaging is required, the acquisition of NMR spectra at low concentration in real-time becomes possible. This enables non-equilibrium, dynamic processes to be followed by NMR with relative ease.

2.5 Stopped-flow NMR

Stopped-flow techniques are the method of choice for the analysis of fast reactions. Combined with optical detection, it is possible to follow reactions with timescales as fast as milliseconds. However, the nature of optical detection means that it is not possible to gather detailed information about the structure of the reactants and products. Furthermore, it is not possible to monitor the progress of reactions involving substrates that do not absorb UV or visible light, or those where there is no change in extinction coefficient or absorption wavelength. Because of these limitations, quenched-flow methods are sometimes used. In these methods, reactions are stopped at discrete time points and the reaction mixture is analyzed in an offline manner using techniques such as NMR or mass spectrometry. However, gathering a considerable number of points is time consuming and may not reveal all of the details of the reaction.

In order to overcome the difficulties faced with optical detection, the rapid-mixing equipment used for stopped-flow studies can be adapted to NMR systems. The use of stopped-flow NMR dates back to the beginning of Fourier transform NMR.[46-48] However, stopped-flow with conventional NMR detection is subject to several limitations. Due to low sensitivity, the only nucleus that can be easily observed is ^{1}H. While ^{1}H NMR is a valuable tool, proton NMR spectra are often severely crowded. Also, solvent resonances are usually orders of magnitude larger than the analyte signal. Additionally, each point in time is acquired by mixing the solutions and then waiting a defined amount of time before acquisition. As signal averaging is often required, the number of experiments quickly becomes large. Since each experiment requires fresh

reagents, systems with limited amounts of reagents are not amenable to being studied by this technique.

When combined with the enhanced signal provided by DNP, all of these issues are resolved. The large signal available at one time means that even insensitive nuclei like ^{13}C are possible to study. Since ^{13}C has a large chemical shift range, spectra are typically sparse and easy to analyze. Also, solvent resonances are generally not an issue. With DNP, it is possible to measure without signal averaging, meaning that only one experiment is required per reaction. It is even possible to measure a series of time points from a single sample, enabling reaction kinetics to be fully characterized in a single experiment. The coming chapters will describe how DNP complements stopped-flow NMR and enables dynamic processes to be characterized with unrivalled detail.

CHAPTER III

DESIGN AND USE OF A RAPID INJECTION AND MIXING SYSTEM*

This chapter details the design and functionality of a system designed to accomplish the rapid transfer of the dissolved sample for NMR measurement. The specific requirements for stable sample injection in the presence of gases due to previous dissolution from cryogenic temperature are discussed, as well as the implications of spin-relaxation, and the achievable frequency resolution of subsequently acquired NMR spectra.

3.1 Introduction

In order to best exploit the signal gains provided by DNP, it is necessary to rapidly transfer samples between the superconducting magnets of the DNP system and NMR spectrometer. The study of chemical reactions imposes an additional constraint that it is also necessary to admix a second reagent prior to acquisition. It is also desirable that the transfer process is repeatable and that the sample be stable for the duration of the NMR experiment. A final requirement is that the sample injection and mixing process is reliable as it is not possible to recover from a failed injection before the NMR signal has been lost by T_1 relaxation.

While the Hypersense system includes an NMR tube adapter, it was unsuitable for our application as it was not designed for stopped-flow experiments. There was also

* Reprinted in part from "Rapid sample injection for hyperpolarized NMR spectroscopy" by Bowen, S.; Hilty, C., *Phys. Chem. Chem. Phys.* **2010,** *12* (22), 5766-5770, Copyright 2010 by the PCCP Owner Societies. *Reproduced by permission of the PCCP Owner Societies*

no way to admix a second reagent as required for chemical reactions. Instead, it was decided to take an alternative approach towards the sample injection process. A new system was designed with the goal of reliable, high-speed injection with the added ability to mix the hyperpolarized sample with a second, unpolarized reagent prior to the NMR experiment.

3.2 Relaxation in Hyperpolarized Samples

In typical NMR experiments, substances with short T_1 are desirable as they allow a higher scan repetition rate. This is because T_1 relaxation is a beneficial process, regenerating equilibrium longitudinal magnetization for the next scan. However, in experiments with hyperpolarized sample, the situation is quite different. The hyperpolarized spin system is in a non-equilibrium state with longitudinal magnetization greater than the equilibrium value. Consequently, T_1 relaxation leads to a loss of polarization with time. A comparison of the time course of transverse magnetization for thermal and hyperpolarized samples is shown in Figure 3.1

Because of this time dependence, dissolution DNP experiments often utilize compounds with long T_1 relaxation time. This is especially true for in vivo imaging studies, where the hyperpolarized compound is injected into a patient. Because of inherent delays in the injection and circulation processes, it is necessary for compounds to have sufficiently long T_1 values so that hyperpolarization is maintained throughout the experiment. Compounds such as urea, pyruvic acid and acetic acid are often chosen for in vivo experiments as they have T_1 values of more than 20 seconds and therefore do not suffer excessive relaxation before the experiment.[44, 49] Alternatively, schemes based

upon long-lived nuclear spin singlet states have been proposed to combat spin relaxation.[50]

Since in vitro spectroscopy experiments do not suffer from inherent time limitations like in vivo experiments, it is possible to combat spin relaxation by minimizing the amount of time the sample remains in the liquid state prior to the experiment. By reducing transfer time, it is possible to utilize compounds such as sugars with rapid T_1 relaxation.

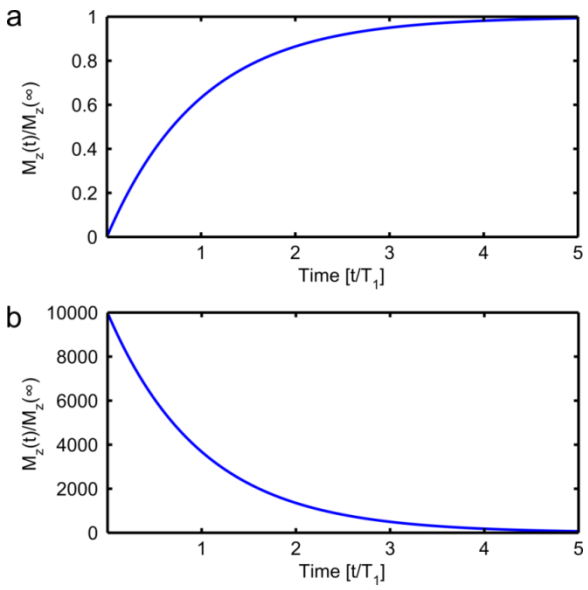

Figure 3.1. Time course of longitudinal magnetization as influenced by T_1 relaxation. (a) Thermal sample with $M_z(0) = 0$ approaching equilibrium longitudinal magnetization. (b) Hyperpolarized sample with $M_z(0) = 10000 \times M_z(\infty)$ approaching equilibrium longitudinal magnetization.

3.3 Materials and Methods

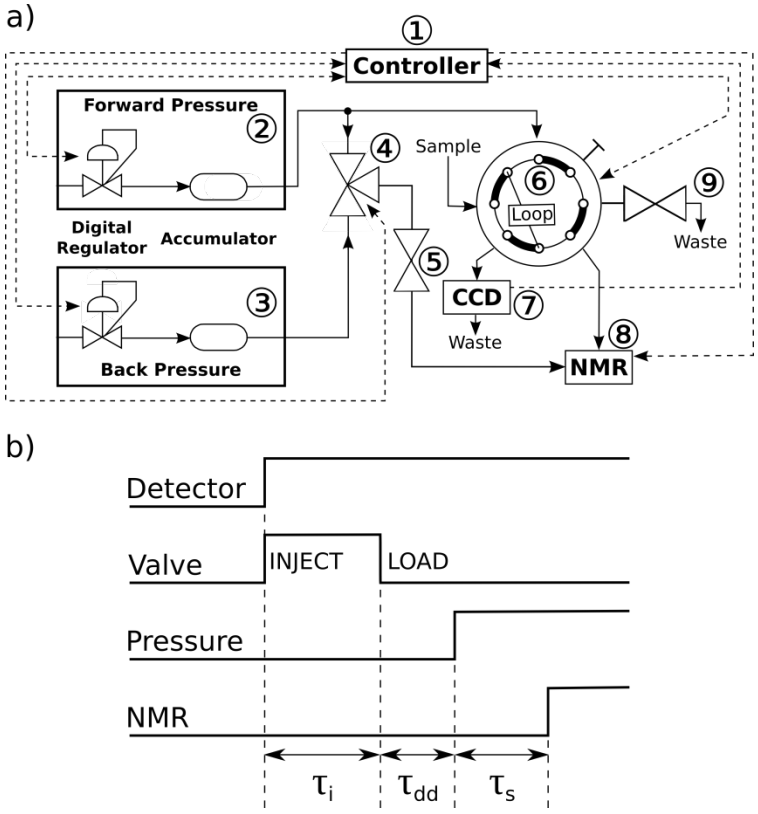

Figure 3.2. a) Block diagram of sample injector. Solid lines indicate pneumatic connections, dashed lines indicate electrical connections. b) Timing diagram for sample injection.

Sample injection is controlled by a Labview program interfaced to the hardware by a data acquisition card (National Instruments PCI-6221, (1) in Figure 3.2a). Both the forward pressure of 1.8 MPa for driving the sample into the NMR tube and the back pressure of 1.0 MPa to prevent outgassing are generated by digital pressure regulators (Marsh-Bellofram T3410S, (2) and (3)). Each regulator is connected to a 500 mL accumulator to buffer the gas flow into the rest of the system as well as to isolate any pressure pulses generated by the regulator from the rest of the system. The pressure

applied to the NMR tube is determined by the three-way solenoid valve (4) and may be shut off via the manual valve (5). An injection valve (VICI-Valco C22-6180, (6)) is fitted with a sample loop of 1.0 mL. This valve may be switched between two positions. During loading of the loop, ports are connected according to the heavy lines. Upon overflow of the sample loop, a contactless conductivity detector[51] or an optical detector (Optek OCB350L125Z) (7) triggers the sequence of events leading to sample injection. The injection valve (6) is switched to the position for sample injection, where ports are connected according to the light lines, for a time τ_i = 400 ms (Figure 3.2b). During this time, 1.8 MPa of nitrogen gas pushes the sample into the NMR spectrometer. The sample is received in the NMR spectrometer by a standard NMR tube, attached to the sample injection system with a home built pressure adapter and pre-pressurized to 1.0 MPa. After a time τ_{dd} < 20 ms after termination of sample injection, an increased pressure of 1.8 MPa is applied to the NMR sample tube. This pressure is maintained throughout the duration of the NMR experiment, which is triggered after a stabilization time τ_s.

Once injection is complete, the NMR experiment (8) is triggered with a transistor-transistor logic (TTL) signal. The NMR spectra shown were measured using a 400 MHz NMR spectrometer equipped with a 5 mm broadband probe (Bruker Biospin, Billerica, MA). At the conclusion of the experiment, the manual depressurization valve (9) is opened to release pressure and to remove solution from the internal tubing and direct it to waste. The fully assembled sample injection system is shown in Figure 3.3.

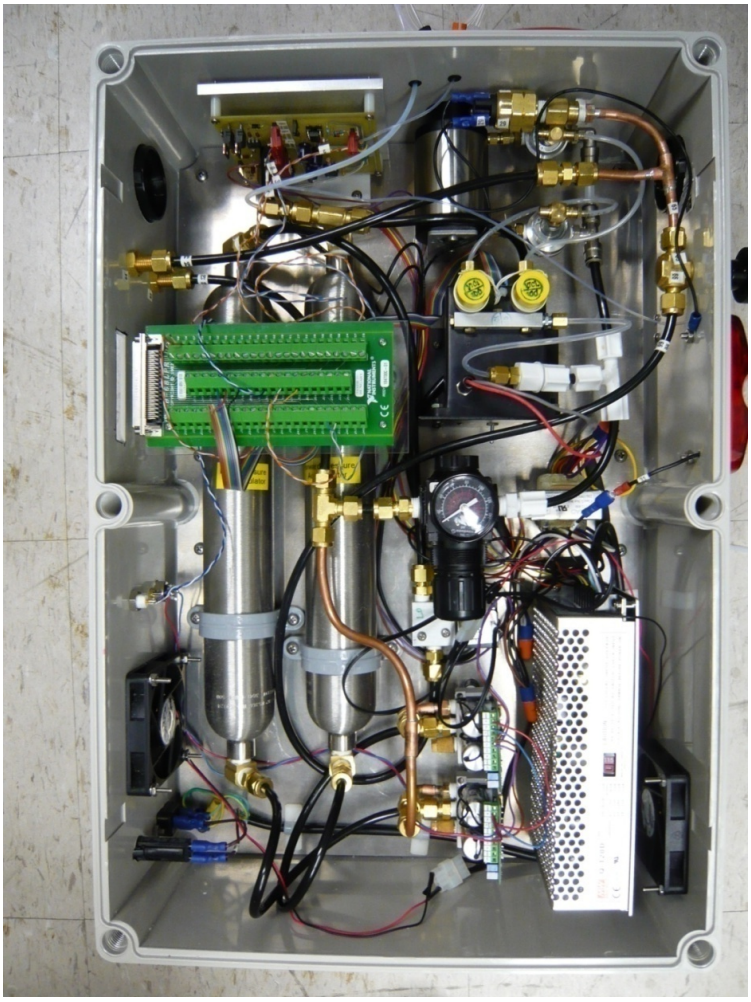

Figure 3.3. Assembled sample injection system. Two position valve and injection loop are located beyond the top and are not shown.

Samples for hyperpolarization consisted of 2 M glucose in D_2O or 1 M glutamic acid in 60:40 ethylene glycol/D_2O, 15 mM Tris{8-carboxyl-2,2,6,6-tetra[2-(1-hydroxymethyl)]-benzo(1,2-d:4,5-d')bis(1,3)dithiole-4-yl}methyl sodium salt (OX63 radical) and 1 mM gadolinium diethylenetriaminepentaacetic acid (Gd(DTPA)). The glutamic acid samples used a glass forming solvent mixture of ethylene glycol and D_2O to ensure uniform dispersion of radical centers. Due to the high concentration of glucose,

the glucose samples were self-glassing, and no supplemental glassing agent was required. Samples were polarized in an Hypersense DNP polarizer (Oxford Instruments, Tubney Woods, United Kingdom) at a nominal field strength of 3.35 T, and a temperature of 1.4 K. Microwave irradiation was applied at 93.974 GHz, at a power of 60 mW for a duration of 2 h. Samples were dissolved into 4 mL of buffer (50 mM potassium phosphate, pH 8.0) heated to 430 K and a pressure of 10 bar, which was rapidly flushed over the sample in the DNP polarizer, as described in ref. [41]. The stream of liquid containing dissolved sample was taken up into a sample injector device,[52-53] and injection into the NMR spectrometer was triggered.

3.4 Injection System Performance

The realization of any gain in sensitivity that solid-to-liquid state DNP can provide over conventional NMR spectroscopy critically depends on minimizing losses during the sample transfer between the point of DNP polarization and the point of NMR measurement. Such losses may occur both through physical loss of sample, as well as through spin relaxation, which causes depolarization of the sample. In order to maximize the signal in the NMR experiment, it is important that the maximum amount of sample is transferred to the NMR tube in the shortest amount of time possible.

In typical experiments, a larger volume of solvent (e.g. 4 mL) is often used for sample dissolution than the volume of a typical NMR sample (ca. 500 μL), to ensure complete dissolution and flushing of the sample from the DNP system.[41] Therefore, complete sample recovery cannot be achieved. However, particularly if a small volume of hyperpolarized sample (0.5 – 10 μL) is to be dissolved, the concentration of dissolved

sample is highest in the first few hundred microliters of solution emerging from the DNP polarizer. A means for ensuring that only this part of the sample is captured is to trigger injection immediately upon sensing the presence of sample in the injection loop.

In the initial implementation, a contactless conductivity detector (CCD) is used for this purpose[54]. The output signal of this detector in reality does not depend solely on conductivity, but also on dielectric constant (Table 3.1). It is obtained through Fourier transformation of an oscillating time-domain signal arising from the coupling between two electrodes via the sample, and its time-resolution and sensitivity is determined by the length of sampling for each output point. In order to maximize sample recovery, a time resolution of 4 ms was chosen. Under these conditions, the standard deviation of random fluctuations is 0.007 relative to the response from air.

Table 3.1. Response from contactless conductivity detector for different solvents. The detector was configured with an operating frequency of 54 kHz and a time resolution of 4 ms. (*) indicates saturation of the detector.

Fluid	Dielectric Constant ε	Relative Response (air =1)
Air	1.0006	1.00
Hexanes	2.0	1.06
THF	7.5	1.39
MeOH	30	3.11
H_2O	80	6.93
100 μM NaCl	n/a	41.1
1 mM NaCl	n/a	197 (*)
10 mM NaCl	n/a	197 (*)
100 mM NaCl	n/a	62.4

While the CCD is an excellent detector for aqueous and polar organic solvent systems, it is less sensitive for non-polar organic solvents. As alternative, it is possible

to employ an optical detector. The optical detectors employed in the later implementations of the system are a simple off-the-shelf product which monitors the light transmitted through the PFA tubing. The optical detector must be able to sense both an increase in light transmission caused by refractive index changes and a non-absorbing sample, as well as a decrease in light transmission caused by an absorbing sample. Therefore the optical sensor must trigger based upon a deviation in transmission outside of a narrow window defined by the empty tubing. The two detectors are complementary, with the optical detector being simple and universal but non quantitative. The CCD is not universal, but is able to deliver a quantitative concentration profile when used with conducting samples.

The amount of sample recovery obtained with the procedure described above was estimated by dissolving and injecting samples of the dye bromocresol green, followed by spectrophotometric assay of the sample concentration in the NMR tube (Table 3.2). It can be seen that the percentage of total material recovered is highest for the smallest sample (1 μL). Therefore it appears advantageous to use the highest possible sample concentration (smallest possible volume of solution) for DNP of mass-limited samples.

Table 3.2. Amount of recovery and final dilution factor for samples of 3 mM bromocresol green in 50% H_2O and 50% ethylene glycol. Samples were dissolved into 4 mL of 50 mM potassium phosphate buffer (pH 8.0), and the final NMR sample volume was 440 ± 10 μL. The dilution factor was obtained by comparing the absorbance of the sample in the DNP system with the absorbance of the sample in the NMR tube. The mass fraction of sample recovered was calculated from the measured concentration and volume of the NMR sample.

Sample Volume in DNP system (μL)	**Dilution Factor**	**Mass Fraction of Sample Recovered**
1	601	73%
5	179	50%
10	90	48%

For ionic samples, sample concentration passing through the CCD was observed from the time dependent response. Figure 3.4a shows such a trace for a sample of 1 μL of 50 mM monopotassium phosphate that was dissolved into 4 mL of H_2O. The arrow in the figure indicates the approximate time of switching of the valve for the injection. The amount of solution that would be injected into the NMR spectrometer can be estimated from the integral of the detector response for the first 1/8 of the total time of solution present in the detector (based on a volume ratio of 500 μL/4000 μL). From this trace, it can also be seen that the appearance of large gas bubbles, as indicated by rapid fluctuations in conductivity, is limited to the tail of the solution emerging from the DNP system.

In order to counteract spin relaxation, which constitutes the second mechanism for loss of signal, minimization of the time utilized for the transfer of the sample is of foremost importance. Using the sample injector as described above, the total time of transfer is the sum of the time required for dissolution of the sample and ejection from

the polarizer, plus the injection time as indicated in Figure 3.2b. A typical time required for dissolution and ejection of the sample from DNP polarizer is estimated at 500 ms (this value is not directly accessible, but based on the length of tubing used is calculated as 60% of the measurable time between triggering of the flow of dissolution solvent into the variable temperature insert of the DNP polarizer, and the emergence of sample solution in the detector at the end of the sample loop of the injector). Therefore, the total time that elapses from the time of dissolution to the time of NMR measurement is 1200 ms.

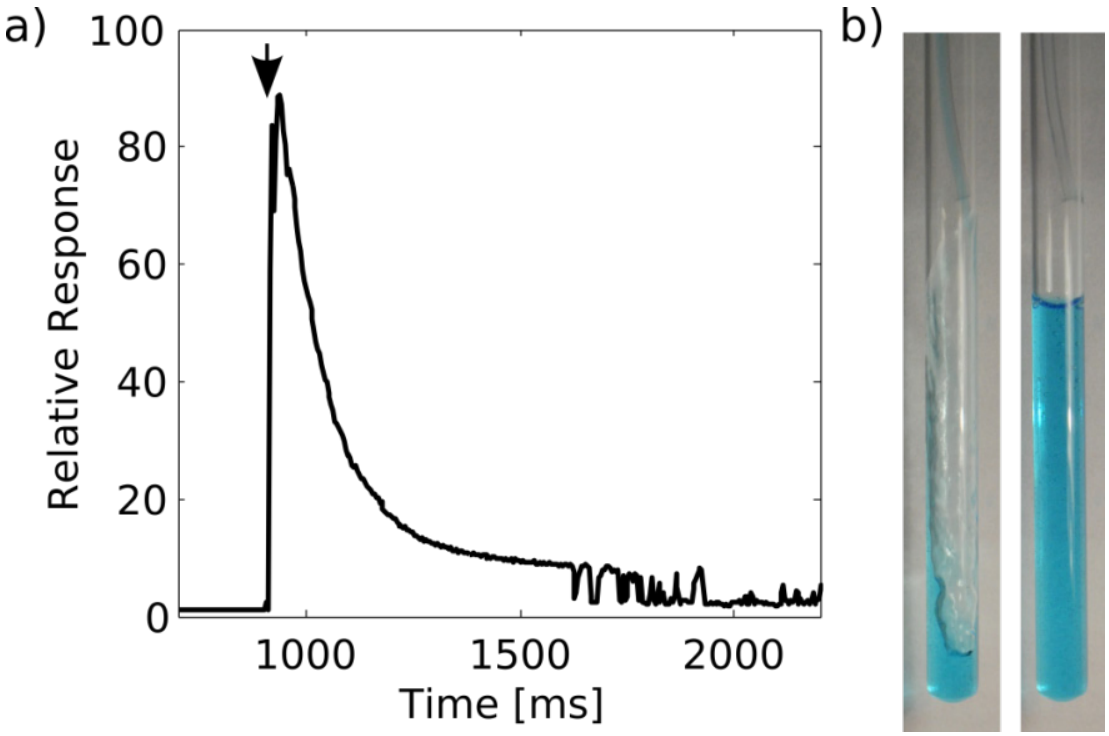

Figure 3.4. a) Conductivity profile for dissolution of a 1 µL sample of 50 mM monopotassium phosphate into 4 mL of H_2O. The arrow indicates the point in time where the injection valve would be switched. b) Image of sample during injection (200 ms) and after stabilization (600 ms). Images were taken with a shutter speed of 1/2500 s.

If the starting polarization is 10^4 times higher than the thermal polarization achievable in the NMR magnet,[41] a significant gain (i.e. of a factor of 500) can still be obtained for compounds that exhibit T_1 relaxation times as short as 1/3 of the injection time, *i.e.* 400 ms. Proton and carbon spins of most small molecules fall within this category[55]. For example, an enhancement factor of 2900 was achieved in the spectra of glucose shown in Figure 3.5a. It may be of further interest to investigate the relaxation behavior due to field fluctuations when passing through regions of low magnetic field during transport. However, qualitatively we have not observed adverse effects for small molecules when care is taken to keep the magnetic field at all points larger than approximately the field of the earth ($5 \cdot 10^{-5}$ T).

3.5 DNP-NMR Spectra Measured With Injection System

The final parameter of interest is the quality of the NMR spectrum that can be obtained at the end of the sample injection process. This parameter is primarily determined by the homogeneity of the solution at the time of measurement, which in turn is particularly sensitive to the presence of small gas bubbles, which would lead to line broadening. Since the injection is carried out against a back pressure of 1.0 MPa, outgassing of the solution is prevented. Through adjustment of the differential between this backpressure, and the forward pressure used to inject the sample, sufficient turbulence can be generated for obtaining a homogeneous solution at the time of NMR measurement (Figure 3.4b). During this step, it is also possible to admix a second solution, most conveniently if this solution is already placed in the NMR tube prior to the start of the experiment.[52] The variation in final sample volume of the NMR should be

kept low both to ensure that sample concentrations are known in rapid mixing experiments, and to enable the use of previously determined shimming parameters for the NMR magnet. Using the buffered digitally controlled pressure regulators to generate the injection pressure, the fluctuation in final sample volumes among different injections is below ±10 μL.

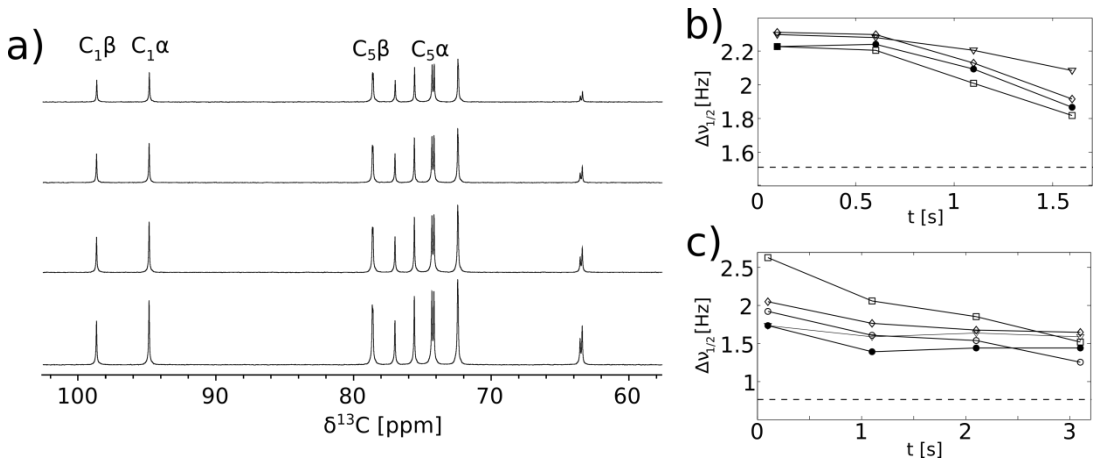

Figure 3.5. a) A series of spectra acquired from a sample of hyperpolarized glucose (20 μl of 2 M glucose in DNP polarizer, dissolved to yield an NMR sample of 440 μl glucose at 30 mM), using small flip angle excitation. Acquisition of the first transient started 600 ms after triggering of injection. Acquisition time was 440 ms for each transient. Flip angles used for excitation were 30°, 35°, 45°, and 90°. b) Line width of resonances from $C_1\beta$ (—●—), $C_1\alpha$ (—▽—), $C_5\alpha$ (—◇—) and $C_5\beta$ (—□—) obtained from the four transients shown in (a). The dashed line indicates the average line width of a thermal sample acquired under the same conditions. c) Line width of resonances from C_1 (—▽—), C_2 (—□—), C_3 (—○—),C_4 (—◇—) and C_5 (—●—) of a sample of hyperpolarized glutamic acid (20 μL of 1 M glutamic acid in DNP polarizer, dissolved to yield an NMR sample of 440 μL at 15 mM), acquisition parameters were similar to those in b, however, the acquisition time was 830 ms for each transient. The dashed line indicates the average line width of a thermal sample acquired under the same conditions.

Figure 3.5a shows a series of NMR spectra measured of hyperpolarized glucose using rapid sample injection as discussed above. The four spectra were obtained using small flip angle excitation, with flip angles adjusted to compensate for polarization used in previous scans (the remaining signal reduction in later scans is due to T_1 relaxation). The line widths of the resonances in these spectra, governed by the relaxation rate T_2*, contain contributions from various sources. Line widths measured as full width at half maximum from peaks of the glucose spectra are shown in Figure 3.5b. For purposes of comparison, Figure 3.5c shows line widths obtained using the same way from a set of spectra measured of a sample of glutamic acid (spectra not shown). The line widths include intrinsic T_2 relaxation, deficiencies in shimming in the steady state, and radiation damping effects, in addition to the broadening caused by inhomogeneities introduced by the sample injection. The minimum achievable line width is further determined by the acquisition time used for each FID, which is given by the total duration of the experiment divided by the number of successive scans that that are applied. An indication of the line broadening introduced specifically due to the sample injection may be obtained by comparing the line width in the first spectrum with the line width in the last spectrum. This difference in line width, plotted in Figure 3.5b and c, indicates that the contribution from such inhomogeneities is approximately 0.5 Hz, which for most applications appears negligible. Inevitably, some deficiencies in shimming occur as a result of the use of an alternate sample to shim prior to the actual experiment. This leads to minor increases in line width in comparison to thermal samples measured under identical conditions. As shown by the difference between the measured line width for the

polarized sample and the thermal sample shown in Figure 3.5b and c, this contribution amounts to approximately 0.5 Hz. In practice, this effect can be mitigated by shimming on the DNP sample just after the conclusion of one experiment and using the optimized values for the next experiment.

3.6 Summary

Solid-to-liquid state DNP up to now has perhaps been most prominently used for in-vivo magnetic resonance imaging and spectroscopy.[49] For such experiments, the focus may primarily be on obtaining the largest possible amount of polarization of a suitably chosen sensor molecule. However, hyperpolarized NMR also has significant potential for advancing NMR spectroscopy in applications related to chemistry and biochemistry. Challenges in this application area lie in the larger variety of compounds that are of interest, some of which exhibit short relaxation times, as well as in the need for obtaining high-resolution spectra. We have presented data to substantiate that true high-resolution NMR, with line widths rivaling those obtained from static samples, can be obtained from DNP polarized small molecules. In this way, hyperpolarization through DNP may open an avenue for structural analysis of minute quantities of small molecule samples, as well as for the study of chemical reactions with previously unmatched time resolution and sensitivity.

CHAPTER IV

KINETICS OF TRYPSIN CATALYZED ESTER HYDROLYSIS*

This chapter details the study of the trypsin catalyzed ester hydrolysis using DNP enhanced NMR. As the reaction kinetics can be measured by UV spectrophotometry, it also provides the "proof of concept" for the use of DNP-NMR for the measurement of reaction kinetics.

4.1 Introduction

NMR has long been used for the measurement of kinetics. However, its applications have largely been limited to slow non-equilibrium processes due to the need to perform signal averaging. A key area of interest is the measurement of chemical reactions in real-time. NMR is an ideal detection method for the measurement of reaction kinetics due to its unrivalled molecular information. When combined with DNP it has the added advantage of significant signal enhancement, while retaining the advantages of carrying out high-resolution NMR measurements in the liquid state. Once spins have been hyperpolarized, the acquisition of an NMR spectrum can be performed rapidly, requiring only a time sufficient to distinguish the spectral frequencies of different resonance lines, which can be as low as 10 ms. On the other hand, obtaining an equivalent signal-to-noise ratio by means of conventional signal averaging typically would take several months.[41, 56] Because hyperpolarization makes this same high signal-

* Reprinted in part with permission from "Time-resolved dynamic nuclear polarization enhanced NMR spectroscopy" by Bowen, S.; Hilty, C., *Angew. Chem. Int. Ed.* ***2008,*** *47, 5235-5237*, Copyright 2008 by Wiley-VCH.

to-noise ratio available in one instant, NMR spectroscopy in this modality seems ideally suited for the study of a dynamic process in real-time.

Trypsin is a serine protease capable of catalyzing the hydrolysis of both amide (peptide) and ester linkages. Both the kinetics and mechanisms of the trypsin catalyzed hydrolysis reaction are well characterized.[57-58] The model substrate N_α-benzoyl-L-arginine-ethyl ester (BAEE) is readily hydrolyzed into N_α-benzoyl-L-arginine (BA) and ethanol as shown in Figure 4.1.

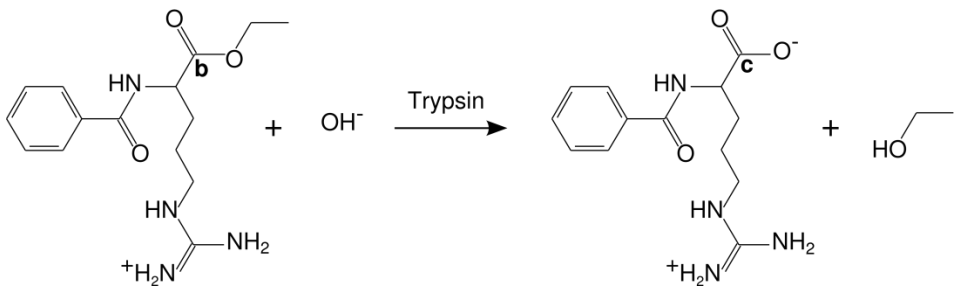

Figure 4.1. Trypsin catalyzed conversion of BAEE into BA and ethanol. “b” and “c” refer to resonances indicated in Figure 4.4.

The trypsin catalyzed hydrolysis of BAEE has the added advantage that it has a well-established spectrophotometric assay.[59] The existence of a spectrophotometric assay means that we can directly compare the results of the DNP-NMR based method to those obtained by the conventional UV method. Note that the DNP-NMR method is far more general, requiring only substrates that contain NMR active nuclei, while the UV method requires a chromogenic substrate.

4.2 DNP Enhanced NMR for Kinetic Measurements

The use of DNP enhanced NMR for measurement of reaction kinetics necessitates a different approach compared to standard NMR experiments. The key point of interest is the non-regenerable nature of the hyperpolarized spin system. In a simple, quantitative one dimensional NMR experiment, a relaxation delay of 3-5 times T_1 is placed between subsequent scans to allow for polarization to fully recover (as shown in Figure 3.1). A 90 degree pulse is used so that each scan uses the full polarization and generates the largest signal. However, relaxation in the hyperpolarized sample does not regenerate the hyperpolarized state, but instead yields equilibrium polarization. Because of this, it is necessary to alter the approach used to measure multiple scans.

There are two major schemes used to enable the acquisition of multiple scans from a single hyperpolarized sample. Both of them involve the use of small-flip angle pulses, which use only part of the available longitudinal magnetization. The first scheme involves the use of a constant, small flip angle for the measurement of each scan and has been used in the measurement of T_1 with hyperpolarized samples.[60] Because a small flip angle pulse uses only some of the available longitudinal magnetization, this scheme enables the measurement of multiple spectra from a single hyperpolarized sample. The key disadvantage of the constant flip angle approach is that each subsequent spectrum will be less intense than the one preceding it. For a given flip angle α and initial longitudinal magnetization $M_Z(0)$, the remaining longitudinal magnetization is

$$M_Z = M_Z(0) \cdot \cos(\alpha) \tag{4.1}$$

while the observable transverse magnetization produced is

$$M_{XY} = M_Z(0) \cdot \sin(\alpha) \tag{4.2}$$

As a consequence, there is no single flip angle capable of generating spectra with consistent intensity. Instead, the intensity profile will be weighted so that most of the available intensity is used in the beginning of the experiment. An approximately uniform profile can be generated with very small flip angle pulses, but this will result in considerable unused longitudinal magnetization.

The alternative is to use a flip angle that increases for each scan, culminating in a 90^o pulse for the last scan. In this approach, it is possible to utilize all of the available longitudinal magnetization while also generating spectra with consistent intensity. For an NMR experiment consisting of n scans, the variable flip angle α_k for the k^{th} scan is

$$\alpha_k = \arcsin\left(1/\sqrt{n+1-k}\right)^{61\text{-}62} \tag{4.3}$$

This variable flip approach neglects the effects of T_1 relaxation. A variable flip angle series which also corrects for T_1 relaxation has been described elsewhere.[62] Figure 4.2 shows the calculated transverse and longitudinal magnetization for a hypothetical 12 scan experiment performed with 15° and 30° constant flip angles, as well as the variable flip angle scheme shown in equation 4.3. It is evident that the variable flip angle scheme is the only one to fully utilize the longitudinal magnetization and, neglecting the effects of relaxation, deliver uniform intensity across all scans.

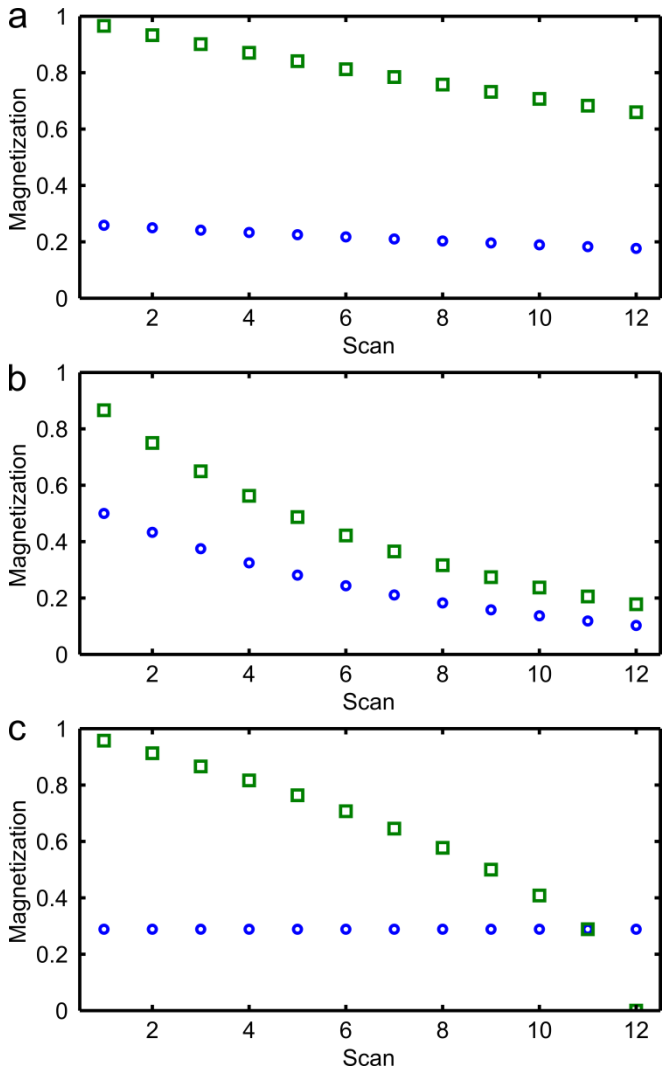

Figure 4.2. Calculated magnetization for a 12 scan experiment using constant and variable flip angle schemes, in the absence of T_1 relaxation. Longitudinal magnetization (M_Z, □) and transverse magnetization (M_{XY}, ○). (a) 15° constant flip angle, (b) 30° constant flip angle, (c) variable flip angle scheme from equation 4.3.

4.3 Experimental Section

For DNP polarization, the sample of BAEE (EMD, Gibbstown, NJ) was mixed with the radical Tris{8-carboxyl-2,2,6,6-tetra[2-(1-hydroxymethyl)]-benzo(1,2-d:4,5-d')bis(1,3)dithiole-4-yl}methyl sodium salt ("OX63"; Oxford Instruments, UK) and glassing mixture of 60% ethylene glycol (Mallinckrodt Baker, Phillipsburg, NJ) and 40% water to yield a 20 µl aliquot of 500 mM BAEE and 15 mM OX63. 5 mM of urea-^{13}C (Cambridge Isotope Laboratories, Andover, MA) was added as an internal standard. This aliquot was polarized using a DNP polarizer (Oxford Instruments, UK), at 1.4 K and 60 mW of 93.976 GHz mm-waves for 120 min. The polarized sample was dissolved by 3 mL of hot buffer solution (90% H_2O / 10% D_2O, 50 mM potassium phosphate, pH 7.6) delivered at 10 bar peak pressure. Sample injection into the 400 MHz NMR (Bruker, Switzerland) was performed with the previously described sample injector using a 5 mm NMR tube. Sample injection was performed using N_2 (17 bar, against a back pressure of 11 bar) to yield 450 µL injected volume. Subsequently, the valve was switched back to the loading position, and an overpressure of 17 bar was applied. A trypsin solution (1 mM, 25 µL, pH 3) was present in the NMR tube prior to sample injection. The two solutions mixed as the polarized sample was injected. NMR data was acquired as a sequence of 6 spectra using the pulse sequence shown in Figure 4.3. The progress of the catalyzed reaction was monitored in real-time by observing a sequence of ^{13}C NMR spectra over the course of 3 sec. For each spectrum, a fraction of the polarization that had previously been generated by the DNP mechanism, and that had been retained by the substrate and product molecules, was converted into NMR

observable spin coherence by a variable flip angle pulse calculated with equation 4.3. Sample temperature was determined by measurement of a representative sample with a small thermocouple. Final substrate concentrations were verified by reverse-phase high performance liquid chromatography. NMR data were processed and integrated using MatNMR.[63]

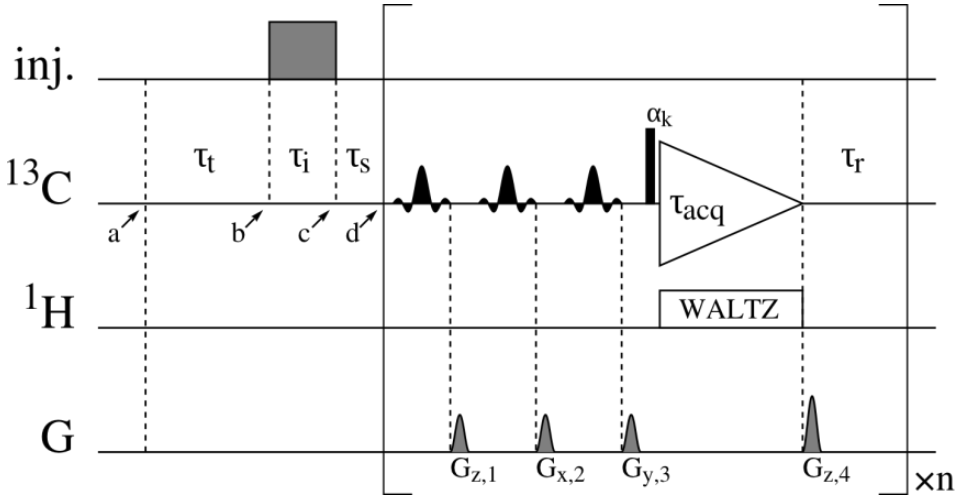

Figure 4.3. NMR experiment for measurement of reaction kinetics using DNP enhanced samples. Sample is delivered from the polarizer to the injector described in the previous chapter between time points a and b. As soon as sample is detected in the CD detector (time point b), the valve of the injector is switched to the inject position. After the injection time τ_i, at time point c, the valve is switched back to the load position. The NMR experiment is triggered after a stabilization time τ_s at time point d. Subsequently, *n* one-dimensional spectra are acquired. Suppression of a resonance from the glassing agent is achieved by three selective $\pi/2$ pulses (shape: $\sin(x)/x$, x=-3π...3π; 10 ms) followed by pulsed field gradients ($G_{z,1}$=70 G/cm; $G_{x,2} = G_{y,3}$ = 35 G/cm; 1 ms; gradients are applied along the axis indicated). The flip angles α_n of the subsequent excitation pulse (pulse strength γB_1=18 kHz) are calculated from equation 4.3. During each acquisition period, 16,384 points are acquired, and τ_{acq} = 275 ms. $G_{z,4}$ = 100 G/cm removes unwanted coherence prior to the next acquisition. τ_r is adjusted so that the repetition rate is 2 s^{-1}. ^{1}H decoupling is applied using WALTZ-16 at a field strength γB_1= 3.3 kHz. The carrier is set to 63.3 ppm on ^{13}C (ethylene glycol) and 4.3 ppm on ^{1}H.

4.4 Results and Discussion

From the spectra in Figure 4.4, the reduction in intensity of the substrate resonance (BAEE; Figure 4.4a&b), as well as the appearance of product (BA; Figure 4.4a&c), can be seen. For a quantitative analysis, the signal intensities were normalized with reference values obtained from a measurement in the absence of trypsin, which was scaled so that the resulting relative intensity extrapolated to t=0 is equal to 1 (intercept in Figure 4.4d). This procedure removes the effect of signal loss due to spin-lattice relaxation during the reaction time.

The normalized intensities are a linear function of time, as is expected for the reaction in the regime where substrate is in large excess (Figure 4.4d).[64] The rate of catalysis, k_{cat} = 12.1 ± 1 s^{-1}, can be read directly from the slope of this line, whereby the error was estimated from the spread of values obtained from different datasets, as well as from different methods for peak integration. To validate the DNP-NMR measurements, we have compared the trypsin activity with a measurement by UV-visible spectrophotometry, which yielded a rate constant of 12.5 s^{-1} for the batch of trypsin used (25 °C, pH 7.6), and is also in good agreement with a published value under similar conditions.[58] While we chose a chromogenic substrate to enable this comparison, there are many naturally occurring substrates that are inaccessible to spectrophotometry, but that can still be directly observed by the DNP-NMR measurements presented here.

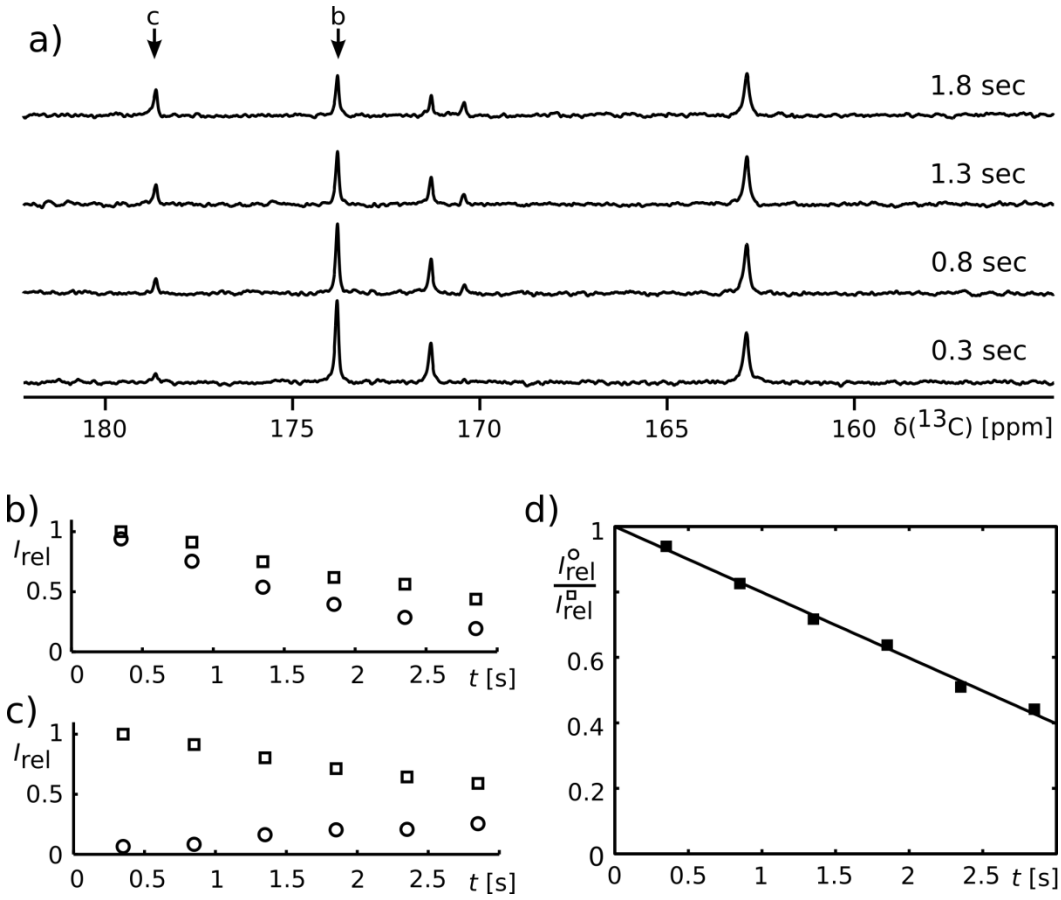

Figure 4.4. Kinetics of BAEE hydrolysis (3.3 mM) by trypsin (54 μM) in 50 mM potassium phosphate buffer, pH 7.6, at 27 °C. Time resolved ^{13}C spectra (a) show loss of BAEE (b), and growth of BA resonances (c). In (b) and (c), intensities from the spectra of the reaction (○) are shown together with intensities from an unreacted reference spectrum (□; scaled as used for (d)). (d) linear regression of the ratio of intensities from (b), yielding k_{cat}=12.1 s^{-1}.

The signal increase in the resonance stemming from the reaction product was also linear (not shown). The apparent rate constant was 9.0 s^{-1}, which is lower than the rate of catalysis. The reason for this difference may be due to a shortening of the spin-lattice relaxation time when substrate is bound to the enzyme. This effect could potentially lead to additional information on the dynamics of the binding of different substrates.

Using the present injection system, the first data point could be acquired with an initial delay of 300 ms. Further improvements of the apparatus will include the design of a NMR flow cell, to increase time resolution close to the theoretical minimum of ~10 ms.[65]

The gain in signal provided by DNP enabled the measurement of ^{13}C spectra without the need for isotopic enrichment, in a single scan (^{13}C concentration of 36 μM at 1.1% natural abundance). A conventionally acquired NMR spectrum of a standard solution of 25 mM BAEE under Ernst-angle conditions[56] yielded a S/N ratio of 31 in 10.7 h. It is extrapolated that a spectrum equivalent to the hyperpolarized dataset (S/N of 62 in first scan), but using conventional signal averaging would require 100 days. The observation of reaction kinetics would thus be impossible. This comparison illustrates the value of using DNP enhanced NMR for enabling the measurement of rapid processes that would otherwise be inaccessible to NMR.

With the present sensitivity, a reaction can be detected at enzyme concentrations on the order of 10 μM, which are typical for biological tissue.[66] Hyperpolarization selectively enhances the signal of the polarized substrate by several orders of magnitude over any background from non-polarized molecules. This property may prove particularly useful for measurements in cells or in crude cell extracts, which contain a large number of substances that would otherwise mask the substrate to be observed, but where reaction kinetics may be dramatically different from those under purified *in-vitro* conditions.[67] Additionally, the ability to observe individual molecular sites by NMR, further enhanced by the large chemical shift range of ^{13}C, can give simultaneous kinetic

information on reactions that occur in parallel. In more complicated situations, direct observation of saturation transfer[68] from an individually addressed spin in the substrate, to the product may also allow the determination of reaction mechanisms by this method.

4.5 Conclusions

In conclusion, we have demonstrated that the increased sensitivity provided by hyperpolarized NMR enables time-resolved observation of enzymatic reactions under near-physiological conditions. This approach is, however, not limited to enzyme kinetics; other applications include the study of unidirectional chemical and biochemical processes as diverse as polymerization reactions, or protein folding. DNP enhanced time-resolved NMR is valuable where conventional NMR observation would require signal averaging, a situation that in practice is often encountered due to the low intrinsic sensitivity of NMR. Under these circumstances, the gain in signal obtained from hyperpolarization directly translates into a reduction of the lower limit of the observable time-scale.

CHAPTER V

CHEMICAL SHIFT CORRELATIONS BY OFF-RESONANCE DECOUPLING*

In this chapter, we discuss the measurement of heteronuclear correlations by off-resonance decoupling. One of the unique features of NMR as compared to other spectroscopic techniques is the ability to measure correlations between atoms. These correlations are invaluable in determining molecular structure. However, when using hyperpolarized samples, it is necessary to use alternative means to obtain them. This is especially true for measurements involving transient species, or those with very short T_1.

5.1 Introduction

In most modern NMR studies, Fourier transform NMR[69] enables the acquisition of multi-dimensional correlation spectra, which yield important information on the structure of a molecule. A multi-dimensional NMR data set is acquired by repeating a one-dimensional experiment with different indirect evolution times, allowing reconstruction of the indirect dimension. Such an experiment relies on a delay between each scan, during which the spin system returns to the equilibrium state, given by the thermal distribution over the Zeeman levels in the magnetic field. Each scan of the experiment thus starts with the same amount of "fresh" longitudinal magnetization. When working with hyperpolarized sample, however, the initial spin state is polarized far beyond equilibrium. The ensuing large magnetization is the basis for the increased signal, but at the same time, the magnetization does not return to the hyperpolarized

* Reprinted in part with permission from "Chemical shift correlations from hyperpolarized NMR by off-resonance decoupling" by Bowen, S.; Zeng, H.; Hilty, C., *Analytical Chemistry* **2008,** *80* (15), 5794-5798, Copyright 2008 by the American Chemical Society.

initial state after an NMR scan has been completed. Rather, the spin system will relax to the thermal equilibrium, which has much lower magnetization. Thus, a two-dimensional NMR spectrum of a hyperpolarized sample cannot be acquired by the means described above.

One elegant way of obtaining a two-dimensional NMR spectrum in a single scan has recently been developed by Frydman.[70] Thereby, using the methods of magnetic resonance imaging (MRI), the sample is divided by the NMR experiment into many small sub-volumes. The coherences corresponding to the multiple scans that are necessary for reconstruction of an indirect spectral dimension are encoded in, and read out from these separate volumes.

Here, we propose an alternative scheme to obtain two-dimensional chemical shift correlations from hyperpolarized samples, which is particularly robust and easy to implement. By a differential scaling of scalar coupling under low-power radio-frequency (RF) irradiation, a second chemical shift dimension is directly encoded into the line shape of the acquired NMR signals. In conventional biomolecular NMR, such an approach has previously been proposed for use with multi-dimensional correlation experiments of isotopically enriched proteins.[71] We demonstrate here that off-resonance decoupling provides a quite general and simple way of obtaining two-dimensional chemical shift correlations with hyperpolarized samples of small molecules.

5.2 Experimental Section

5.2.1 Sample Preparation

Samples for determination of ^{1}H-{^{13}C} spectra consisted of 0.5 μL of 3.6 M vanillin (MP Biomedicals, Solon, OH) solution in 72% dimethylsulfoxide-D_6 (DMSO-D_6; Cambridge Isotope Laboratories, Andover, MA) and 28% D_2O (Cambridge Isotope Laboratories, Andover, MA) containing 15 mM 4-Hydroxy-2,2,6,6-tetramethylpiperidine 1-oxyl (TEMPOL; Sigma-Aldrich, St. Louis, MO) free radical. Samples for ^{13}C-{^{1}H} spectra consisted of 0.5 μL of 3.6 M vanillin solution in 72% DMSO-D_6 and 28% D_2O containing 15 mM of Tris{8-carboxyl-2,2,6,6-tetramethyl-benzo(1,2-d:4,5-d')bis(1,3)dithiole-4-yl}methyl sodium salt ("Finland"; Oxford Instruments, Tubney Woods, UK) free radical. After dissolution into the NMR spectrometer, samples were analyzed by high pressure liquid chromatography (HPLC). A C_{18} column (ODS, 3 μM, 250 x 4.0 mm) from SGE (Austin, TX) was used with a mobile phase of 60% acetonitrile / 40% H_2O + 0.1% trifluoroacetic acid (TFA). Vanillin concentrations were determined by comparing peak integral values for vanillin to standard samples of vanillin in mobile phase.

5.2.2 DNP Polarization

DNP polarization took place at a temperature of 1.4 K in a Hypersense DNP polarizer (Oxford Instruments, Tubney Woods, UK). Samples for ^{1}H observation were polarized for 30 min at a microwave frequency of 94.270 GHz and a power of 100 mW. Samples for ^{13}C observation were polarized for 3 h at 93.976 GHz and 60 mW. Samples

were dissolved in acetonitrile, and transferred to the NMR spectrometer using a sample injector described in Chapter III. The total time of sample injection, from the point of dissolution to the point of NMR measurement, is < 2.5 sec. After sample injection, NMR experiments are automatically started.

5.2.3 NMR Spectroscopy

The purpose of the NMR experiment is to determine the chemical shifts of a pair of heteronuclei that are coupled via scalar coupling. The information obtained is the same as from a heteronuclear correlation spectroscopy experiment.[72-73] In contrast to the aforementioned techniques, however, the chemical shift of the coupled nucleus is determined from the same transient that shows a spectrum of the directly observed nucleus. When continuous-wave (CW) decoupling is applied near the resonance frequency of the coupled nucleus, the scaling in the observed scalar coupling constant, J_{obs}, allows direct inference of the chemical shift of the coupled nucleus. Specifically, the NMR experiment (Figure 5.1) acquires a small number of scans, typically from n = 3 to 5. The first scan is a reference scan without CW radiation, while the subsequent scans apply CW at different frequencies within the chemical shift range of the indirectly observed nucleus. To distribute the signal available from the hyperpolarized sample evenly across the n scans, a variable flip angle α_k is used for excitation. Since the spin polarization should not reach equilibrium conditions, there is no delay between the successive scans. Figure 5.1 presents two alternative schemes to obtain the chemical shift correlations. In (a), the acquired dimension is ^{13}C, and the indirect dimension is ^{1}H (^{13}C-{^{1}H} experiment). In this case, the free induction decay (FID) is obtained directly

after the excitation pulse. In Figure 5.1b, the acquired dimension is ^{1}H (^{1}H-{^{13}C} experiment). In this experiment, the abundance of the NMR active isotope of the indirectly observed nucleus, ^{13}C, is only 1%. If a sequence analogous to Figure 5.1a were used, most of the acquired signal would not carry the desired information on the ^{13}C chemical shift. Therefore, an isotope selective pulse sequence is used, which includes coherence selection by pulsed field gradients. By this pulse sequence, only the coherence transferred from ^{1}H to ^{13}C and then back to ^{1}H contributes to the signal.

As in any other heteronuclear experiment, this pulse sequence requires the adjustment of an additional delay, τ_j, which is a function of the J_{CH} scalar coupling constant. Since the final signal intensity depends on $\sin^2(\pi/2 \cdot J/J_0)$, where $J_0 = 1/(2\ \tau_j)$ is the presumed and J the actual coupling constant, this delay is however quite forgiving to small maladjustment. For example, a variation of 20% in the coupling constant translates into a sensitivity loss of only 10%.

5.3 Results and Discussion

For purposes of comparison, two-dimensional chemical shift correlations of the molecule vanillin, at 0.9 mM concentration and without isotopic enrichment, were recorded. In the first case (Figure 5.1a), ^{13}C spectra were acquired while CW radiation was applied at different frequency values within the ^{1}H frequency range (^{13}C-{^{1}H} experiment). The obtained one-dimensional traces are shown in Figure 5.2, the lowest one representing the spectrum without CW. In the upper traces, the offsets of CW irradiation on the ^{1}H channel are indicated on the right. From the expanded view of the resonance around 191.9 ppm (Figure 5.2b), the effect of the ^{1}H CW irradiation can be

observed directly. The distance between the two observed peaks in the lowest trace corresponds to the actual ^{1}H-^{13}C coupling constant J_0 = 173.6 Hz. In the traces with CW irradiation, this coupling constant is scaled depending on the difference between the CW frequency and the ^{1}H chemical shift attached to the observed carbon.

The observed coupling constant, J_{obs}, is given by

$$\frac{J_{obs}}{J_0} = \frac{\left|\delta - \delta_{CW}\right|}{\sqrt{(\delta - \delta_{CW})^2 + (10^6 \cdot B_{1,CW} / B_0)^2}} \tag{5.1}$$

where $B_{1,CW}$ is the amplitude of the decoupling field ($B_{1,CW} = 1/(4\gamma\tau_{90})$ with τ_{90} the 90° pulse length corresponding to the applied power), δ is the chemical shift of the spin, and δ_{CW} the chemical shift at which CW irradiation takes place.[74] Figure 5.3 shows the dependence of the scaling factor on chemical shift of the indirectly observed ^{1}H nucleus, plotted using the parameters δ_{CW} and $B_{1,CW}$ from the ^{13}C-{^{1}H} experiments. The offset frequencies are chosen so that at any point in the desired frequency range, the scaling factors in at least two scans are strongly dependent on the chemical shift.

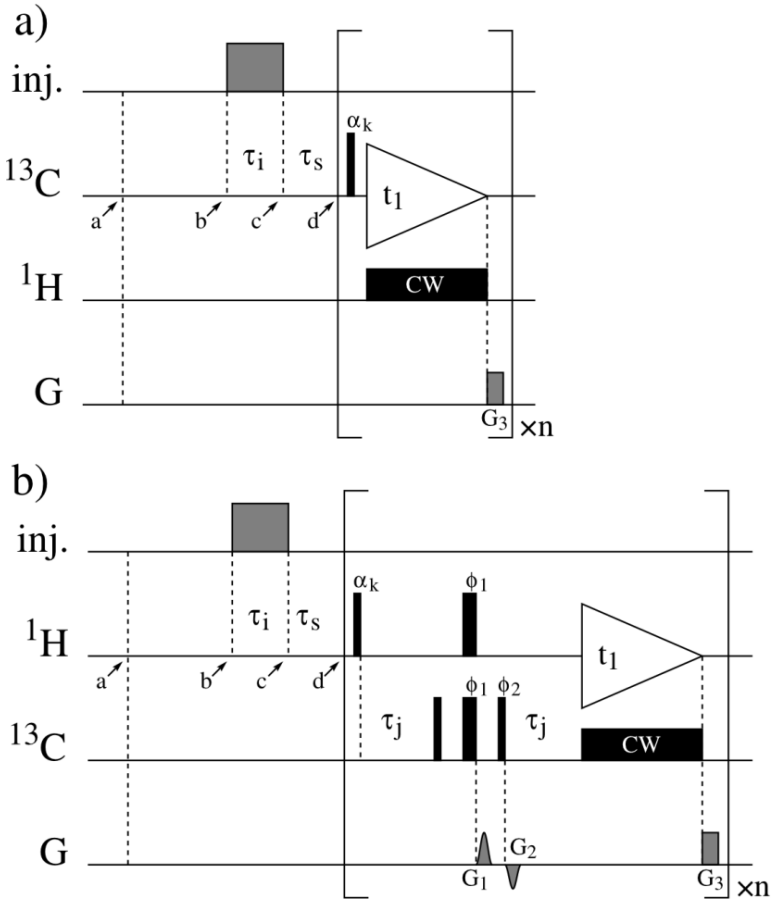

Figure 5.1. NMR experiments for measurement of 2D chemical shift correlations of hyperpolarized sample. Injection ("inj.") into the NMR takes place during τ_i=350 ms, and the NMR experiment is started after a stabilization time τ_s=300 ms at time point d. Narrow and wide black bars denote π/2 and π hard pulses, unless otherwise indicated ($\gamma_H B_{1,H}$ = 25 kHz; $\gamma_C B_{1,C}$ =20 kHz). Flip angles on excitation pulses are given by $\alpha_k = \arcsin\left(\frac{1}{\sqrt{n+1-k}}\right)$, with *k*=1..*n*. Pulse phases are x, unless indicated. A pulsed field gradient G_3 = 50 G/cm, 2.5 ms duration is applied along the z axis. In (a), the offset on the ^{13}C channel is 120 ppm. Three spectra with off-resonance decoupling ($\gamma_H B_{1,H}$ = 1.67 kHz) at offset 11 ppm, 7 ppm, and 3 ppm are acquired. The acquisition time $t_{1,max}$=324 ms. In (b), coherence selection is achieved by the pulsed field gradients G_1 (50 G/cm, 1000 μs applied along x, y and z axes) and G_2 (-37.4 G/cm, 1000 μs applied along x, y and z axes). The delay τ_j=1/(2 J_{CH})=3.45 ms. Pulse phases are φ_1=y; φ_2=-x. The offset on the ^1H channel is 6 ppm. Four spectra with off-resonance decoupling ($\gamma_C B_{1,C}$ = 6.0 kHz) at offset 210 ppm, 150 ppm, 90 ppm and 30 ppm are acquired. The acquisition time $t_{1,max}$=426 ms.

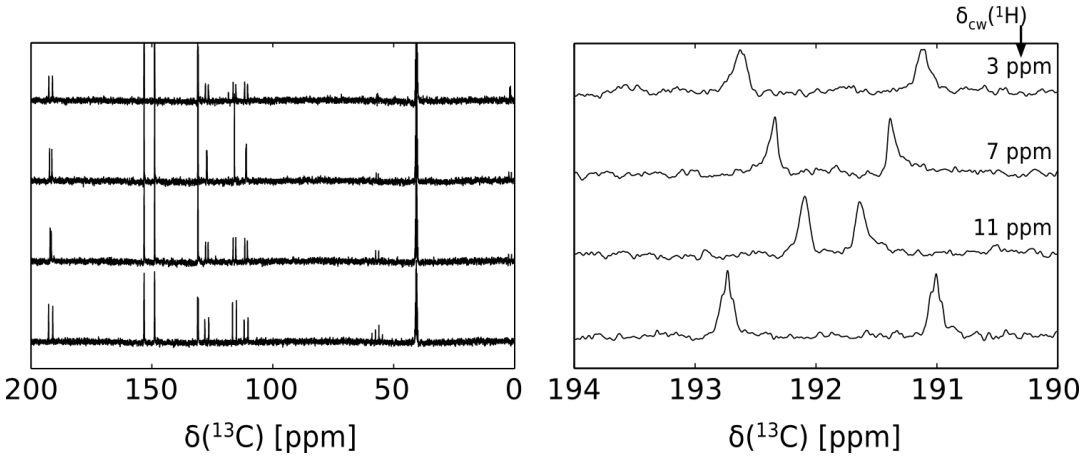

Figure 5.2. Series of ^{13}C NMR spectra recorded from one single DNP polarized sample, which permits the reconstruction of a two-dimensional chemical shift correlation. (a) full spectrum. (b) expanded spectrum around 192 ppm. The frequency for off-resonance CW irradiation is indicated near each trace. The lowest trace is the reference spectrum without irradiation. Chemical shifts were calibrated against a standard of tetramethyl silane (TMS), using the substitution method.[9]

Rewriting equation 5.1 yields

$$\left|\delta_{CW,i} - \delta_i\right| = 10^6 \frac{B_{1,CW}}{B_0} \tan\left(\arcsin\left(\frac{J_{obs}}{J_0}\right)\right) \tag{5.2}$$

$\delta_{CW,i}$ is the chemical shift at which CW irradiation takes place in a given trace *i*, and δ_i is the chemical shift value of the spin to be determined from trace *i*. From measurement of J_{obs} in a one-dimensional trace, the difference between the ^1H chemical shift and the respective offset of CW irradiation can thus be determined. Comparing these differences from all the acquired traces allows unambiguous determination of the ^1H chemical shift values.

Since the accuracy of each obtained chemical shift difference depends on the slope of the respective curve shown in Figure 5.3, it is possible to use a weighted average that depends on this slope, for determining the final chemical shift value,

$$\delta = \frac{\sum_{i=1}^{n} \alpha_i \delta_i}{\sum_{i=1}^{n} \alpha_i}, \tag{5.3}$$

with the weighting factor

$$\alpha_i = \left(\frac{1}{\sqrt{(\delta_i - \delta_{CW,i})^2 + (10^6 \cdot B_{1,CW} / B_0)^2}} \right)^3 . \tag{5.4}$$

Using this procedure has the further advantage that an estimate for the error in the indirectly detected chemical shift can be obtained,

$$\Delta\delta = \frac{\sum_{i=1}^{n} \alpha_i \left| \delta_i - \delta \right|}{\sum_{i=1}^{n} \alpha_i} \tag{5.5}$$

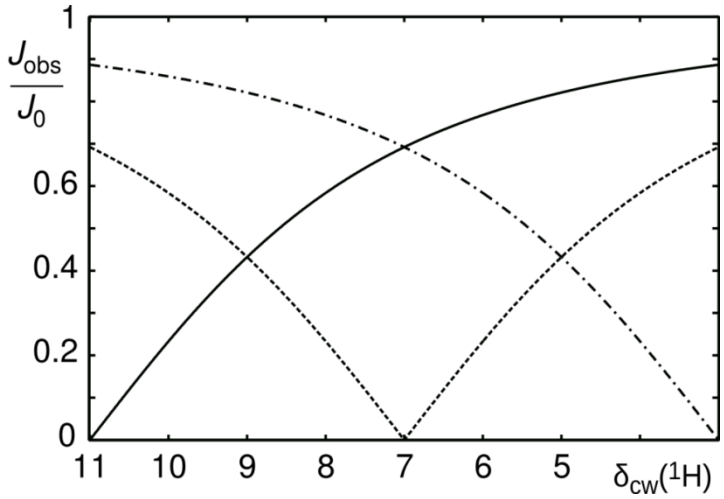

Figure 5.3. Scaling of the observed *J*-coupling constant as a function of resonance offset of the CW irradiation. The scaling factor is plotted against ^{1}H chemical shift for CW frequencies corresponding to 11 ppm (—), 7 ppm (– –), and 3 ppm (– · –).

The observed coupling constants and the derived chemical shifts for the ^{13}C-{^{1}H} data set in Figure 5.2, are presented in

Table 5.1. The assignments of these chemical shifts to the atoms in the vanillin molecule are shown in Figure 5.4.[75-76] It can be seen that the indirectly detected chemical shifts could be determined with an error of 0.1 ppm for all resonances, using a total of 4 scans on a single hyperpolarized sample.

Table 5.1. Observed coupling constants and chemical shifts in the ^{13}C-{^{1}H} spectrum.

^{1}H cw offset / ppm[a]	no CW	11	7	3		
^{13}C Chemical shift / ppm	J / Hz				^{1}H chemical shift / ppm	Site
191.9	173.6	44.8	94.6	150.1	9.8 ± 0.1	E
153.2	No proton is attached to these carbons.					G
148.9						H
130.9						F
127.3	161.9	102.6	18.8	116.4	7.5 ± 0.1	D
115.8	162.4	108.0	0	109.7	7.0 ± 0.1	C
111.0	161.9	103.5	18.8	114.3	7.4 ± 0.1	B
56.8	145.5	123.8	84.9	30.7	4.0 ± 0.1	A

[a] Offset values in the table are nominal values. The values after calibration against the standard of TMS are: 10.92, 6.92, 2.92 ppm.

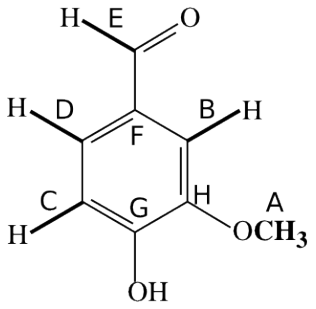

Figure 5.4. Vanillin, with sites indicated as in tables 1 and 2.

The inverse experiment, where a proton spectrum is acquired (^{1}H-{^{13}C} experiment; Figure 5.5 and Table 5.2) works by the same principle. However, since 98.9% of the observable ^{1}H nuclei are attached to a NMR inactive ^{12}C nucleus, a heteronuclear ^{13}C filter element was included in this experiment. This filter element suppresses the large central peak that would otherwise be present in the spectra. Due to the larger ^{13}C chemical shift dispersion (0-200 ppm), it was necessary to acquire 5 instead of 4 traces. In Table 5.2, it can be seen that chemical shifts could be determined with an uncertainty of 3 ppm.

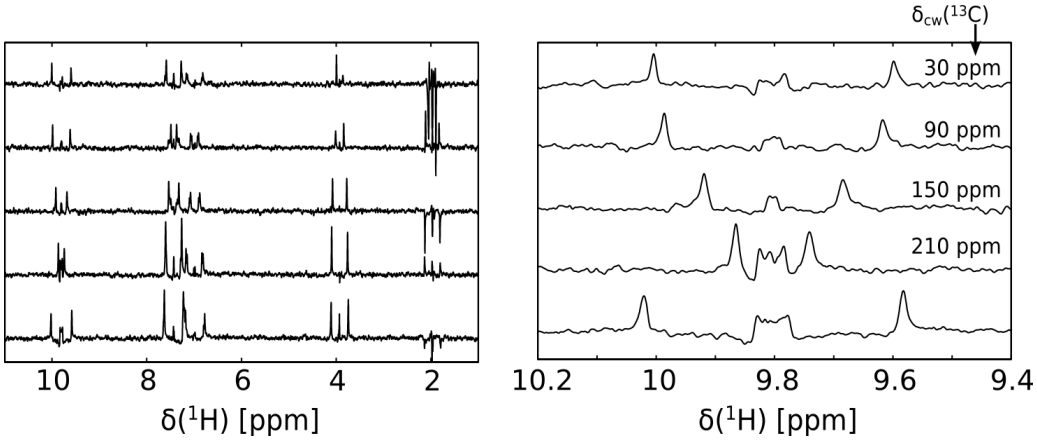

Figure 5.5. Series of ^{13}C filtered ^{1}H NMR spectra for the reconstruction of two-dimensional chemical shift correlation.

Table 5.2. Observed coupling constants and chemical shifts in the ^{1}H-{^{13}C} spectrum.

^{13}C cw offset / ppm[a]	no CW	210	150	90	30		
^{1}H Chemical shift / ppm	J / Hz					^{13}C chemical shift / ppm	Group
9.81	175.9	49.9	94.5	147.9	162.2	190 ± 3	E
7.43	162.3	129.1	56.4	79.8	143.0	129 ± 3	D
7.43	161.1	135.4	85.4	47.8	125.2	111 ± 3	B
6.99	162.3	133.9	77.6	59.4	129.9	116 ± 3	C
3.93	145.4	134.2	120.9	69.1	53.8	58 ± 3	A

[a] the offset values in the table are nominal values. The values after calibration against the standard of TMS are: 211.0, 151.0, 91.0, 31.0 ppm.

The concentration of vanillin was determined by HPLC to be 0.9 mM in both samples. Since the compound was not ^{13}C enriched, the concentration of the observable ^{13}C nuclei was 10 μM. For calculation of the obtained polarization level, it is necessary to compare the S/N ratio to a conventionally acquired spectrum. Due to the low concentration, it was however not practical to use the samples that were previously polarized for this purpose, as an excessively long measurement time would be needed. Therefore, we acquired a one-dimensional ^{13}C spectrum, as well as a one-dimensional ^{13}C-filtered ^{1}H spectrum using reference samples of vanillin at concentrations of 69 mM and 45 mM, respectively. The S/N ratio of the reference ^{13}C spectrum was 13 to 32, depending on the resonance line, after an acquisition time of 12 hours under Ernst-angle conditions.[74] This compares to an SNR of 8 to 20 in the first trace of the dataset obtained from hyperpolarized sample shown in Figure 5.2.

We estimate that a conventional spectrum with the same S/N ratio would require >200 days when acquired on the same NMR spectrometer. In the case of the ^{1}H

experiment, the S/N ratio was 26 to 88 for the ^{13}C filtered ^{1}H experiment after an acquisition time of 1 hour, and 11 to 21 for the first trace of the hyperpolarized experiment. Based on these numbers, a conventionally acquired spectrum with the same S/N ratio would thus take 4 to 18 days.

In both cases, a significant gain in sensitivity is achieved by hyperpolarization, since the polarization time is only on the order of hours (3 h for ^{13}C polarization and 30 min for ^{1}H polarization), while the actual NMR measurement time for the two spectra is below 3 seconds. The level of polarization can be calculated from this comparison, using

$$p_p = p_t \sqrt{n_t} \cdot \frac{1 - e^{-t_r/T_1}}{1 - e^{-t_r/T_1}\cos(\alpha_t)} \frac{\sin(\alpha_t)}{\sin(\alpha_p)} \frac{s_p}{s_t} \frac{c_t}{c_p}, \tag{5.6}$$

with the thermal polarization

$$p_t = \frac{\hbar \gamma B_0}{2kT}. \tag{5.7}$$ [74]

Here, the subscripts *p* and *t* refer to the polarized and the thermal samples, respectively. *n* is the number of scans, *s* the obtained signal-to-noise ratio, *c* the concentration, α the flip angle for excitation, t_r the recycle time in the conventional experiment, T_1 the spin-lattice relaxation time, and *T* the temperature of NMR measurement. Eq. 6 and 7 yield polarization levels between 2 and 7% for ^{13}C and between 2 and 3% for ^{1}H, depending on the observed resonance line.

The level of polarization that is observed in the NMR depends on the polarization in the solid state, and on losses due to T_1 relaxation during dissolution and injection into the NMR spectrometer. Because of the latter process, the liquid state polarization level is

generally higher for spins with longer relaxation time. This observation stands in contrast to the situation in a conventional NMR spectrum, where it is the signals from spins with long relaxation time that are typically attenuated due to incomplete recovery during the delay between subsequent scans.

For demonstration of the present experiments, we have chosen the vanillin molecule because it contains a variety of proton and carbon containing chemical groups, including a methyl group, an aromatic ring and an aldehyde group. In our experience, most small molecules are polarizable, and the presented method should be quite generally applicable. The most limiting factor determining the type of molecule suitable for solid-to-liquid state DNP polarization is the loss to relaxation during the time required for sample dissolution and injection into the NMR spectrometer. Using our present, "home-built" sample injector, this time is approximately 2.5 seconds. Spins with a T_1 relaxation time of a few seconds are thus ideal for polarization using our DNP instrument. Chemical groups belonging to this class include aromatic rings, ketones or aldehydes, and also many aliphatics. The limitation imposed by T_1 relaxation is not as stringent as it may seem at first glance, as appreciable signal gain can still be realized for spins with a T_1 relaxation time as low as one-third of the injection time (*i.e.* currently $T_1 \approx 700$ ms). We have also successfully polarized molecules containing spins with relaxation times in this range, including peptides and glucose.

5.4 Conclusions

Using the presented method, the entire set of $^{13}C,^{1}H$ chemical shift correlations from a single hyperpolarized sample, here 0.9 mM vanillin, can be determined with high

sensitivity. In the spectra shown, 10 μM of ^{13}C atoms were observed with a total experiment time of three hours, including the time required for hyperpolarization. Certainly, this method does not resolve overlapping resonances in the second dimension, as would be done in a two-dimensional data set with indirect chemical shift evolution. However, the hyperpolarization offers the ability to directly detect the ^{13}C spectrum, rather than the ^{1}H spectrum. Therefore, the ^{13}C-{^{1}H} experiment yields chemical shifts of carbon atoms without attached protons, in addition to the ^{13}C,^{1}H chemical shift correlations. At the same time, the large chemical shift range of the carbon spectrum alleviates potential signal overlap problems. To further reduce the number of lines in the spectra, it would also be possible to include a spin-state selective pulse sequence[71, 77-78] to select only one component of the peak doublet. However, this was not done here because it would require the acquisition of additional one-dimensional traces, and thus decrease the overall sensitivity of the experiment somewhat.

Even though we determined both ^{1}H-{^{13}C} and the ^{13}C-{^{1}H} spectra, either one is sufficient to reconstruct the ^{1}H-^{13}C chemical shift correlations. Comparing the spectra from Figures 5.2 and 5.5, the signal-to-noise ratio of an individual trace of the ^{1}H-{^{13}C} and the ^{13}C-{^{1}H} experiment is comparable under the experimental conditions used. The latter, however, has the advantage that (1) it enables at the same time the observation of the chemical shifts of carbons without attached protons, and (2) signal overlap is reduced due to the larger chemical shift range.

A major advantage of this method over other techniques of NMR spectroscopy with hyperpolarized samples lies in its robustness and ease of implementation. For this

reason, the presented technique seems to lend itself well for routine use in the identification and structure determination of compounds originating from organic synthesis, as well as for other applications to small molecules, where the obtainable sample quantity is severely limited.

CHAPTER VI

TEMPORAL CHEMICAL SHIFT CORRELATIONS*

In this section, DNP enhanced NMR is utilized to enable the measurement of temporal correlations. These correlations are valuable for the elucidation of reaction mechanisms as they permit direct connections between atoms in reactants and products. Despite the utility of these correlations, they are often difficult and/or costly to measure. In the absence of DNP, the only means to measure such correlations is to selectively isotopically label the starting material in a specific position. The transfer of the label from reactant to product can then be analyzed by conventional means. The utility of this method is however mitigated by the high cost of selective isotope labeling. Through the use of hyperpolarized sample and selective RF pulses, we can follow an atom of interest through the course of a reaction; thus providing a reliable and cost effective method capable of mapping atoms between reactant and product.

6.1 Introduction

Chemical structure and dynamics are routinely studied by nuclear magnetic resonance spectroscopy (NMR),[56] a major advantage of which is the availability of chemical shift. In single- or multidimensional NMR, chemical shift permits the resolution of individual atomic sites in a molecule. Moreover, much of the power of NMR derives from its capability to correlate the chemical shifts of atoms that are located close in space (nuclear Overhauser effect spectroscopy; NOESY) or that are linked

through chemical bonds (correlation spectroscopy; COSY). Such correlations are routinely used in the process of structural determination of molecules by NMR.[79] However, in contrast to other spectroscopic techniques a drawback of NMR is that in most cases it requires long experimental times to obtain a sufficiently high signal level or to record indirect spectral dimensions. For this reason, NMR is most typically applied to samples under equilibrium conditions.

Recent advances in NMR technology dramatically enhance the obtainable signal level by pre-polarizing nuclear spin systems prior to an NMR measurement. Ex-situ dynamic nuclear polarization (DNP) is a hyperpolarization technique, which can increase the liquid state NMR signal by several orders of magnitude in a single scan.[41] The availability of such a high signal level for one rapid scan suggests a powerful means of studying processes far from equilibrium. Using DNP polarized substrates, irreversible reactions can be followed in real time. Recently, for example, we have obtained time-resolved NMR data of an enzyme catalyzed reaction by this method.[52] Due to the signal increase provided by hyperpolarization, two-dimensional NMR spectra can also be measured within seconds or less, either in a single scan with gradient encoding,[70, 80] or using sequential scanning by means of small flip angle excitation.[61, 81]

By using real-time NMR for studying non-equilibrium processes, an additional type of chemical shift correlation becomes possible, namely the correlation of chemical shifts between a reactant and a reaction product, over the dimension of time. Because spin states can be preserved even if the spin carrying atoms undergo a chemical reaction, the different chemical shifts of such an atom in the reactant and the product molecule

can not only be observed, but a direct experimental correlation can be established between them. An existing NMR technique, termed “exchange spectroscopy”, exploits this property to study chemical exchange under equilibrium conditions.[82] Thereby, the chemical shifts of atoms in two conformations of a molecule are correlated if the molecule undergoes continuous chemical exchange between the two forms. For irreversible reactions, however, such correlations would only be available in a steady-state experiment if the reaction were studied under continuous flow conditions.[83] Hyperpolarization in conjunction with stopped-flow NMR[48] on the other hand allows a more powerful use of this mechanism, because it provides sufficient sensitivity for observation of a series of single transient ^{13}C spectra, at natural isotope abundance. Here, we show direct temporal correlations measured in real-time, from a single hyperpolarized sample on the example of an irreversible organic reaction, the Grignard addition of methylmagnesium bromide to 3-methylbenzophenone.[84]

6.2 Materials and Methods

For DNP polarization in non-polar organic solvents, the necessary concentration of unpaired electron spins can conveniently be provided by addition of the free radical α,γ-bisdiphenylene-β-phenylallyl (BDPA; Sigma Aldrich, St. Louis, MO).[85] The optimal microwave frequency for DNP polarization using BDPA was determined by recording a frequency dependent profile of polarization buildup using a ^{13}C solid state probe for the HyperSense DNP polarizer (Oxford Instruments, Tubney Woods, UK). A sample of 200 µl of 3-methylbenzophenone (Alfa Aesar, Ward Hill, MA) with 15 mM BDPA was irradiated with 60 mW of mm-wave power at frequencies ranging from 93.95 to 94.03

GHz in steps of 1 MHz, for 60 s per step. After each step, a single ^{13}C NMR spectrum of the solid sample was acquired, using a carrier frequency of 35.9037 MHz and a $\pi/2$ pulse length of 62 μs at 7.5 W forward power. Prior to the start of each polarization step, spins were saturated by a train of $\pi/4$ pulses. The acquired free induction decays (FIDs) were subsequently Fourier transformed in Matlab.

For the liquid state experiments, samples of 5 μl of neat 3-methylbenzophenone containing 15 mM BDPA were polarized using 60 mW of 93.965 GHz mm-wave power for 2 h. Samples were dissolved using 4 mL of tetrahydrofuran (THF; Malinckrodt Baker, Phillipsburg, NJ). The first 475 μL of this solution was injected into the NMR tube which already contained 25 μL of 3 M methylmagnesium bromide in diethyl ether (Strem Chemicals, Newburyport, MA) using a gas driven sample injector as previously described.[52] The injector applied 245 psi nitrogen gas pressure against a back-pressure of 150 psi for a duration of τ_i = 360 ms. The total transfer time of the sample from the point of dissolution to the point of NMR measurement was 2 s, and the mixing dead time was 200 ms. The effective dilution factor of the sample during the dissolution process was estimated by comparison with other samples to be 375×. This dilution yields a sample containing 15 mM 3-methylbenzophenone and 150 mM methylmagnesium bromide at the start of the NMR experiment. All reagents contained ^{13}C at the natural isotope abundance of 1.1 %.

The NMR experiment for determining temporal chemical shift correlations (Figure 6.1) was carried out using a Bruker 400 MHz spectrometer equipped with a broadband probe with actively shielded triple gradients. A data set consisted of n = 30

transients separated by 340 ms, started after an initial delay of τ_s = 400 ms. The total experimental time was 10.3 s. To equalize the signal from individual transients, a variable flip angle α_k was used for each excitation. The flip angles were calculated as described in[52] using a nominal $\pi/2$ pulse length of 10 μs.

The experiment in Figure 6.1 employs a selective inversion of the spin of interest prior to the first excitation. The inversion yields a negative signal in the subsequent spectra of the reactant, which is then transferred to the reaction product during the course of the experiment. For selective inversion, an adiabatic pulse p1 (flip angle π, hyperbolic secant shape with a truncation level of 1%, 10 ms duration, R=20 [*i.e.* 20 Hz sweep width at nominal 1 s duration]) was applied at the beginning of the pulse sequence followed by a pulsed field gradient $G_{1,x}$ = 50 G/cm.[86] The offset of this pulse was chosen to coincide with the chemical shift of the carbonyl carbon of 3-methylbenzophenone at 195.9 ppm. For each transient, 18432 complex points were recorded with a total acquisition time $t_{1,max}$ = 310 ms. During acquisition, broadband decoupling was applied on the ^{1}H channel using the WALTZ-16 scheme[87] at a field strength of γB_1 = 12 kHz. After the acquisition, remaining transverse magnetization was removed by application of a pulsed field gradient $G_{2,z}$ = (50 G/cm) so as to not interfere with the next acquisition.

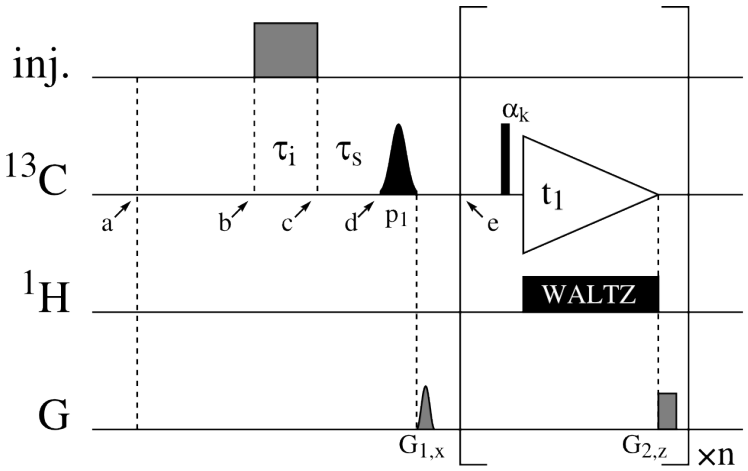

Figure 6.1. NMR pulse sequence for measuring temporal chemical shift correlations in reactions of hyperpolarized sample. Acquisition parameters are given in the text.

6.3 Results and Discussion

Dynamic Nuclear Polarization (DNP) operates by transferring polarization from highly polarizable electron spins to nuclear spins. In the present "ex-situ" experiments, samples were polarized in the solid state at a temperature of 1.3 K and subsequently dissolved into a dissolution solvent for NMR measurement. Efficient polarization in the solid state takes place only if electron spin carrying free radicals are interspersed with the sample molecules in a glass like aliquot.[41, 88] The choice of radical and solvent used for DNP polarization is an important determinant of the success of an experiment. In addition, when using the polarized aliquot as a component of a reaction to be observed by NMR, the additional components that are required for DNP polarization must also be compatible with the reaction conditions. In the present case, 3-methylbenzophenone was found to be self-glassing; it did not require an additional solvent for DNP polarization. Additionally, the free radical α,γ-bisdiphenylene-β-phenylallyl (BDPA) was found to be directly soluble in 3-methylbenzophenone.

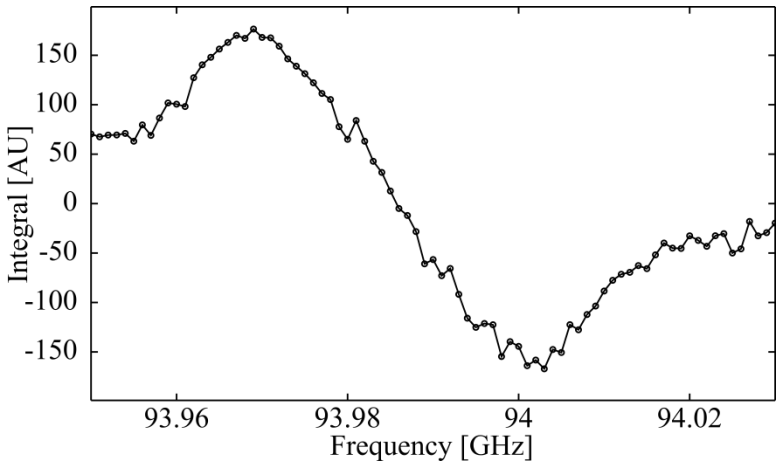

Figure 6.2. Solid state polarization efficiency (signal integral) as a function of frequency for the radical BDPA dissolved in 3-methylbenzophenone

Polarization conditions for the BDPA radical in 3-methylbenzophenone were determined as described above. The frequency dependence of the DNP enhancement of 3-methylbenzophenone containing 15 mM BDPA is shown in Figure 6.2. Maximum enhancements were found to lie at frequencies of 93.969 GHz and 94.003 GHz, with a center frequency ν_0 = 93.986 GHz. For purposes of identification of the prevalent DNP mechanism, the following values are of interest: ν_0-ν_C = 93.950 GHz, and ν_0+ν_C = 94.022 GHz, where ν_C = 35.9037 MHz is the ^{13}C NMR frequency in the 3.35 T field of the DNP polarizer. In the case of a predominant contribution from the solid effect, the positive and negative enhancement maxima would lie at the above calculated values and therefore be separated by two times the NMR frequency; however, contributions from thermal mixing will reduce the separation. As may be expected, the mechanism of polarization under these conditions appears to contain a significant contribution from the thermal mixing effect.[89]

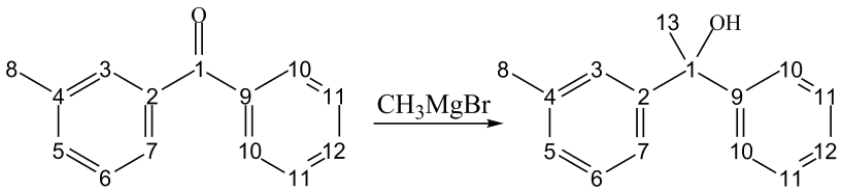

Figure 6.3. Scheme for the Gringard addition, where 15 mM of DNP polarized 3-methylbenzophenone was reacted with 150 mM of methylmagnesium bromide.

The key advantage of ex-situ DNP, however, is that the polarized sample can be dissolved after the polarization process has been completed in the solid state, and the NMR experiments can be carried out in the liquid state. In the context of the present experiments, the high signal obtained from hyperpolarization enables the rapid acquisition of a succession of single-scan ^{13}C NMR spectra, at natural isotope abundance, from a substance that undergoes an irreversible chemical change. Recently, we have reported real-time DNP-NMR spectra of an enzyme catalyzed reaction obtained in this way. A specially constructed sample injection system was used for rapid mixing of the DNP polarized substance with a second, non-polarized reactant.[52] The same technique is well suited for the determination of kinetics and mechanisms in many chemical transformations, also including organic or organometallic reactions. An example of such a reaction, the Grignard addition of methylmagnesium bromide to 3-methylbenzophenone, was selected as a model system for the present work (Figure 6.3). In the course of this reaction, three carbon atoms experience dramatic changes in chemical shift. Namely, the quaternary carbon in the center of the molecule (#1 in Figure 6.3) experiences a change $\Delta\delta[^{13}C] = -120$ ppm, and the quaternary aromatic carbons (#2 and #9 in Figure 6.3) experience a change $\Delta\delta[^{13}C] = 15$ ppm (see supplementary

materials for spectra and chemical shift assignments of the reactant and the product species).

Time resolved DNP-NMR as described previously is capable of showing the resonances of reaction product that appear with time, and allows for example the determination of kinetic parameters.[52] *A priori,* such an NMR experiment cannot be used to determine the identity of the atoms giving rise to those chemical shifts. However, using the pulse sequence in Figure 6.1, which in addition selectively inverts the signal of a spin of interest; it is possible to establish a direct temporal correlation between reactant and product. In the experiment shown in Figure 6.4, the resonance of the carbonyl carbon atom in the hyperpolarized 3-methylbenzophenone reactant at 195.9 ppm (marked #1 in Figure 6.3) was inverted after admixing of the non-polarized methylmagnesium bromide reaction component. As can be seen in Figure 6.4, the signal from this carbon atom remains negative throughout the reaction. More importantly, the appearance of a negative product signal at 77 ppm (#1') after a few seconds indicates that this resonance in the product species arises from the carbonyl carbon atom (#1) in the reactant. This experiment therefore provides direct proof of the origin of that particular atom in the product. At the same time, the peaks from all of the other carbon atoms in the reactant and product molecules remain positive. Without prior knowledge of the reaction mechanism, this type of information cannot easily be obtained from a conventional NMR measurement at equilibrium, which is carried out after the reaction has completed. To yield the same information, a conventional experiment would require the use of a reactant that is selectively isotope enriched at the position of interest.[90]

Generally, the synthesis of a selectively labeled organic compound requires considerable effort and expense. Moreover, any molecule that has been produced with a selective label can only be used to probe the position of that particular label. On the other hand, if more information is required, the hyperpolarized ^{13}C-NMR experiment can be repeated under the same conditions, while choosing another ^{13}C spin in the molecule for selective inversion.

An expanded view of some peaks of interest in this experiment is shown in Figure 6.5. Because of the large chemical shift distribution of ^{13}C, most of the resonances of the reactant and product species can be individually resolved. The signal from the initially inverted peak (left panels) translates as a negative signal to the corresponding product resonance (right panel). The peaks from other spins in reactant and product (center panel) keep their positive intensities. The three distinct peaks in the right panel of Figure 6.5 further indicate that three forms of the product with similar chemical shift appear to build up. The appearance of these three distinct resonances could potentially be attributed to complexation of the reaction product under the given experimental conditions; however, this effect is currently under investigation.

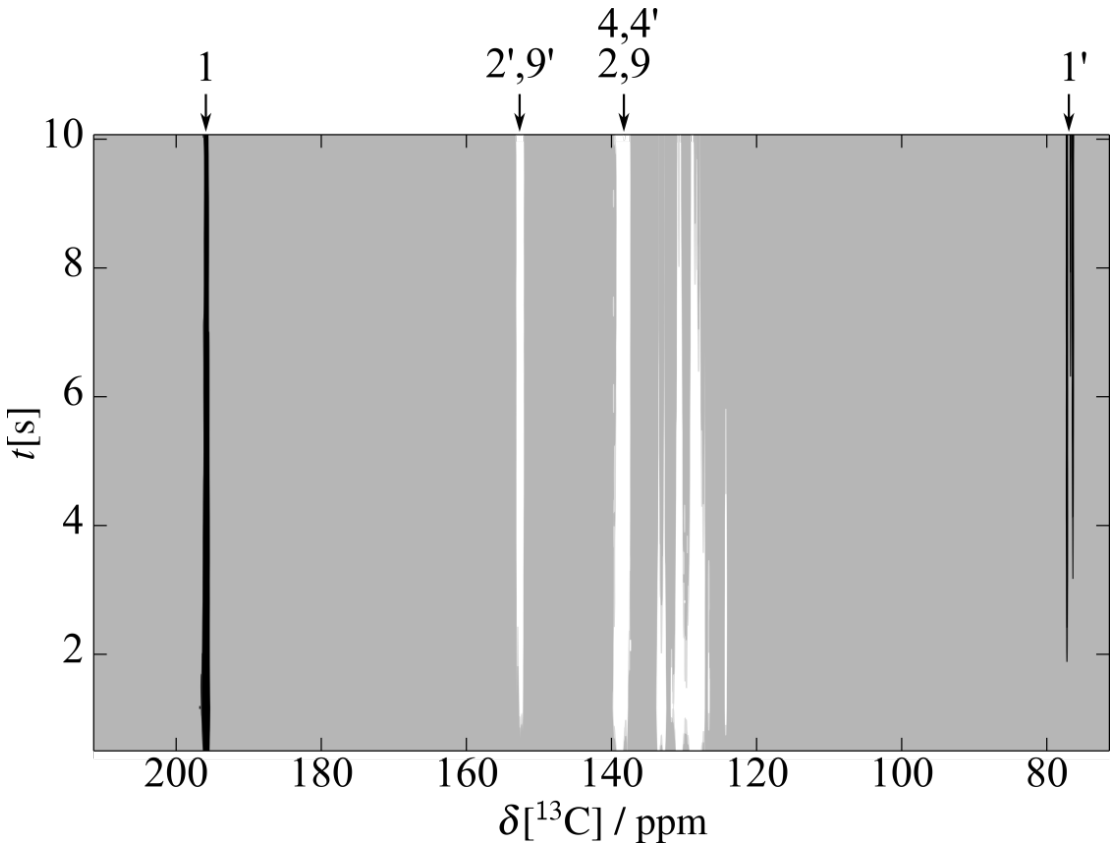

Figure 6.4. Correlation experiment showing chemical shift vs. time. Against a gray background, positive peaks are white and negative peaks are black. The atom numbers from Figure 6.3 that correspond to individually resolved peaks are indicated at the top. Initially inverted was the reactant resonance #1, which yields the product resonance #1' after the reaction. Also indicated are the non-inverted reactant and product resonances #2, 2', 4, 4', 9, and 9'.

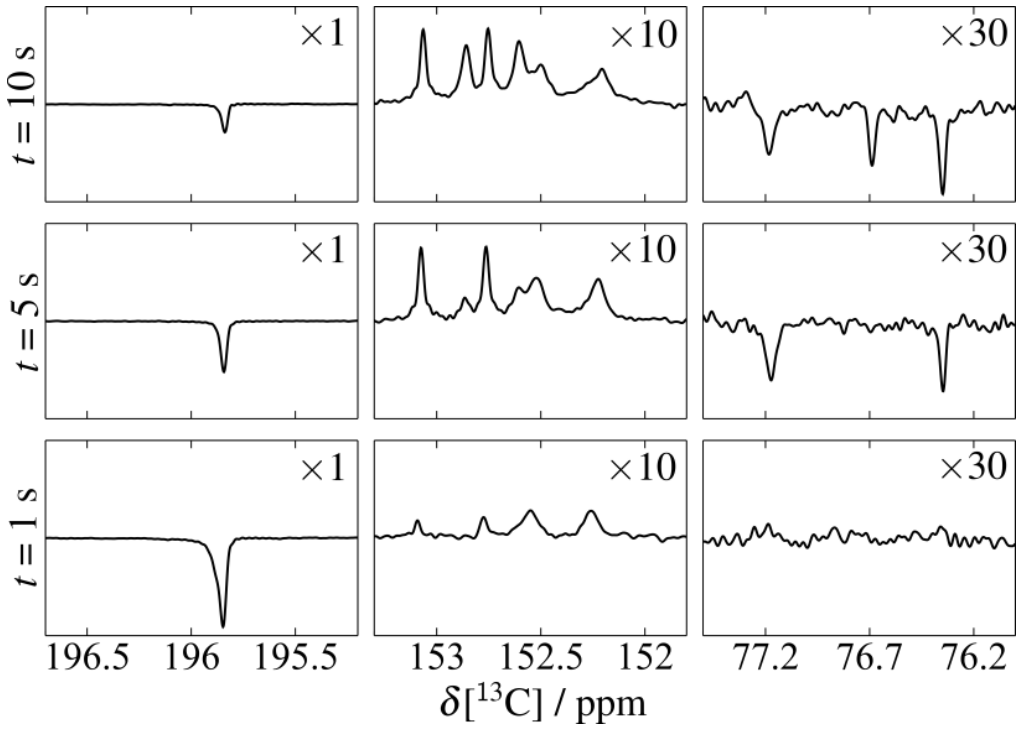

Figure 6.5. Expanded views of the temporal correlation experiment, for reaction times t=1 s, t=5 s and t=10 s on the vertical axis in Figure 6.4. Scaling factors that were applied to the individual traces are indicated.

Apart from providing increased sensitivity, which enables the observation of real-time ^{13}C NMR at natural isotope abundance, hyperpolarization has an additional important benefit for the temporal correlation experiment. Namely, with hyperpolarized sample the effect of relaxation is simply the disappearance of a resonance; the signal from the same spin system in thermal equilibrium is typically too weak to be observed under given experimental conditions. A NMR experiment of the type described here, but without hyperpolarization could yield a false result if a previously inverted spin relaxes back to yield a positive signal. In the hyperpolarized experiment, on the other hand, the loss of correlation due to relaxation merely manifests itself as a loss in signal, and not in the later appearance of a positive signal. This property ensures that from the

hyperpolarized experiment, the correct information is obtained from a peak as long as it is visible. The only remaining effect that needs to be considered is the possibility for transfer of magnetization due to cross-relaxation (NOE) between individual atomic sites in a molecule, which can potentially lead to undesired changes in signal intensity. As seen from the data in Figure 6.4 and Figure 6.5, cross relaxation in the present experiments however did not appear to give rise to a change in the peak intensities that would be detrimental to the experiment (a quantitative discussion of this effect will be published elsewhere).

The upper limit of the observable time window of this technique is given by the spin-lattice relaxation time of the polarized reactant. In our experience, a reasonable signal-to-noise ratio can be obtained for a reaction time of up to ca. 3 times the spin-lattice relaxation time, *i.e.* for seconds or tens of seconds. Clearly, the amount of signal depends on the concentration of the reactants, as well as on the amount of transients over which the signal is distributed. In the experiment presented in Figure 6.4, the concentration of reactant was relatively high (15 mM), and the signal could be distributed over 30 transients. It is, however, possible to use lower reactant concentrations. The present limit of detection is a 100 μM sample with ^{13}C at natural isotope abundance (1.1 μM ^{13}C), in which case however the number of transients may be reduced to 6. It would also be possible to obtain up to 90 times more signal by employing ^{13}C enriched substrate, if available. In the experiments presented here, we chose to polarize and detect carbon spins, which provides the advantage of the relatively large chemical shift dispersion of this nucleus. Individual peaks can be more readily

distinguished from each other, and the selective inversion is accomplished more easily. It is, however, also possible to polarize other nuclei, including for example protons.[81]

The lower limit of the observable time scale using the described method for sample injection and mixing is given by the mixing dead time, which is ca. 200 ms. By implementing a more rapid stopped-flow system,[65] this limit could however be reduced to the acquisition time required to obtain a NMR spectrum with sufficient resolution to distinguish chemical shifts, which could be as low as 10 ms.

The Grignard addition is an example of a reaction that is sensitive to both oxygen and water.[84] The DNP polarizer in conjunction with our rapid sample injection system provides an environment that is isolated from the atmosphere, and that can easily be purged with an inert gas prior to sample loading. During the experiment, the only gases with which the sample is in contact are helium and nitrogen. Dry, oxygen free conditions were confirmed by the absence of discoloration or precipitation of the methylmagnesium bromide. In a more general sense, reactions in a variety of solvent systems are amenable to this technique, as long as the solvent can safely be heated during the dissolution process. A non-exhaustive list of suitable solvents includes water, aqueous buffers, methanol, acetonitrile and toluene. Apart from the dissolution solvent, the conditions for the DNP polarization also need to be considered. In the present experiment, efficient polarization could be achieved by adding BDPA to the neat reactant. More generally, it may be necessary to mix the sample with a glass-forming solvent for DNP polarization.[41] For example when using an aqueous solution, the addition of ethylene glycol produces a glass-forming mixture. In this case, carbon spins in the solvent will

also be hyperpolarized and give rise to a strong NMR signal. Suppression of a solvent resonance may optionally be implemented by applying, after the initial inversion pulse, an additional $\pi/2$ pulse on the ^{13}C channel, followed by a pulsed field gradient.[52]

6.4 Conclusions

The temporal correlation experiment enables the direct observation of the transfer of an atom from reactant to product in an irreversible reaction. Using hyperpolarization, this transfer can be followed in real-time, and with sufficient sensitivity to allow ^{13}C spectroscopy at natural isotope abundance. The large chemical shift distribution of ^{13}C allows for the resolution of most atomic positions in a small organic molecule. The assignments of these chemical shifts in reactant and product may be obtained using conventional NMR spectroscopy under equilibrium conditions. Given this assignment, the ability to establish a direct correlation between the two states, using the experiment presented here, allows the determination of reaction mechanisms even if the identity of a transferred chemical group is ambiguous. Further, if a reaction passes through a transient intermediate that cannot be accessed by conventional NMR, a temporal chemical shift correlation will enable the assignment of resonances in the intermediate as well. The application of this experiment to multi-step reactions opens the possibility for an additional interesting variation. Namely, the inversion of a chemical shift does not necessarily need to be carried out immediately after mixing, but can take place at a later time and be targeted towards a chemical shift of an intermediate species. A succession of such experiments can potentially follow atoms through several reaction steps. Structure determination of intermediate forms may in addition be enabled by

modeling to NMR observable parameters including chemical shift and scalar coupling constants. These capabilities have the potential to provide insights into problems as varied as the stereospecificity of organic reactions, and the mechanisms of enzyme catalyzed reactions and of protein folding.

CHAPTER VII

ANALYSIS OF BIOSYNTHETIC PATHWAYS*

In this chapter, we detail the application of DNP enhanced NMR to the analysis of biosynthetic pathways. In this work, we have used the power of DNP to enable the acquisition of ^{13}C NMR spectra with excellent signal to noise. When combined with fractional isotope labeling techniques, it is possible to observe correlations that directly point to the biosynthetic pathways used to synthesize the molecule of interest.

7.1 Introduction

The synthesis of proteins and of ribonucleic acids in cells follows well established and highly conserved pathways. Biosynthesis of other, predominantly small molecules is more variable, and involves a large number of enzyme catalyzed reactions. These reactions are characterized in classical enzymology using a variety of approaches, including but not limited to isotope labeling or the use of suicide substrates. An array of techniques may be used for analyzing samples, such as chromatography, mass spectrometry, nuclear magnetic resonance (NMR) or fluorescence.[91-93] Of these, NMR is particularly informative due to its chemical shift resolution, which allows the identification of individual molecular species. NMR spectra can reveal further information about biosynthetic pathways, if samples are produced using fractional ^{13}C isotope labeling.[94-97] Such a labeling pattern is typically achieved by growing the source organism on a medium that contains a fraction of its carbon carrying feed compounds in

* Reprinted from "Rapid determination of biosynthetic pathways using fractional isotope enrichment and high-resolution dynamic nuclear polarization enhanced NMR" by Bowen, S.; Sekar, G.; Hilty, C, *NMR in Biomedicine* **2011**, Copyright 2011 by John Wiley & Sons.

fully or partially ^{13}C labeled form. Fragments that are incorporated into the biosynthetic product from the same feed molecule will then exhibit $^{13}C - ^{13}C$ spin coupling patterns, whereas fragments incorporated from two different feed molecules will show a statistical distribution of such couplings. Fractional isotope labeling is therefore a powerful tool aiding in the characterization of biosynthetic pathways.

An impediment for using NMR spectroscopy in such studies can be the relative insensitivity of the technique, which for ^{13}C spectroscopy is further compounded by the low gyromagnetic ratio and typically long relaxation time of carbon nuclei. This is especially true for biosynthetic compounds that are not readily available in large quantity. In the recent years, however, hyperpolarization techniques have been developed that are capable of significantly increasing the signal level in NMR spectroscopy. In particular, solid-to-liquid state dynamic nuclear polarization (DNP) has been shown to provide an increase in signal of up to 10^4 for ^{13}C spectroscopy of small molecules.[41] While a major thrust of this technique currently is towards metabolic imaging, high-resolution spectroscopy of DNP polarized biomolecules can provide important and complementary information.[49] DNP-NMR appears especially well suited for the analysis of a large variety of small-molecule biosynthetic products, since highly polarized NMR samples can typically be produced of small organic molecules. This capability further opens the possibility of studying the pathways leading to their synthesis, even if only small amounts of sample are available.

Here, we present a DNP-NMR study of membrane lipid biosynthesis in *E. coli*, using fractional isotope labeling. We compare the results to the known pathways for type

II fatty acid synthesis in this organism, characterize the incorporation preferences into various chemical groups in the presence of glucose and acetate feed molecule mixtures, and discuss the utility of this approach for the identification of characteristic metabolic "fingerprints" in biomedical science.

7.2 Experimental

7.2.1 Sample Preparation

Starter cultures of *E. coli* BL21(DE3) were grown overnight at 37 °C in 5 mL Luria Bertani (LB) medium. Cells were pelleted by centrifugation, washed (20 mM sodium phosphate, 150 mM NaCl, pH 6.8), and pelleted again. Cells were then resuspended in 200 mL minimal medium, and grown for 12-16 h to OD_{600} = 3 (in glucose medium) or for 24 h to OD_{600} = 1.5 (in acetate medium). Minimal medium was M9 buffered to pH 7, and supplemented with trace metals.[98] Minimal media contained a total of 3 g/L of ^{13}C labeled or unlabeled glucose and sodium acetate mixture. Sample 1 – 0.6 g $^{13}C_6$-glucose (Sigma-Aldrich, St. Louis, MO). Sample 2 – 0.06 g $^{13}C_6$-glucose, 0.54 g unlabeled glucose. Sample 3 – 0.06 g 1,2-$^{13}C_2$-sodium acetate (Cambridge Isotope Laboratories, Andover, MA), 0.54 g unlabeled glucose. Sample 4 – 0.06 g 1-^{13}C-sodium acetate, 0.54 g unlabeled glucose. Sample 5 – 0.06 g 2-^{13}C-sodium acetate, 0.54 g unlabeled glucose. Sample 6 – 0.06 g 1,2-$^{13}C_2$-sodium acetate, 0.54 g unlabeled sodium acetate. Sample 7 – 0.06 g 1-^{13}C-sodium acetate, 0.54 g unlabeled sodium acetate. Sample 8 – 0.06 g 2-^{13}C-sodium acetate, 0.54 g unlabeled sodium acetate. A control sample (Sample 9) was grown in 200 mL unlabeled LB medium.

Cells were harvested by centrifugation, and resuspended in 5 mL of 1 M sodium chloride and 18.75 mL 2:1 methanol / chloroform mixture. The cell suspension was shaken at 200 rpm and room temperature for 10 min; 6.25 mL chloroform was added and shaken for 1 min; 6.25 mL of 1 M NaCl was added and shaken for 1 min. The solution was centrifuged to separate the organic layer. The organic layer was washed with 1 M NaCl, separated again, and solvent was evaporated (modified from [99]). Transesterification was accomplished by dissolving lipids in 200 µL of toluene, adding 600 µL of 1 M of sodium methoxide in methanol and incubating for 20 min at 60 °C. 2 mL of water and 4 mL of pentane were subsequently added, the organic layer was separated by centrifugation, and the solvent was evaporated.

DNP samples of fatty acid esters were prepared by mixing 2.5 µL of ester with an equal amount of 1,2-dimethoxyethane, and α,γ-bisdiphenylene-β-phenylallyl free radical (BDPA; Sigma-Aldrich) to a final concentration of 15 mM.

7.2.2 DNP Polarization and NMR Spectroscopy

Samples were hyperpolarized on ^{13}C in a Hypersense DNP polarizer (Oxford Instruments, Tubney Woods, UK) for 4 h, at a temperature of 1.4 K, and under microwave irradiation of 60 mW at a frequency of 93.969 GHz. [41, 100] Polarized samples were dissolved into a stream of heated 1,2-dimethoxyethane, and taken up by a loop in a sample injector.[52, 101] The first 450 µL of sample solution was subsequently injected into a NMR tube already located in the NMR magnet, using a pressure of 1.69 MPa nitrogen gas, against a backpressure of 1.03 MPa. The NMR experiment was triggered 500 ms after sample injection, which corresponds to a total elapsed time of 1.8 s from sample

dissolution. ^{13}C NMR spectra were measured on a 400 MHz spectrometer (Bruker, Billerica, MA) equipped with a 5 mm broadband observe probe with three axis gradients. From each polarized sample, a single transient was acquired using the scheme $p_1 – G_x – p_2 – G_y – p_3 –$ acq. Solvent suppression was achieved by p_1 and p_2, which were selective EBURP $\pi/2$ pulses [102] of 25 ms duration, at the solvent resonances of 59 ppm and 75 ppm respectively. G_x and G_y were applied at 50 G/cm for 1 ms, with a sine bell shape. p_3 stands for a hard $\pi/2$ pulse, which was followed by a signal acquisition period of 2.2 s. During acquisition, protons were decoupled using WALTZ-16 [87] at a radio-frequency field strength of 12 kHz.

For the assignment of the fatty acid chemical shifts, a conventional correlation spectrum (COSY) was measured of a fully ^{13}C labeled sample. Chemical shifts were referenced to an internal standard of tetramethylsilane (TMS; Cambridge Isotope Laboratories). For the DNP-NMR experiments, a secondary standard of toluene was referenced against TMS.

7.3 Results and Discussion

Variability in membrane lipid structure is amplified combinatorially by joining instances from a set of head groups (primarily phosphatidyl ethanolamine, phosphatidyl glycerol and cardiolipin head groups) with fatty acid chains that can contain different structural features. For assessing the biosynthetic pathways leading to fatty acid synthesis, the presence of different head groups introduces unnecessary complexity. Therefore, head groups were removed by transesterification with methanol. An additional advantage of the transesterification process specifically for DNP-NMR is that

the product is a hydrophobic liquid, which after mixing with 1,2-dimethoxyethane is readily glass-forming. Depending on the application, a variety of methods for sample preparation could be also envisaged, including the use of unmodified lipids, or trans-esterification with other alcohols to introduce alternative functionality or avoid toxic products of hydrolysis.

Structural elements in fatty acid chains from *E. coli* include unsaturated carbon–carbon bonds and cyclopropyl groups [103-104]. Chain lengths are variable between 12 and 18 carbon atoms [105]. Fatty acid chains can also exhibit branch points; this feature is however not common for cells grown under the present conditions [106]. Figure 7.1 shows a DNP-NMR spectrum of 2.5 μL of the fatty acid extract (see Experimental section). Characteristic chemical shifts are readily observed for several carbon atoms at the chain ends, as well as for the unsaturated and for the cyclopropyl groups. As expected, the two carbon atoms forming an unsaturated bond are degenerate. The same is true for the carbon atoms in the middle of polymethylene stretches of the chain. From Figure 7.1, it can be seen that all expected peaks are observed in the hyperpolarized spectra. Although a larger amount of sample was prepared, the required amount of substance for measuring these spectra would be available from less than 50 mL unlabeled cell culture. Based on a comparison with conventional ^{13}C spectroscopy, the signal enhancement for the $^{13}C{=}O$ carbon atom (carbon 1) obtained due to DNP hyperpolarization, was estimated to be approximately 2000. A measurement on the model compound methyl linoleate in chloroform using conventional NMR indicated that the $^{13}C{=}O$ group exhibits a spin-lattice relaxation time of 20 s, while the aliphatic carbon atoms showed relaxation times

between 2 and 6 s. Rapid injection of the hyperpolarized sample into the NMR spectrometer is therefore of importance in order to obtain a high-quality spectrum of all of the carbon atoms in the compound.

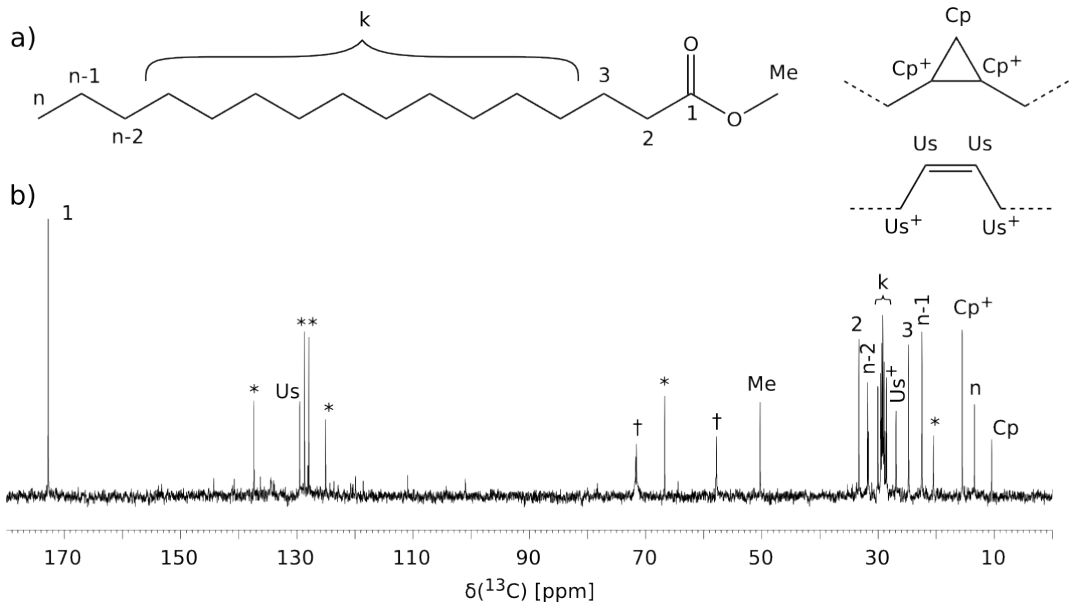

Figure 7.1. a) Representative structural features of fatty acids found in *E. coli* membrane lipids. The cyclopropyl and unsaturated groups on the right hand side may be substituted for two methylene carbons in the chain of the fatty acid. The methyl group (Me) is added by the transesterification process. b) DNP-NMR spectrum of the transesterification product from unlabeled lipid extract of *E. coli*. Numbers and letters indicate the assignment of peaks to the respective sites shown in (a). * are resonances from solvents (toluene and dioxane), † designates the residual signal from a resonance of the polarization solvent (1,2-dimethoxyethane), which was suppressed using selective pulses.

The information on the biosynthetic processes leading to the synthesis of the fatty acid chains is contained in the spectra of samples produced with fractional labeling [94-97]. As can be seen in Figure 7.2, the observed ^{13}C-^{13}C splitting patterns are strongly dependent on the type of label used. For example, for position 1 (carbonyl group), the fully labeled sample #1 shows a doublet due to coupling with the neighboring carbon 2. The same peak is present as a singlet in the unlabeled sample #9. In the presence of 10% (w/w) of fully ^{13}C labeled glucose (sample #2) or fully labeled acetate (sample #3) on an unlabeled background, predominantly the split peak is observed. This is in contrast to the a priori expectation that a ~10% random ^{13}C labeling should give rise to a peak pattern containing predominantly the central singlet peak.

The reason for the appearance of the observed pattern lies in the way that the fatty acids are synthesized by *E. coli*. The process of biosynthesis utilizes an enzyme catalyzed condensation reaction (Claisen condensation) of acyl-ACP with malonyl-ACP, which is synthesized from an acetyl coenzyme A precursor [107-108]. The carbon atoms in the acetyl moiety that is transferred originate from a single acetate molecule [109]. A scheme for this process is drawn in Figure 7.3. After insertion of a new acetyl moiety at the site of the thioester, the β-keto group is reduced and subsequently dehydrated, leaving a trans unsaturated site. This site is either reduced, forming a saturated link, or is converted by allyl rearrangement into an adjacent cis unsaturated site [104]. This process is repeated until the final chain length is achieved.

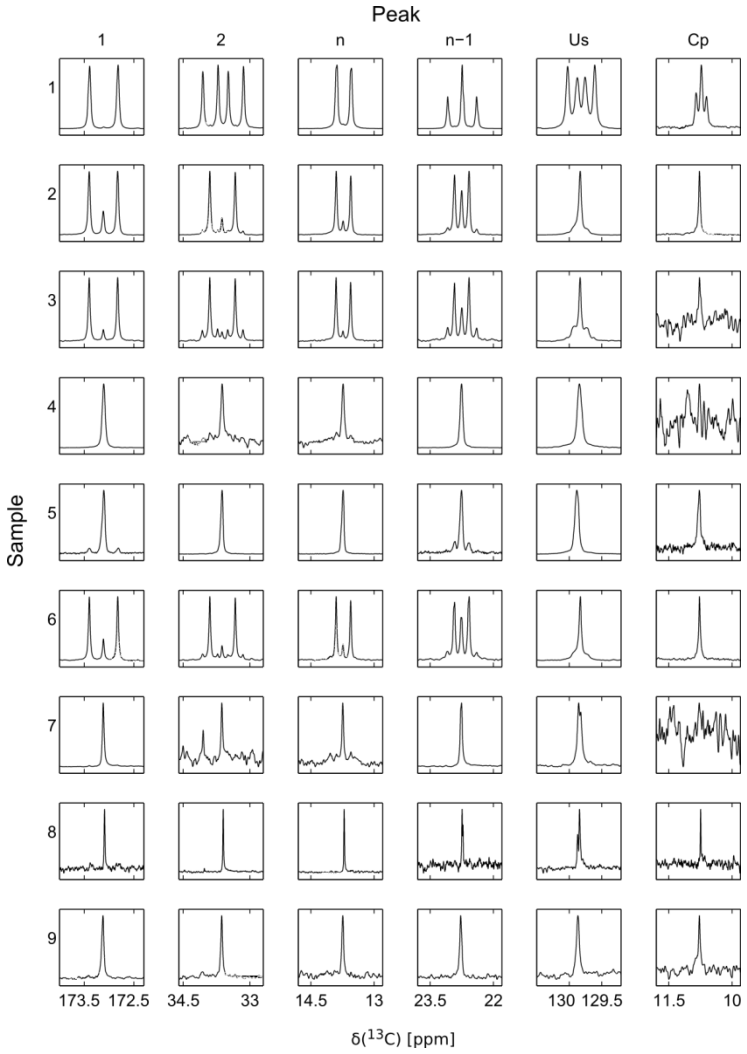

Figure 7.2. Peak multiplets due to scalar coupling in fractionally labeled samples of transesterified *E. coli* membrane lipids. The peak labels correspond to those used in Figure 7.1. The growth conditions are as follows: Sample 1 – 100% $^{13}C_6$-glucose. Sample 2 – 10% $^{13}C_6$-glucose, 90% unlabeled glucose. Sample 3 – 10% 1,2-$^{13}C_2$-sodium acetate, 90% unlabeled glucose. Sample 4 – 10% 1-^{13}C-sodium acetate, 90% unlabeled glucose. Sample 5 – 10% 2-^{13}C-sodium acetate, 90% unlabeled glucose. Sample 6 – 10% 1,2-$^{13}C_2$-sodium acetate, 90% unlabeled sodium acetate. Sample 7 – 10% 1-^{13}C-sodium acetate, 90% unlabeled sodium acetate. Sample 8 – 10% 2-^{13}C-sodium acetate, 90% unlabeled sodium acetate. Sample 9 – unlabeled. Samples 1 – 8 were grown in minimal medium. Sample 9 was grown in LB medium. Spectra in each panel are scaled vertically to fit the available space.

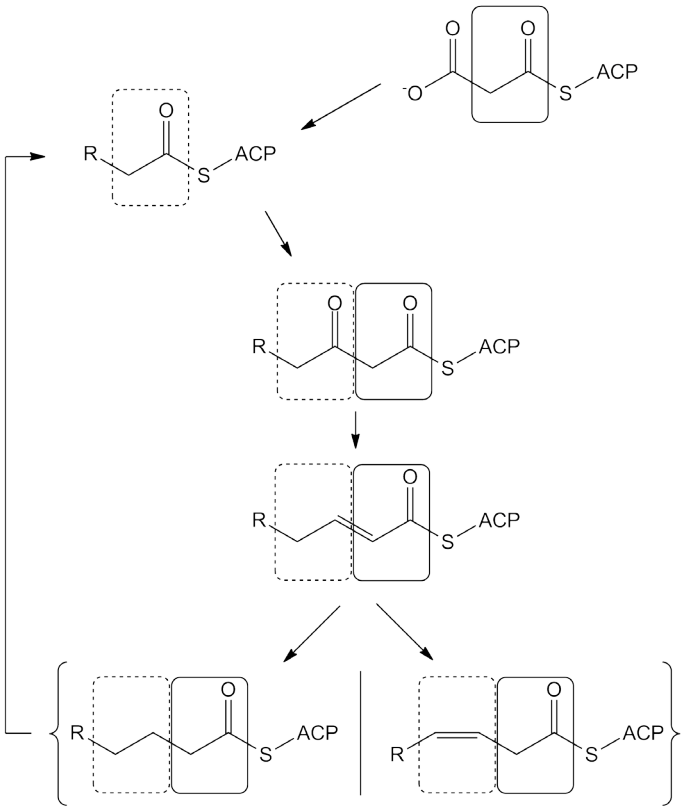

Figure 7.3. Simplified scheme illustrating a part of the fatty acid synthesis pathway in *E. coli*. The rectangular boxes designate moieties that originate from a single acetate molecule. ACP stands for acyl carrier protein. The last step of the cycle accounts for the formation of a saturated linkage (left branch) or unsaturated linkage (right branch).

The boxes in Figure 7.3 highlight those carbon atoms, which are incorporated from one acetate molecule. Since 1,2-^{13}C acetate feed molecules give rise to a significantly higher signal than the unlabeled molecules at 1.1% natural abundance of ^{13}C, in the case of sample #3 most of the fatty acid molecules containing ^{13}C in position 1 also contain ^{13}C in position 2, giving rise to the split peak. Considering that the acetyl coenzyme A precursor is also produced from a single molecule of glucose by decarboxylation of pyruvate emerging from the glycolysis pathway [110], a similar pattern is observed for sample #2. Expected peak intensities can easily be calculated by

assuming random incorporation of the different feed molecules present in the media. The DNP-NMR spectra may not be quantitative in their relative signal intensities due to differences in the polarization process for different chemical groups, as well as due to different losses that occur during dissolution and sample transfer. In fact, in contrast to conventional ^{13}C NMR, where spins with short relaxation time typically give the highest signal, in DNP-NMR spectra, the highest signal is often obtained from peaks with long relaxation times. For these reasons, the ^{13}C spectra do not lend themselves easily to direct comparison with calculated intensities. However, it appears reasonable to compare the intensities of multiplets from the same site in the molecule. Such a comparison is straightforward in the case, where a carbon atom is coupled to only one other carbon atom, as is the case for positions 1 (carboxyl group) and n (methyl group). Table 7.1 shows the calculated and observed fractions of doublet peak intensity r_{calc} and r_{obs} for these carbon atoms, according to

$$r = \frac{I_d}{I_d + I_s} \tag{7.1}$$

In this equation, I_d is the integrated intensity of both peaks from the doublet combined, and I_s is the integrated singlet peak intensity. The values have been calculated from the known weight of labeled and unlabeled glucose and acetate feed molecules that were added to the growth medium. For unlabeled sites in the molecules, a random ^{13}C isotope incorporation of 1.1% was assumed, and for the labeled sites an incorporation level of 99% was used. Even though the weight percentage of labeled feed molecules is always 10%, glucose and acetate molecules contain a slightly different amount of carbon

per molecular weight unit. Therefore, the calculated percentages for isotope incorporation, and consequently the r_{calc} values, are not exactly the same for all samples. It can be seen that the observed fraction of doublet intensity for carbons at position 1 and n is in the case of growth media containing only one chemical species as feed molecule (sample 2 for glucose and sample 6 for acetate) are, as expected, approximately equal to the calculated ratio. It should be noted that any recombination of feed molecules in the metabolic pathway ("scrambling") would lower this ratio. Interestingly, the sample using 10% 1,2-$^{13}C_2$-sodium acetate in 90% unlabeled glucose (sample #3) shows a doublet peak intensity that is significantly higher than expected ($r_{obs} > r_{calc}$). The likely reason is that the (labeled) acetate feed molecule is more readily available than glucose for incorporation into malonyl-ACP, the precursor for lipid biosynthesis.

The same considerations apply to the carbon atoms at position 2 and n-1. These atoms are coupled to carbon atoms at positions 1 or n, respectively, which gives rise to the same splitting patterns. In the fully labeled sample #1, it can be seen that these atoms are also coupled to their other respective neighbors at positions 3 of n-2. In all of the fractionally labeled samples, however, the effect of this coupling is quite small, since carbon atoms at positions 2 and 3, as well as carbon atoms at positions n-1 and n-2 are not incorporated from the same acetate molecule, and therefore are not expected to show a correlation in their labeling. For this reason, the peak pattern for the carbon atom at position 2 is similar to the pattern for carbon at position 1, and the pattern for position n-1 is similar to the pattern for position n in the fractionally labeled samples.

Table 7.1. Calculated and observed fractions of signal in the doublet peak for carbon positions 1 (carboxyl group) and n (methyl group). The accuracy of the small ratio indicated by the ~ sign is limited by the signal-to-noise ratio. The calculation is based on the assumption of random inclusion of the different feed molecules (see text).

Labeled Component	Unlabeled Component	Sample #	r_{calc}	r_{obs} (position 1)	r_{obs} (position n)
10% $^{13}C_6$-glucose	90% glucose	2	0.90	0.85	0.92
10% 1,2-$^{13}C_2$-sodium acetate	90% glucose	3	0.87	0.93	0.95
10% 1-^{13}C-sodium acetate	90% glucose	4	0.011	-	-
10% 2-^{13}C-sodium acetate	90% glucose	5	0.084	0.09	-
10% 1,2-$^{13}C_2$-sodium acetate	90 % sodium acetate	6	0.90	0.86	0.92
10% 1-^{13}C-sodium acetate	90 % sodium acetate	7	0.011	-	-
10% 2-^{13}C-sodium acetate	90 % sodium acetate	8	0.11	~0.16	-

It may be of further interest to consider the other, less abundant structural features of the *E. coli* fatty acids, namely the unsaturated group and the cyclopropyl group. From Figure 7.2, it can be seen that for all labeling conditions, predominantly a single peak without splitting is observed for position Us. In the synthesis pathway for an unsaturated fatty acid, the allyl rearrangement leaves a cis unsaturated site, which is not further reduced (lower right part of Figure 7.3), yielding an unsaturated final product. Because the position of the double bond changes during the rearrangement reaction [104], both of the carbon atoms in the bond originate from the same acetate molecule, whereas their neighbors originate from different molecules. Therefore, there is no correlation between the labels on the unsaturated carbon atoms and their neighbors, and indeed only one peak is expected.

The cyclopropyl ring can be formed from an unsaturated site after the fatty acid chain has been attached to a head group. This process requires the addition of a carbon atom, which is derived from the methyl group of S-adenosyl methionine.[103] The isotope labeling probability for this atom is not correlated in any way to the atoms from the unsaturated bond; therefore, the peak at position Cp appears as a singlet in all of the partially labeled samples. Except for the sample grown in LB medium, the intensity of this peak is generally low. This may indicate that the cyclopropyl species is not favored under the growth conditions in minimal medium. The minimal medium was buffered at pH 7, whereas cyclopropyl groups often appear in response to stress induced by low pH. [111]

From Figure 7.2, it can further be noted that the peak corresponding to the cyclopropyl group is entirely absent in samples #4 and #7. These are the two samples that contain acetate, which is not labeled in the carbon 2 position. This observation may indicate a preference for the methyl group of acetate in the biosynthesis of methionine, which is the precursor of the carbon atom in question in the cyclopropyl group. Interestingly, the biosynthetic origin of the methyl group of methionine can be traced to the carbon 2 of acetate via a pathway including gluconeogenesis followed by serine biosynthesis. The β-methylene group of serine, which originates from the carbon 2 position of acetate, is subsequently transferred to tetrahydrofolate, which is the methyl donor in the production of methionine [112]. This result illustrates that through highly sensitive DNP-NMR spectroscopy, the origin of individual functional groups may be traced through large biosynthetic networks. In a broader context, it would also be

possible to use auxotrophic cell lines, which are deficient in a metabolic pathway, for monitoring such networks in further detail.

7.4 Conclusions

The discussed structural features of fatty acid chains among others change the melting temperature of the lipid mixture, and contribute to membrane fluidity [103, 113-114]. For *E. coli*, variation of these properties allow for tuning in response to stress and nutrient availability. More generally, lipid fingerprinting is commonly used to identify bacterial species.[115] We have shown that DNP-NMR data of fractionally labeled fatty acid extracts can be used to explain in detail their biosynthetic pathway. Even though labeling in general imparts an increase in sensitivity, in the case of fractional labeling for the determination of metabolic pathways, this is not strictly true. In order to gain information on the origin of neighboring atoms in the biosynthetic product, it is also necessary to observe the minor multiplets of the peaks, which may be present only at the level of natural ^{13}C abundance. DNP-NMR is particularly well suited for obtaining highly sensitive spectra of small amounts of substance, or for locating minor components in a sample. This technique therefore presents an opportunity for the rapid determination of metabolic pathways, even if it is difficult to obtain large amounts of substance.

CHAPTER VIII

STUDY OF URONATE ISOMERASE CATALYZED CONVERSION OF GLUCURONATE TO FRUCTURONATE

This chapter details a case study for the application of our DNP-NMR methods for real-time analysis of chemical reactions. The reaction is non-chromogenic and is not amenable to ^{1}H NMR analysis due to spectral crowding. Furthermore, concomitant mutarotation processes for both reactant and product mask data regarding anomeric specificity.

8.1 Introduction

The enzyme uronate isomerase (URI) catalyzes the isomerization of D-glucuronate into D-fructuronate as shown in Figure 8.1. This process serves as the first step in glucuronate metabolism which leads into the glycolysis and the citric acid cycle. Overall kinetics for this reaction have previously been characterized by a coupled assay involving the NADH dependent enzyme mannonate dehydrogenase.[116]

Mechanistically, it has been determined that the enzyme binds the open form of glucuronate, abstracts a proton from C_2 and proceeds through a cis-enediol mechanism. The mechanism is supported by X-ray structures of the enzyme bound to D-glucuronate, D-fructuronate and mimics of the cis-enediol intermediate. Additionally, the proton exchange with solvent has been studied with NMR by incubating glucuronate with URI in D_2O and observing the loss of intensity of the proton bound to C_2. It was found that the proton exchange rate is four orders of magnitude slower than the turnover rate,

indicating that the proton removed from the substrate is not well exposed to the solvent.[117-118]

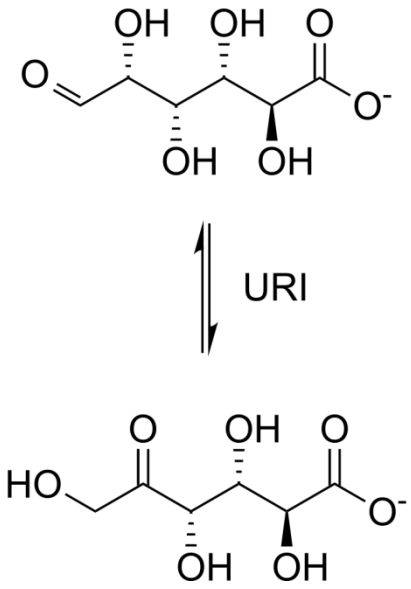

Figure 8.1. Uronate isomerase catalyzed conversion of D-glucuronate into D-fructuronate.

While the mechanism has been characterized, knowledge of the mechanism does not automatically entail knowledge of the kinetics. Specifically, the coupled assay utilized in previous studies is unable to resolve different forms of the substrate. Because of this, we desire to design a real-time assay capable of probing the reaction kinetics and mechanism. This requires the ability to rapidly acquire site-specific information about the species involved in the reaction. It must also be capable of operating without additional reactions which may complicate the process by imparting their own kinetics on the overall process.

Enzyme activity assays are often used to probe the kinetics of enzyme catalyzed reactions. As spectrophotometric detection is the most amenable to real-time detection, it is commonly the detection technique of choice. However, many substrates do not absorb ultraviolet or visible light, or there is no change in absorption properties between reactant and product. Furthermore, the absorption spectrum of the substrate may overlap with the enzyme or other substances required for the reaction. To overcome these issues, enzymatic assays are often coupled to other chromogenic reactions. Often nicotinamide adenine dinucleotide (NAD^+ / NADH) dependent enzymes are used in the coupled reaction with NAD^+ and NADH as the chromogenic pair.[119]

While this approach is effective in terms of making the reaction amenable to optical detection, it has the potential to alter the reaction kinetics. In the case of coupled enzyme assays, it is possible to analyze the kinetic behavior of the coupled system[120-121]; however, it is not possible to observe transient species or examine differential behavior with multiple substrates.

Nuclear magnetic resonance (NMR) has properties of an ideal detection method for enzyme catalyzed reactions. In combination with DNP, it is possible to obtain high quality ^{13}C NMR spectra in real time. We have previously shown the applicability of DNP enhanced NMR for the kinetic analysis of enzyme catalyzed reactions[52], as well as mechanistic analysis through the measurement of temporal correlations[100]. As the uronate isomerase reaction is non-chromogenic, DNP-NMR offers a means to study the reaction in real time, while taking advantage of the site-specific information delivered by NMR to make both mechanistic and kinetic observations simultaneously.

As the uronate isomerase catalyzed isomerization reaction occurs concomitantly with process of anomerization of both reactant and product; it is necessary to consider both α and β anomers of the glucuronate and fructuronate. NMR is one of the few methods able to discern the anomers even in the presence of glucuronate and fructuronate. Because of this, NMR is well suited to the analysis of the differential kinetics for the two anomers. For the related enzyme phosphoglucose isomerase, the anomeric specificity of the enzyme was probed using conventional NMR techniques.[122-123] However analogous measurements with uronate isomerase have proven unfeasible by conventional NMR techniques.[124]

8.2 Experimental Section

8.2.1 Sample Preparation

Uronate isomerase was recombinantly expressed in *E. coli* as described in [118]. sodium D-glucuronate (Alfa Aesar, Ward Hill, PA) was commercially obtained and used without further purification. Samples for DNP polarization containing the equilibrium mixture of α- and β-glucuronate were prepared using 10 μL of 2 M sodium D-glucuronate solution in D_2O mixed with 10 μL of 30 mM free radical (OX63, Oxford Instruments, Tubney Woods, UK), and 2 mM Gd(DTPA) (Sigma Aldrich, St. Louis, MO) in ethylene glycol. The final sample of 20 μL contained 1 M sodium D-glucuronate, 15 mM OX63, and 1 mM Gd(DTPA) in 50% D_2O / 50% ethylene glycol mixture (v/v). The sodium D-glucuronate solution was allowed to equilibrate for at least 24 hours so that its anomeric forms reached equilibrium.

In order to validate the choice of ethylene glycol as a glassing agent, alternate samples were prepared using dimethyl sulfoxide-d6 (DMSO-d6) as a glassing agent. Samples were prepared in an analogous fashion to the description above, but had a final solvent composition of 60% D_2O / 40% DMSO-d6 (v/v).

10% ^{13}C samples: sodium U-10% ^{13}C D-glucuronate was synthesized by the Raushel lab from U-10% ^{13}C D-glucose as previously described. Samples were prepared in an analogous fashion to the equilibrium samples in ethylene glycol.

Samples containing primarily β-D-glucuronate were prepared from sodium D-glucuronate that had previously been recrystallized. 10 μL of freshly made 2 M sodium D-glucuronate solution in D_2O was mixed with 10 μL of 30 mM OX63 free radical, and 2 mM Gd(DTPA) in ethylene glycol. The final sample of 20 μL contained 1 M sodium D-glucuronate, 15 mM OX63, and 1 mM Gd(DTPA) in 50% D_2O / 50% ethylene glycol (v/v).

8.2.2 Hyperpolarization and NMR Spectroscopy

Samples were hyperpolarized at a temperature of 1.4 K, by irradiation with microwaves of frequency 94.976 GHz and 60 mW power, for a duration of 3 h. Hyperpolarized samples were dissolved into heated 50 mM potassium phosphate, 50 mM “substoichiometric” potassium borate, or 500 mM “superstoichiometric” potassium borate buffer at pH 8.0 in H_2O, and injected into the NMR spectrometer using a home-built injection system[101]. The time from dissolution to NMR measurement was less than 2 s. For experiments involving enzyme catalysis, 20 μL of a solution of 0.1-0.5 mM

uronate isomerase in 4-(2-hydroxyethyl)-1-piperazineethanesulfonic acid (HEPES) buffer, was preloaded in the NMR tube prior to sample injection, and mixed with the hyperpolarized sample upon injection. In different experiments, final sample concentrations ranged between 10 mM and 20 mM glucuronate, and between 5-25 μM uronate isomerase. For experiments conducted without enzyme catalysis, 20 μL of dissolution buffer was preloaded in the NMR tube prior to sample injection. This ensured that the dilution and mixing of all samples was identical.

DNP-NMR spectra were measured on a 400 MHz spectrometer (Bruker, Billerica, MA) equipped with a broadband observation probe with actively shielded triple axis gradients. The NMR experiment for measurement of a time series consists of a selective $\pi/2$ pulse applied to the glassing solvent followed by a pulsed field gradient (PFG), and a series of variable flip angle scans. A PFG was applied after each scan to suppress any remaining transverse magnetization. Selective inversion experiments were measured with the addition of a selective π pulse between the solvent suppression and acquisition phases. Concentrations measured by integration of the ^{1}H NMR spectrum of each sample and comparison to a standard reference sample.

8.2.3 Data Processing

DNP-NMR spectra were Fourier transformed and integrated using MATLAB (Mathworks, Natick, MA). Conventional NMR spectra were processed using TopSpin (Bruker, Billerica, MA).

8.2.4 Chemical Shift Assignments

For purposes of chemical shift assignment, conventional NMR spectra were measured at 298 K on a 500 MHz spectrometer (Bruker, Billerica, MA) equipped with a TCI cryoprobe with actively shielded Z-axis gradient. These included [^{1}H,^{1}H]-TOCSY, [^{1}H,^{1}H]-COSY, [^{13}C,^{1}H]-HSQC and [^{13}C,^{1}H]-HMBC spectra. The URI used to prepare samples containing fructuronate was thermally denatured by heating samples to 95 °C for 5 minutes. The precipitated URI was then removed by centrifugation prior to measurement.

In order to characterize the structure of the fructuronate-borate complex, a [^{1}H,^{1}H]-TOCSY spectrum was measured on the previously described 400 MHz NMR spectrometer at 243 K in 30% DMSO-d6 and 70% potassium borate buffer in H_2O at pH 8.0. As the low temperature reduced the OH proton exchange rate, it was possible to assign the location of the borate by observing which sites lacked OH protons. Chemical shifts were assigned from conventionally acquired one and two dimensional experiments.

8.3 Results and Discussion

The NMR spectra of the substrates and products of the uronate isomerase reaction are shown in Figure 8.2. Figure 8.2a contains the spectrum of glucuronate, in anomeric equilibrium. The spectrum in Figure 8.2b was measured with an equilibrium mixture of 40% fructuronate and 60% glucuronate as generated by uronate isomerase. In this spectrum it is possible to see both α and β anomers of glucuronate and fructuronate. While the reaction reaches equilibrium in phosphate buffer, it has been

shown that it proceeds fully towards fructuronate in borate buffer.[116] This is shown in Figure 8.2c. It is worth noting that the spectra in Figure 8.2b and Figure 8.2c differ, most conspicuously by the appearance of a resonance at 113 ppm. As these are conventional, thermally polarized spectra, species with extended T_1 times appear with reduced intensity due to incomplete relaxation between scans.

Figure 8.3 shows a hyperpolarized spectrum of glucuronate and fructuronate. In this case, the manifestation of relaxation is the opposite of the thermally polarized case. Resonances stemming from sites with long T_1 will appear more intense than those with short T_1. Hyperpolarization is necessary for studying the reaction as it is necessary to acquire a series of 12 ^{13}C spectra over the course of four seconds. With the concentrations used in this work, acquisition of even a single spectrum of comparable signal to noise would require signal averaging for weeks.

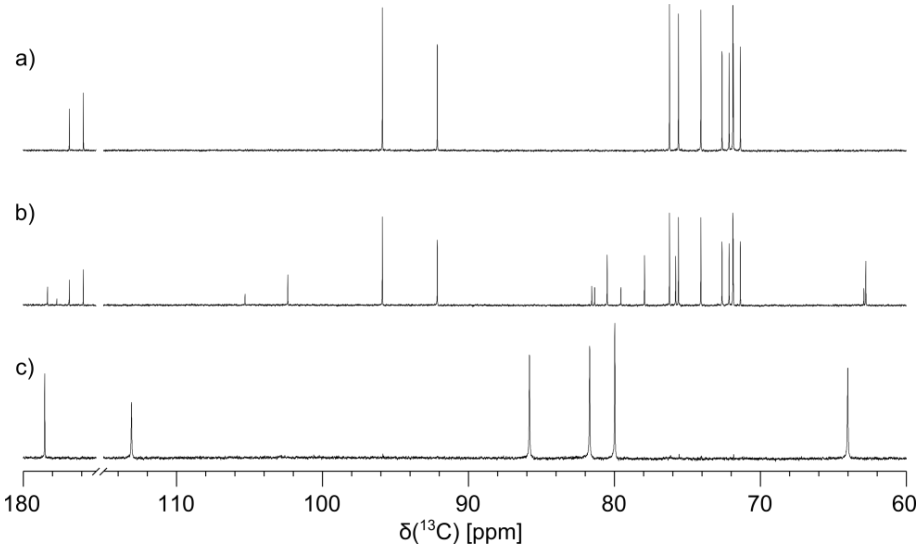

Figure 8.2. ^{13}C spectra of a) glucuronate in 50 mM phosphate buffer (pH 8.0), b) enzymatically prepared glucuronate/fructuronate mixture in 50 mM phosphate buffer (pH 8.0), c) enzymatically prepared fructuronate, in 500 mM borate buffer (pH 8.0).

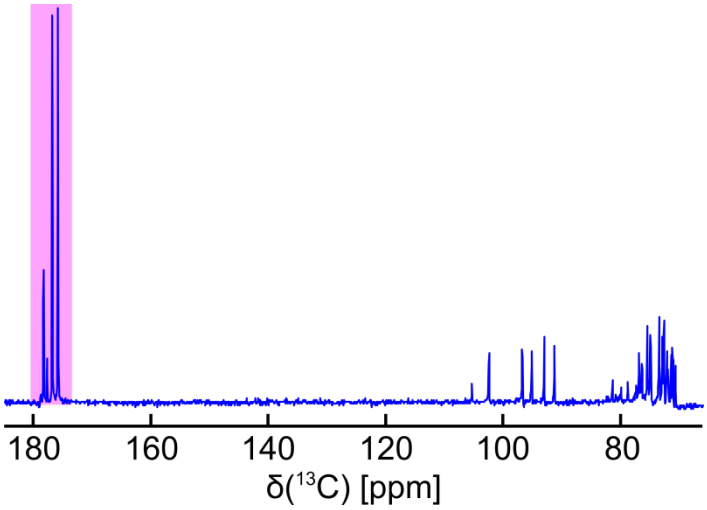

Figure 8.3. Hyperpolarized proton coupled ^{13}C NMR spectrum of glucuronate and fructuronate measured in phosphate buffer. This spectrum is the sum of 12 scans measured during the course of the URI catalyzed isomerization of glucuronate into fructuronate. The region containing carboxyl (C_6) resonances is highlighted.

As we desire to follow the progress of the reaction over time, it is beneficial to use resonances with long T_1 relaxation times and strong signal. The long T_1 relaxation time of these atoms ensures that minimal relaxation occurs during the course of the reaction. Minimizing relaxation is important both for preserving signal for later scans as well as simplifying the data analysis. These resonances also demonstrate good dispersion and are far from potential interferences such as the glassing solvent used for DNP polarization.

In Figure 8.4, the first 6 of a total of 12 scans acquired from the URI catalyzed isomerization of glucuronate into fructuronate. It is possible to see the disappearance of glucuronate with time as well as the appearance of product. In particular, two distinct product peaks are visible at 113 ppm and 178 ppm. These peaks are consistent with the thermal spectrum of fructuronate in borate presented in Figure 8.2c. It is evident that the

carboxyl resonances have the highest initial intensity and the lowest signal loss due to relaxation.

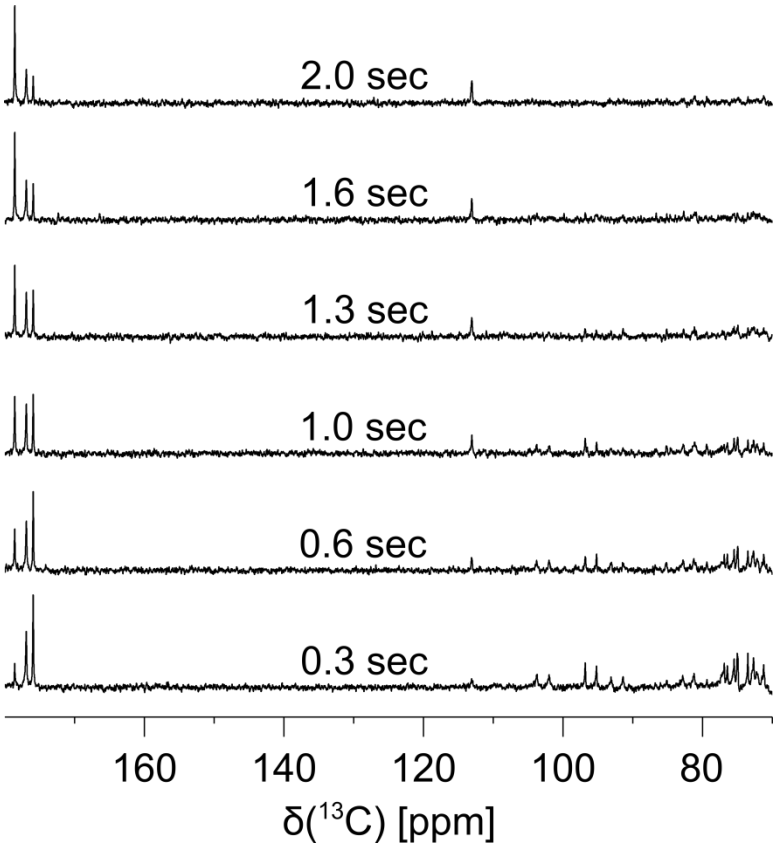

Figure 8.4. Series of time-resolved DNP-NMR spectra of the URI catalyzed isomerization of glucuronate into fructuronate measured in superstoichiometric borate buffer.

As a prerequisite to analyzing the mechanism of the reaction by DNP-NMR, it was necessary to assign the NMR spectra of each of the forms. Most assignments were easily obtained using conventional NMR techniques (see Materials and Methods). Because the reaction undergoes an equilibrium shift towards fructuronate and yields a different NMR spectrum in borate buffer; we aimed to characterize the species formed in borate. We used a hyperpolarized temporal correlation experiment (Chapter VI) to

determine the source of the resonance near 113 ppm that appears in borate buffer. Resonances belonging to different carbon atoms in β-D-glucuronate were selectively inverted. Only when the resonance corresponding to C_2 of β-D-glucuronate was selectively inverted, was it possible to observe the inversion of the resonance near 113 ppm; the results are shown in Figure 8.5. In all of the other experiments, no change was observed for the resonance at 113 ppm. This experiment was the only one to utilize uniformly 10% ^{13}C labeled substrate, which was required due to the low intensity of the inverted product resonances. The low intensity may be attributed to both short T_1 relaxation and the occurrence of the reaction before and during the selective RF inversion pulse. Based upon the temporal correlation experiment, it is possible to conclude that the resonance at 113 ppm is the atom in a reaction product, which corresponds to the C_2 resonance from β-D-glucuronate. It is also possible to see the anticipated correlation to β-D-fructuronate near 102 ppm. The spectrum further suggests that the resonance at 113 ppm may be a borate complex of fructuronate, as it is broadened considerably.[125]

The borate binding locations were verified using an [^1H,^1H]-TOCSY spectrum measured at -30 °C in a mixture of borate buffer and DMSO-d_6 as shown in Figure 8.6. At this low temperature, the OH exchange rate decreases to the point that the OH protons are visible on the NMR spectrum. While exchange in this regime is still rapid enough that the OH proton resonances are broadened, it is possible to measure correlation spectra. As cross peaks are observable between the CH and OH protons, it is clear that positions 1 and 4 have protonated OH groups and therefore are not bound to

borate. Consequently the borate must be bound to positions 2 and 3. Borate-sugar complexes are well known and quite stable.[125-126] Under the present conditions, this complex forms only with the beta form of fructuronate. As glucuronate overwhelmingly favors the pyranose form, neither anomer is able to form a stable complex.

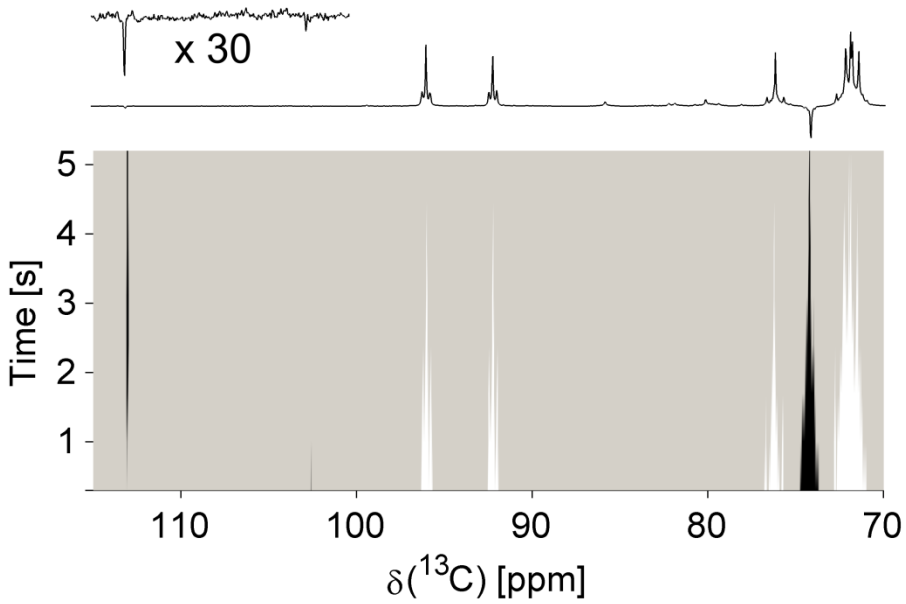

Figure 8.5. Correlation experiment showing chemical shift vs. time. Against a gray background, positive peaks are white and negative peaks are black. Initially inverted was the β-glucuronate C_2 resonance, which yields the β-fructuronate borate complex. A small amount of uncomplexed β-fructuronate is also visible.

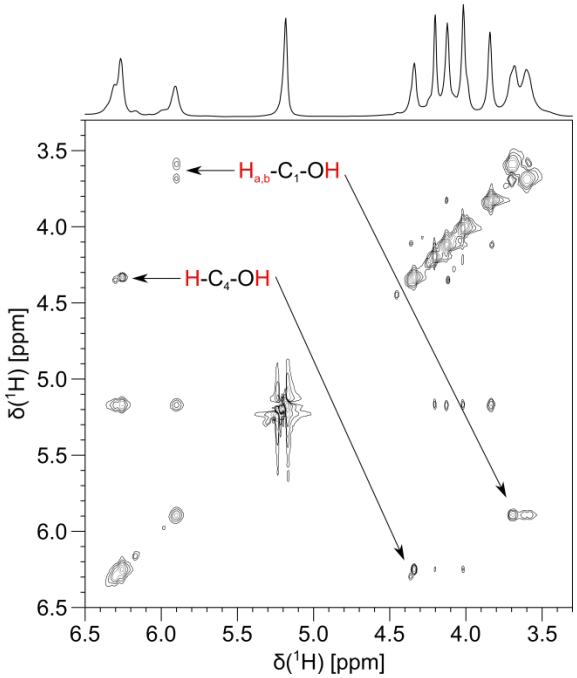

Figure 8.6. [^{1}H,^{1}H]-TOCSY spectrum of fructuronate-borate complex in 30% DMSO-d6 and 70% potassium borate buffer (pH 8.0), measured at -30 °C. Cross peaks between hydroxyl groups and C-H protons are indicated with arrows.

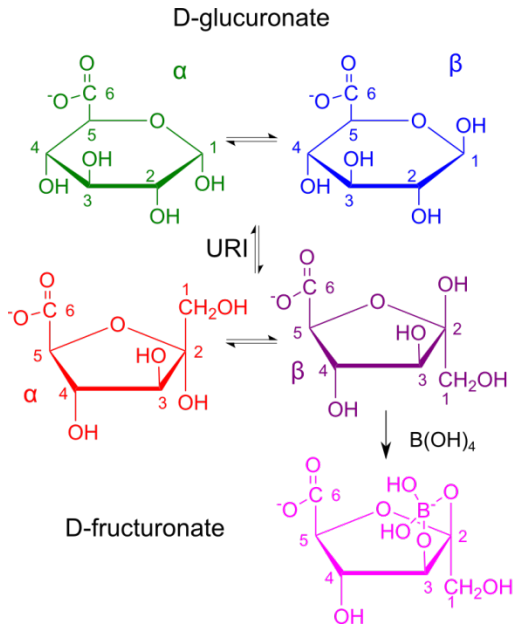

Figure 8.7. All observed forms of substrate and product for the uronate isomerase catalyzed reaction. Top row: D-glucuronate anomers, Middle row: D-fructuronate anomers, Bottom row: D-fructuronate borate complex.

The structures and chemical shifts of all species are summarized in Table 8.1. The reaction scheme containing the key forms and their structures is shown in Figure 8.7.

Table 8.1. NMR spectral parameters for glucuronate and fructuronate species involved in the reaction.

Compound	Atom	$\delta[^1H]$ (ppm)	$\delta[^{13}C]$ (ppm)	$^1J_{CH}$ (Hz)	J_{HH} (Hz)
α-D-Glucuronate 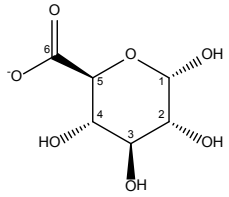	1	5.10	92.14	170.4	3.75 (d)
	2	3.43	71.37	145.1	3.83, 9.85 (dd)
	3	3.58	72.63	144.6	9.59 (t)
	4	3.35	72.15	145.6	9.61 (t)
	5	3.94	71.86	147.4	10.09 (d)
	6	-	176.84	-	-
β-D-Glucuronate 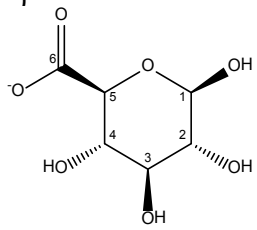	1	4.50	95.90	161.7	8.05 (d)
	2	3.15	74.08	144.5	7.88, 9.51 (dd)
	3	3.36	75.62	143.0	9.33 (t)
	4	3.37	71.89	146.4	9.67 (t)
	5	3.59	76.24	144.2	9.72 (d)
	6	-	175.88	-	-
α-D-Fructuronate 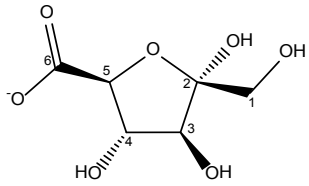	1	3.57	62.92	144.5	2.62 (d)
	2	-	105.32	-	-
	3	4.18	81.55	151.0	6.08 (d)
	4	4.03	79.57	149.8	4.65, 6.01 (dd)
	5	3.93	81.38	149.4	4.67 (d)
	6	-	177.71	-	-
β-D-Fructuronate 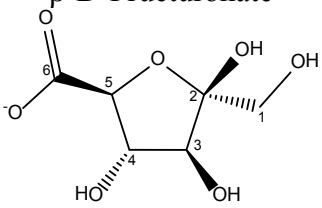	1	3.45	62.78	143.6	1.84 (d)
	2	-	102.39	-	-
	3	3.91	75.82	145.7	7.56 (d)
	4	4.14	77.95	147.8	7.55 (t)
	5	3.94	80.53	150.3	7.06 (d)
	6	-	178.34	-	-
β-D-Fructuronate Borate Complex 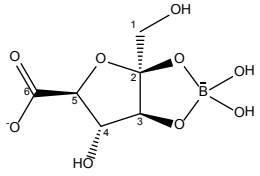	1	3.50, 3.55	64.07	144.3	11.96 (d)
	2	-	113.02	-	-
	3	3.93	81.76	153.2	1.03 (d)
	4	4.21	80.00	155.1	1.28 (t)
	5	4.12	85.80	148.9	1.42 (d)
	6	-	178.48	-	-

Apart from enabling the real-time observation of all species in the reaction, an additional benefit of DNP enhanced NMR is the ability to choose the degree of reversibility of the reaction. The kinetic behavior of the reaction was analyzed under reversible, semi-reversible, and fully reversible conditions. These conditions were generated through the use of phosphate, substoichiometric borate, and superstoichiometric borate buffers respectively. When using borate buffer, the high stability of the borate complex means that complexed molecules remain inaccessible to the URI. In the case of the phosphate buffer, the fructuronate product is fully uncomplexed and is free to undergo the reverse reaction. As the borate concentration is increased, the amount of complexed fructuronate also increases and the reaction is rendered increasingly irreversible. When the concentration of borate exceeds the amount of glucuronate/fructuronate, all of the fructuronate will be complexed and the reaction rendered irreversible. As it is also a vicinal diol, ethylene glycol which is used as a glassing agent in the hyperpolarized sample has the potential to form complexes with borate that would prevent borate from complexing fructuronate. To eliminate ethylene glycol as a source of error, DMSO was used as an alternative glassing agent and the results were found to be identical to those obtained with ethylene glycol. As ethylene glycol yields higher polarization with glucuronate samples, it was used for the data presented in this chapter.

Figure 8.8 shows the integrated signals from the time-course of the uronate isomerase catalyzed conversion of glucuronate into fructuronate. In these experiments, the glucuronate was at anomeric equilibrium prior to the experiment. The data in the

figure are presented as the fraction of the total signal. As we have verified that the polarization efficiencies and spin-lattice relaxation rates are similar for all forms, the signal fraction is approximating the mole fraction of species present. Additionally, we assume that the relaxation time constants are identical for the carboxyl carbons of all species; the procedure of calculating signal fraction simultaneously eliminates the effect of relaxation. Therefore, there is no need to directly compensate for it using data measured in the absence of enzyme.

Figure 8.8a shows the results obtained when measuring the reaction in phosphate buffer. In this reaction, consumption of α and β glucuronate is observable as is the formation of α and β fructuronate. In this reaction, it can be further noted that the concentration of β glucuronate remains larger than that of α glucuronate at all times. It is fully expected that the equilibrium shifts towards fructuronate in the presence of increasing concentrations of borate. In Figure 8.8b, the presence of a substoichiometric amount of borate causes the appearance of an additional peak corresponding to the borate-fructuronate complex. As expected, the equilibrium shifts towards fructuronate. However, we also note an interesting trend, as the borate concentration is increased the rate of consumption of β increases in comparison to α. This is best illustrated in Figure 8.8c where in the presence of a superstoichiometric amount of borate, the amount of β actually decreases to less than the amount α. This is the opposite of the equilibrium situation, where $[\beta] / [\alpha] = 1.4$.

This depletion of the β form is particularly noteworthy as it indicates that the enzyme shows a preference for β glucuronate, which is not simply due to a concentration

effect. If the higher rate of β consumption were based solely upon the fact that the β form is more abundant, it would be expected that the concentrations of α and β would become equal and establish a dynamic equilibrium.

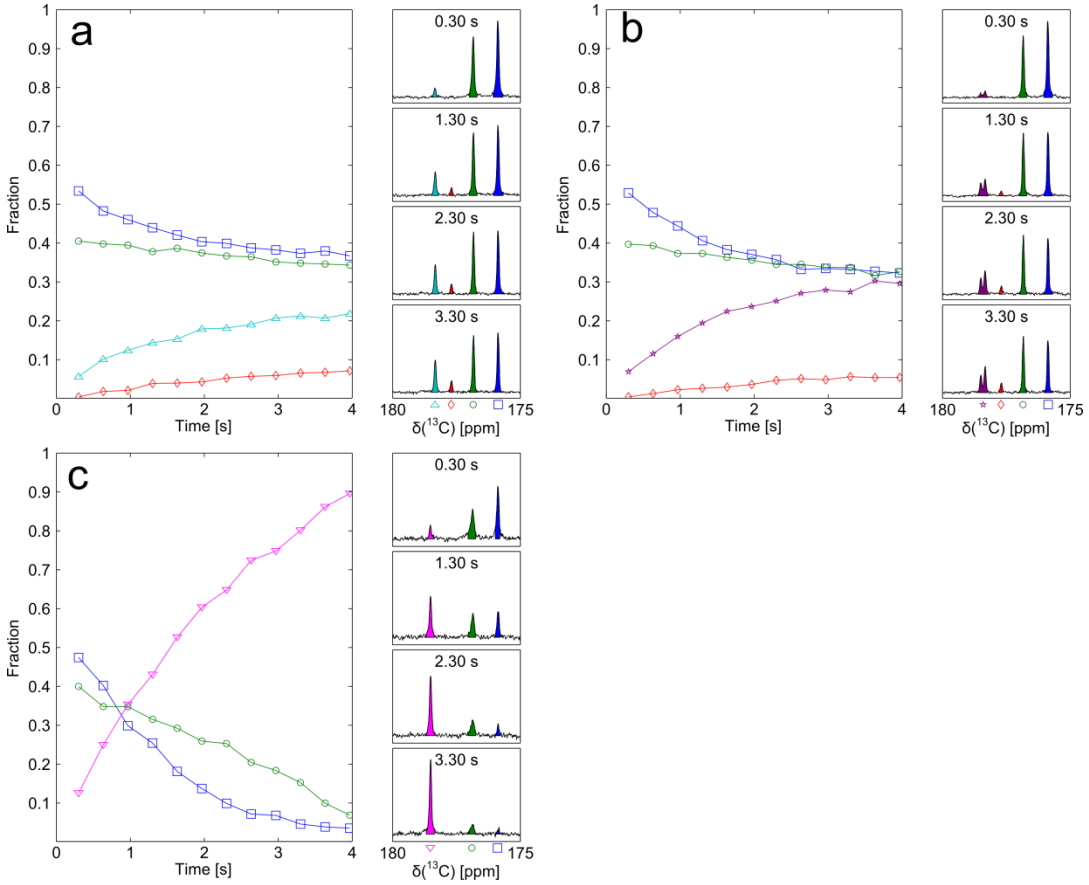

Figure 8.8. Time course of signal fraction and subset of spectra for the reaction of glucuronate at anomeric equilibrium catalyzed by uronate isomerase in a) phosphate buffer, b) substoichiometric borate buffer, and c) superstoichiometric borate buffer. α-glucuronate - ○, β-glucuronate - □, α-fructuronate - ◊, β-fructuronate -△, β-fructuronate borate complex - ▽, mixture of β-fructuronate and borate complex -☆

Figure 8.9a shows the ratio of β glucuronate to α glucuronate for each of the conditions, starting from an equilibrium mixture of α and β. It is clear that the ratio decreases in all cases, with the borate containing samples decreasing below unity. In the

case of phosphate buffer, the ratio tends to level off at a value just greater than unity. The variable depletion of β-glucuronate under the different conditions of reversibility suggests that the anomeric specificity of the enzyme is connected to the degree of reversibility of the reaction. This is an important point for comparison to in vivo conditions as the conventional coupled assay renders the reaction completely irreversible. While the mannonate dehydrogenase reaction is coupled to the uronate isomerase reaction in vivo, it cannot be said that the concentration of mannonate dehydrogenate is substantially higher than uronate isomerase as in the assay.[127] Additionally, we do not see an absolute preference for β-glucuronate, but instead a weak one. The reaction rate is significantly faster than the mutarotation rate in the absence of enzyme, so it is not possible for the results to occur solely because of non-enzymatic mutarotation processes. Indeed, the reaction rate itself combined with evidence from the X-ray structure that the enzyme binds the open form strongly implies that the enzyme is active in the mutarotation process.

Figure 8.9b shows the ratio [β] / [α] of the fructuronate product which initially appears in the β form, but rapidly reaches a value near the equilibrium value of [β] / [α] = 3. This indicates that the rate of β-fructuronate formation is faster than that of α-fructuronate. This potentially indicates that the enzyme is active in the ring-closing process of the fructuronate product.

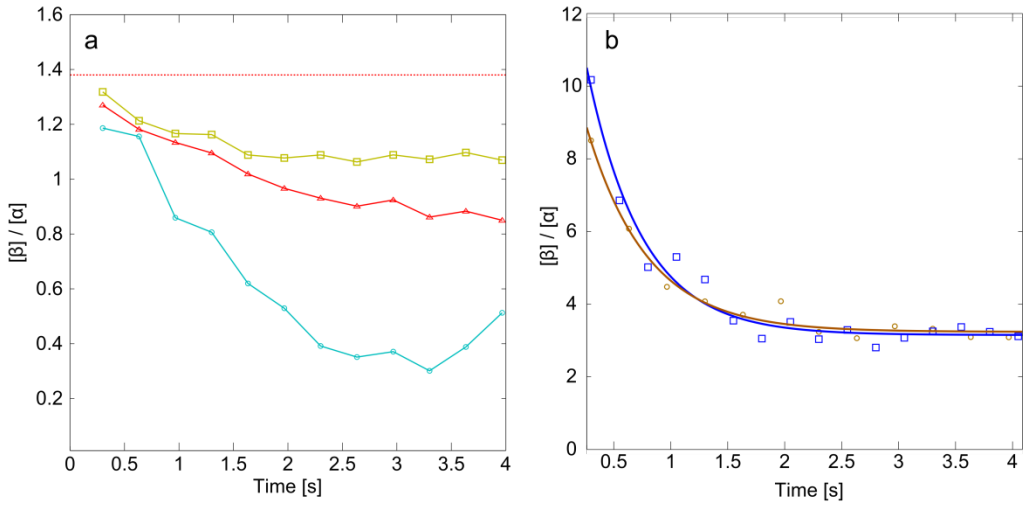

Figure 8.9. Ratios of signal integral fractions between β and α form of (a) substrate and (b) product. In (a), open circles represent the reaction in phosphate, filled triangles the reaction in substoichiometric borate, and filled circles the reaction in superstoichiometric borate. The horizontal dashed line indicates the equilibrium concentration ratio. In (b), only the reaction in phosphate is shown. Open squares represent the reaction starting from substrate at equilibrium ratio of β:α species, and open circles starting from substrate with β:α > 5:1.

For further analysis of the impact of mutarotation, samples containing primarily β-glucuronate are utilized ([β] / [α] > 5). The results of these experiments are shown in Figure 8.10. As these samples are far from anomeric equilibrium, it is possible for enzymatic mutarotation to cause an increase in the amount of α-glucuronate. Barring deviations due to differences in relaxation rates, Figure 8.10a appears to show such an increase. The same reaction was also conducted under irreversible conditions, shown in Figure 8.10b. Here, the fraction of β-glucuronate uniformly decreases. Additionally experiments without uronate isomerase show that mutarotation in the absence of enzyme is slow (Figure 8.10c The results obtained with samples at anomeric equilibrium and

samples far from anomeric equilibrium suggest that the reduced anomeric specificity shown in phosphate buffer may stem from the reverse reaction.

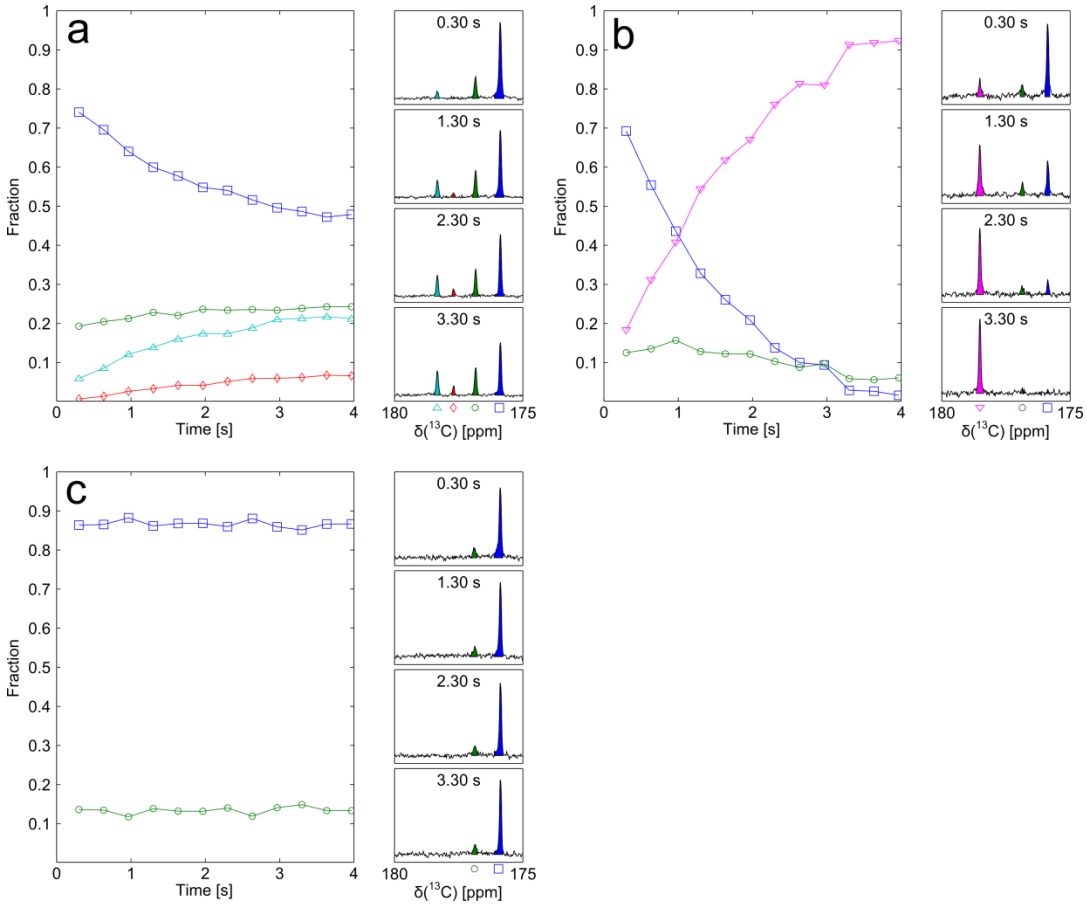

Figure 8.10. Time course of signal fraction and subset of spectra for the reaction of β-glucuronate catalyzed by uronate isomerase in a) phosphate buffer, b) superstoichiometric borate buffer. For comparison, panel c shows the results in the absence of uronate isomerase. α-glucuronate - ○, β-glucuronate - □, α-fructuronate - ◊, β-fructuronate -△, β-fructuronate borate complex - ▽

8.4 Conclusions

The uronate isomerase catalyzed conversion of glucuronate into fructuronate has been characterized using DNP enhanced NMR. Unlike spectrophotometric assays, the reaction was followed in real-time while observing all anomeric forms of reactant and

product. This enabled measurements of anomeric specificity, which indicate a preference of the enzyme for consuming β-glucuronate, as well as a preference for releasing β-fructuronate. This property would be interesting to investigate in the context of the substrate preference of the subsequent enzyme in the metabolic pathway.

The source of the previously observed equilibrium shift in borate buffer has been ascribed to the formation of a 2,3 borate complex of β-D-fructuronate. The formation of this complex has been used to render the reaction of glucuronate partially or fully irreversible. This data indicated that the enzyme appears to catalyze mutarotation of the substrate, primarily by means of the reverse reaction. It further suggests that the enzyme may be active in the ring-closing process of the fructuronate product.

Compared to conventional assays, which use a coupled reaction that is typically irreversible, the ability to tailor the degree of reversibility is an advantage of the DNP technique.. As the optional coupled reaction used to alter the equilibrium need not be chromogenic, depending on the system under study, a variety of coupled reactions are tolerated, it is possible to analyze the reaction under conditions similar to those experienced in vivo.

CHAPTER IX

GENERAL CONCLUSIONS

The work presented in this dissertation demonstrates that solid-to-liquid state DNP enhanced NMR has significant potential for advancing NMR spectroscopy in applications related to chemistry and biochemistry. Through the design and construction of a high-speed sample injector, it becomes possible to extend DNP-NMR to systems exhibiting short relaxation times. Additionally, true high-resolution NMR data, with line widths rivaling those obtained from static samples, can be obtained. These features enable the NMR measurement of chemical reactions with previously unmatched time resolution and sensitivity.

The capabilities of the high speed sample injector enable the use of the increased sensitivity provided by hyperpolarized NMR for time-resolved observation of enzymatic reactions under near-physiological conditions. For kinetic measurements of model systems, the DNP-NMR method yields rates which are comparable to those obtained by conventional, optical methods. Unlike optical methods, the DNP-NMR method does not require chromophoric reagents. This means that DNP-NMR can be applied to reactions that would otherwise be difficult to follow in real-time.

DNP enhanced NMR is not limited to simple one-dimensional measurements. For purposes of obtaining crucial heteronuclear correlation data, we have introduced an off-resonance decoupling based scheme. It is ideal for systems where the additional dispersion of a true two-dimensional spectrum is not required. Through the acquisition of a series of one-dimensional spectra, heteronuclear correlations are obtained in a rapid

and straightforward manner. Furthermore, the fast nature of the technique means that correlations could even be obtained during the course of a chemical reaction. As shown, the off-resonance decoupling method delivers heteronuclear correlation data which compare favorably to those obtained via conventional two-dimensional spectroscopy.

Heteronuclear correlations are a vital part of the structural elucidation process and prove invaluable in cases where the structure of a product or intermediate is unknown.

We also use DNP to acquire temporal correlations between atoms in reactant and product. Conventionally, this sort of atom mapping would be performed with costly, selectively isotope labeled reagents. As DNP enables observation of reactions in real-time, it is possible to measure these correlations through selective inversion of a resonance of interest. This permits multiple atoms to be mapped without the use of multiple labeled samples. In the case of the Grignard reaction demonstrated in this work, it is possible to observe a clear correlation between reactant and product. Additionally, it is possible to map atoms involved in the formation of transient species such as complexes or intermediates.

While DNP-NMR yields high quality spectra with small quantities of sample, it is not possible to obtain quantitative integrals from different resonances. Nonetheless, it is possible to compare peak multiplets obtained from fractionally isotope labeled samples. These peak multiplets are indicative of the isotopic enrichment of neighboring sites within the molecule and the biosynthetic pathways for the molecule Because of the

high sensitivity of the DNP-NMR technique even minor components present at natural isotope abundance can be measured.

In order to demonstrate the applicability of the aforementioned DNP-NMR methods to new systems, the uronate isomerase catalyzed isomerization of glucuronate to fructuronate was studied. Unlike optical methods, it is possible to observe all anomeric forms of the reactant and product. Real-time observation allowed the anomer specific determination of kinetics for substrate and product. This real-time data reveals the anomeric specificity of the enzyme. Additionally, the lack of a requirement for a coupled, chromogenic reaction enabled the reaction kinetics to be probed without the complications of a second reaction.

Combining the benefits of high-resolution NMR coupled to the signal enhancement through DNP, it may become possible to obtain detailed information on kinetics and mechanisms from a variety of reactions. These measurements are possible under a wide variety of conditions. For biological reactions, the ability to measure under conditions similar to those encountered in vivo permits more accurate characterization of reactions. This allows for the real-time measurement of many reactions under conditions which accurately reproduce those encountered in the real-world.

REFERENCES

1. Bifulco, G.; Dambruoso, P.; Gomez-Paloma, L.; Riccio, R., Determination of relative configuration in organic compounds by NMR spectroscopy and computational methods. *Chem. Rev. (Washington, DC, U. S.)* **2007,** *107*, 3744-3779.

2. Rizzo, V.; Pinciroli, V., Quantitative NMR in synthetic and combinatorial chemistry. *J. Pharm. Biomed. Anal.* **2005,** *38*, 851-7.

3. Zuccaccia, C.; Stahl, N. G.; Macchioni, A.; Chen, M. C.; Roberts, J. A.; Marks, T. J., NOE and PGSE NMR spectroscopic studies of solution structure and aggregation in metallocenium ion-pairs. *J. Am. Chem. Soc.* **2004,** *126*, 1448-1464.

4. Fukushi, E., Advanced NMR approaches for a detailed structure analysis of natural products. *Biosci. Biotechnol. Biochem.* **2006,** *70*, 1803-12.

5. Exarchou, V.; Krucker, M.; van Beek, T. A.; Vervoort, J.; Gerothanassis, I. P.; Albert, K., LC-NMR coupling technology: recent advancements and applications in natural products analysis. *Magn. Reson. Chem.* **2005,** *43*, 681-687.

6. Derome, A. E., The use of NMR spectroscopy in the structure determination of natural products: two-dimensional methods. *Nat. Prod. Rep.* **1989,** *6*, 111-41.

7. Meyer, B.; Peters, T., NMR Spectroscopy techniques for screening and identifying ligand binding to protein receptors. *Angew. Chem., Int. Ed.* **2003,** *42*, 864-890.

8. Sharman, G. J.; Griffiths-Jones, S. R.; Jourdan, M.; Searle, M. S., Effects of amino acid phi, psi propensities and secondary structure interactions in modulating H alpha chemical shifts in peptide and protein beta-sheet. *J. Am. Chem. Soc.* **2001,** *123*, 12318-12324.

9. Harris, R. K.; Becker, E. D.; De Menezes, S. M. C.; Goodfellow, R.; Granger, P., NMR nomenclature. Nuclear spin properties and conventions for chemical shifts - (IUPAC recommendations 2001). *Pure Appl. Chem.* **2001,** *73*, 1795-1818.

10. Weil, J. A.; Bolton, J. R., *Electron Paramagnetic Resonance : Elementary Theory and Practical Applications*; 2nd ed.; Wiley-Interscience: Hoboken, N.J., 2007.

11. Kelly, A. E.; Ou, H. D.; Withers, R.; Dotsch, V., Low-conductivity buffers for high-sensitivity NMR measurements. *J. Am. Chem. Soc.* **2002,** *124*, 12013-12019.

12. Kovacs, H.; Moskau, D.; Spraul, M., Cryogenically cooled probes - a leap in NMR technology. *Prog. Nucl. Magn. Reson. Spectrosc.* **2005,** *46*, 131-155.

13. Schneider-Muntau, H. J., High field NMR magnets. *Solid State Nucl. Magn. Reson.* **1997,** *9*, 61-71.

14. Olson, D. L.; Peck, T. L.; Webb, A. G.; Magin, R. L.; Sweedler, J. V., High-resolution microcoil ^{1}H NMR for mass-limited, nanoliter-volume samples. *Science* **1995,** *270*, 1967-1970.

15. Frossati, G., Polarization of 3He, D2 (and possibly 129Xe) using cryogenic techniques. *Nucl. Instrum. Meth. A* **1998,** *402*, 479-483.

16. Biskup, N.; Kalechofsky, N.; Candela, D., Spin polarization of xenon films at low-temperature induced by 3He. *Physica B (Amsterdam, Neth.)* **2003,** *329-333*, 437-438.

17. De Graaf, R. A., *In vivo NMR Spectroscopy: Principles and Techniques*; 2nd ed.; John Wiley & Sons: Hoboken, NJ, 2007.

18. Happer, W., Optical pumping. *Rev. Mod. Phys.* **1972,** *44*, 169-249.

19. Spence, M. M.; Rubin, S. M.; Dimitrov, I. E.; Ruiz, E. J.; Wemmer, D. E.; Pines, A.; Yao, S. Q.; Tian, F.; Schultz, P. G., Functionalized xenon as a biosensor. *Proc. Natl. Acad. Sci. U. S. A.* **2001,** *98*, 10654-10657.

20. Hilty, C.; Lowery, T. J.; Wemmer, D. E.; Pines, A., Spectrally resolved magnetic resonance imaging of a xenon biosensor. *Angew. Chem., Int. Ed.* **2006,** *45*, 70-73.

21. Bowers, C. R.; Weitekamp, D. P., Para-hydrogen and synthesis allow dramatically enhanced nuclear alignment. *J. Am. Chem. Soc.* **1987,** *109*, 5541-5542.

22. Duckett, S. B.; Sleigh, C. J., Applications of the parahydrogen phenomenon: A chemical perspective. *Prog. Nucl. Magn. Reson. Spectrosc.* **1999,** *34*, 71-92.

23. Overhauser, A. W., Polarization of nuclei in metals. *Phys. Rev.* **1953,** *92*, 411.

24. Carver, T. R.; Slichter, C. P., Experimental verification of the Overhauser nuclear polarization effect. *Phys. Rev.* **1956,** *102*, 975.

25. Carver, T. R.; Slichter, C. P., Polarization of nuclear spins in metals. *Phys. Rev.* **1953,** *92*, 212.

26. Maly, T.; Debelouchina, G. T.; Bajaj, V. S.; Hu, K. N.; Joo, C. G.; Mak-Jurkauskas, M. L.; Sirigiri, J. R.; van der Wel, P. C. A.; Herzfeld, J.; Temkin, R. J.; Griffin, R. G., Dynamic nuclear polarization at high magnetic fields. *J. Chem. Phys.* **2008,** *128*.

27. Lingwood, M. D.; Han, S., Dynamic nuclear polarization of 13C in aqueous solutions under ambient conditions. *J. Magn. Reson.* **2009,** *201*, 137-145.

28. Drago, R. S., *Physical Methods for Chemists*; 2nd ed.; Saunders College Pub.: Ft. Worth, 1992.

29. Abragam, A.; Proctor, W. G., Spin temperature. *Phys. Rev.* **1958,** *109*, 1441.

30. Kittel, C.; Kroemer, H., *Thermal Physics*; 2nd ed.; W. H. Freeman: San Francisco, 1980.

31. Chen, H.-Y.; Lee, Y.; Bowen, S.; Hilty, C., Spontaneous emission of NMR signals in hyperpolarized proton spin systems. *J. Magn. Reson.* **2011,** *208*, 204-209.

32. Borghini, M., Dynamic polarization of nuclei by electron-nucleus dipolar coupling ("effet solide"). *Phys. Rev. Lett.* **1966,** *16*, 318.

33. Abragam, A.; Goldman, M., Principles of dynamic nuclear polarization. *Rep. Prog. Phys.* **1978,** *41*, 395-467.

34. Goldman, M., Overview of spin temperature, thermal mixing and dynamic nuclear polarization. *Appl. Magn. Reson.* **2008,** *34*, 219-226.

35. Song, C. S.; Hu, K. N.; Joo, C. G.; Swager, T. M.; Griffin, R. G., TOTAPOL: A biradical polarizing agent for dynamic nuclear polarization experiments in aqueous media. *J. Am. Chem. Soc.* **2006,** *128*, 11385-11390.

36. Thurber, K. R.; Yau, W.-M.; Tycko, R., Low-temperature dynamic nuclear polarization at 9.4 T with a 30 mW microwave source. *J. Magn. Reson.* **2010,** *204*, 303-313.

37. Lumata, L.; Jindal, A. K.; Merritt, M. E.; Malloy, C. R.; Sherry, A. D.; Kovacs, Z., DNP by thermal mixing under optimized conditions yields >60,000-fold enhancement of 89Y NMR signal. *J. Am. Chem. Soc.* **2011,** *133*, 8673-8680.

38. Hall, D. A.; Maus, D. C.; Gerfen, G. J.; Inati, S. J.; Becerra, L. R.; Dahlquist, F. W.; Griffin, R. G., Polarization-enhanced NMR spectroscopy of biomolecules in frozen solution. *Science* **1997,** *276*, 930-932.

39. Torrezan, A. C.; Seong-Tae, H.; Mastovsky, I.; Shapiro, M. A.; Sirigiri, J. R.; Temkin, R. J.; Barnes, A. B.; Griffin, R. G., Continuous-wave operation of a frequency-tunable 460-GHz second-harmonic gyrotron for enhanced nuclear magnetic resonance. *IEEE T. Plasma Sci.* **2010,** *38*, 1150-1159.

40. Joo, C.-G.; Hu, K.-N.; Bryant, J. A.; Griffin, R. G., In situ temperature jump high frequency dynamic nuclear polarization experiments: enhanced sensitivity in liquid state NMR spectroscopy. *J. Am. Chem. Soc.* **2006,** *128*, 9428-9432.

41. Ardenkjaer-Larsen, J. H.; Fridlund, B.; Gram, A.; Hansson, G.; Hansson, L.; Lerche, M. H.; Servin, R.; Thaning, M.; Golman, K., Increase in signal-to-noise ratio of > 10,000 times in liquid-state NMR. *Proc. Natl. Acad. Sci. U. S. A.* **2003,** *100*, 10158-10163.

42. Leggett, J.; Hunter, R.; Granwehr, J.; Panek, R.; Perez-Linde, A. J.; Horsewill, A. J.; McMaster, J.; Smith, G.; Kockenberger, W., A dedicated spectrometer for dissolution DNP-NMR spectroscopy. *Phys. Chem. Chem. Phys.* **2010,** *12*, 5883-5892.

43. Ardenkjaer-Larsen, J. H.; Leach, A. M.; Clarke, N.; Urbahn, J.; Anderson, D.; Skloss, T. W. Dynamic nuclear polarization polarizer for sterile use intent. *NMR Biomed.* [Online early access]. DOI: 10.1002/nbm.1682. Published Online: Mar 18, 2011. http:/dx.doi.org/10.1002/nbm.1682 (accessed May 15, 2011).

44. Jóhannesson, H.; Macholl, S.; Ardenkjaer-Larsen, J. H., Dynamic nuclear polarization of [1-13C]pyruvic acid at 4.6 tesla. *J. Magn. Reson.* **2009,** *197*, 167-175.

45. Jannin, S.; Comment, A.; Kurdzesau, F.; Konter, J. A.; Hautle, P.; van den Brandt, B.; van der Klink, J. J., A 140 GHz prepolarizer for dissolution dynamic nuclear polarization. *J. Chem. Phys.* **2008,** *128*, 241102.

46. Grimaldi, J.; Baldo, J.; McMurray, C.; Sykes, B. D., Stopped-flow nuclear magnetic resonance spectroscopy. *J. Am. Chem. Soc.* **1972,** *94*, 7641-7645.

47. Grimaldi, J. J.; Sykes, B. D., Stopped flow fourier-transform nuclear magnetic resonance spectroscopy - Application to α-chymotrypsin catalyzed hydrolysis of tert-butyl-L-phenylalanine. *J. Am. Chem. Soc.* **1975,** *97*, 273-276.

48. Kuhne, R. O.; Schaffhauser, T.; Wokaun, A.; Ernst, R. R., Study of transient chemical reactions by NMR - fast stopped-flow fourier-transform experiments. *J. Magn. Reson.* **1979,** *35*, 39-67.

49. Golman, K.; in't Zandt, R.; Thaning, M., Real-time metabolic imaging. *Proc. Natl. Acad. Sci. U. S. A.* **2006,** *103*, 11270-11275.

50. Warren, W. S.; Jenista, E.; Branca, R. T.; Chen, X., Increasing hyperpolarized spin lifetimes through true singlet eigenstates. *Science* **2009,** *323*, 1711-1714.

51. Fracassi da Silva, J. A.; do Lago, C. L., An oscillometric detector for capillary electrophoresis. *Anal. Chem.* **1998,** *70*, 4339-4343.

52. Bowen, S.; Hilty, C., Time-resolved dynamic nuclear polarization enhanced NMR spectroscopy. *Angew. Chem., Int. Ed.* **2008,** *47*, 5235-5237.

53. Hilty, C.; Bowen, S. Rapid nuclear magnetic resonance analysis system. US Patent Application 12/539,486, 2009.

54. da Silva, J. A. F.; do Lago, C. L., An oscillometric detector for capillary electrophoresis. *Anal. Chem.* **1998,** *70*, 4339-4343.

55. Levy, G. C.; Kerwood, D. J., Carbon-13 Relaxation Measurements: Organic Chemistry Applications. In *Encyclopedia of Nuclear Magnetic Resonance*, Grant, D. M.; Harris, R., Eds. Wiley: Weinheim, 1996; Vol. 2, pp 1147-1156.

56. Ernst, R. R.; Bodenhausen, G.; Wokaun, A., *Principles of Nuclear Magnetic Resonance in One and Two Dimensions*; Oxford University Press: Oxford, 1986.

57. Foucault, G.; Seydoux, F.; Yon, J., Comparative kinetic properties of alpha, beta and psi forms of trypsin. *Eur. J. Biochem.* **1974,** *47*, 295-302.

58. Villalonga, M. L.; Reyes, G.; Fragoso, A.; Cao, R.; Fernández, L.; Villalonga, R., Chemical glycosidation of trypsin with O-carboxymethyl-poly-beta-cyclodextrin: catalytic and stability properties. *Biotechnol. Appl. Biochem.* **2005,** *41*, 217-223.

59. Schwert, G. W.; Takenaka, Y., A spectrophotometric determination of trypsin and chymotrypsin. *Biochim. Biophys. Acta* **1955,** *16*, 570-575.

60. Day, I. J.; Mitchell, J. C.; Snowden, M. J.; Davis, A. L., Applications of DNP-NMR for the measurement of heteronuclear T1 relaxation times. *J. Magn. Reson.* **2007,** *187*, 216-224.

61. Zhao, L.; Mulkern, R.; Tseng, C. H.; Williamson, D.; Patz, S.; Kraft, R.; Walsworth, R. L.; Jolesz, F. A.; Albert, M. S., Gradient-echo imaging considerations for hyperpolarized Xe-129 MR. *J. Magn. Reson. Ser. B* **1996,** *113*, 179-183.

62. Zeng, H.; Bowen, S.; Hilty, C., Sequentially acquired two-dimensional NMR spectra from hyperpolarized sample. *J. Magn. Reson.* **2009,** *199*, 159-165.

63. van Beek, J. D., matNMR: A flexible toolbox for processing, analyzing and visualizing magnetic resonance data in Matlab((R)). *J. Magn. Reson.* **2007,** *187*, 19-26.

64. Michaelis, L.; Menten, M. L., The kenetics of the inversion effect. *Biochem. Z.* **1913,** *49*, 333-369.

65. Yushmanov, P. V.; Furo, I., A rapid-mixing design for conventional NMR probes. *J. Magn. Reson.* **2005,** *175*, 264-270.

66. Srere, P. A., Enzyme concentrations in tissues. *Science* **1967,** *158*, 936-937.

67. Wienkers, L. C.; Heath, T. G., Predicting in vivo drug interactions from in vitro drug discovery data. *Nat. Rev. Drug Discovery* **2005,** *4*, 825-833.

68. Forsen, S.; Hoffman, R. A., Study of moderately rapid chemical exchange reactions by means of nuclear magnetic double resonance. *J. Chem. Phys.* **1963,** *39*, 2892-2901.

69. Ernst, R. R.; Anderson, W. A., Application of Fourier Transform Spectroscopy to Magnetic Resonance. *Rev. Sci. Instrum.* **1966,** *37*, 93-102.

70. Frydman, L.; Scherf, T.; Lupulescu, A., The acquisition of multidimensional NMR spectra within a single scan. *Proc. Natl. Acad. Sci. U. S. A.* **2002,** *99*, 15858-15862.

71. Grace, C. R. R.; Riek, R., Pseudomultidimensional NMR by spin-state selective off-resonance decoupling. *J. Am. Chem. Soc.* **2003,** *125*, 16104-16113.

72. Bodenhausen, G.; Ruben, D. J., Natural abundance nitrogen-15 NMR by enhanced heteronuclear spectroscopy. *Chem. Phys. Lett.* **1980,** *69*, 185-189.

73. Bax, A.; Griffey, R. H.; Hawkins, B. L., Correlation of proton and nitrogen-15 chemical shifts by multiple quantum NMR. *J. Magn. Reson.* **1983,** *55*, 301-315.

74. Cavanagh, J.; Fairbrother, W. J.; Palmer, A. G.; Skelton, N. J., *Protein NMR Spectroscopy: Principles And Practice*; Academic Press, Inc. : San Diego, 1996.

75. AIST Spectral Database for Organic Compounds, SDBS. http://riodb.ibase.aist.go.jp/sdbs/cgi-bin/cre_index.cgi?lang=eng (accessed February 25, 2008).

76. Caytan, E.; Remaud, G. S.; Tenailleau, E.; Akoka, S., Precise and accurate quantitative 13C NMR with reduced experimental time. *Talanta* **2007,** *71*, 1016-1021.

77. Schulte-Herbruggen, T.; Briand, J.; Meissner, A.; Sorensen, O. W., Spin-state-selective TPPI: A new method for suppression of heteronuclear coupling constants in multidimensional NMR experiments. *J. Magn. Reson.* **1999,** *139*, 443-446.

78. Sorensen, M. D.; Meissner, A.; Sorensen, O. W., C-13 natural abundance (SE)-E-3 and (SCT)-C-3 experiments for measurement of J coupling constants between C-13(alpha) or H-1(alpha) and other protons in a protein. *J. Magn. Reson.* **1999,** *137*, 237-242.

79. Wüthrich, K., *NMR of Proteins and Nucleic Acids*; Wiley, New York: 1986.

80. Frydman, L.; Blazina, D., Ultrafast two-dimensional nuclear magnetic resonance spectroscopy of hyperpolarized solutions. *Nat. Phys.* **2007,** *3*, 415-419.

81. Bowen, S.; Zeng, H.; Hilty, C., Chemical shift correlations from hyperpolarized NMR by off-resonance decoupling. *Anal. Chem.* **2008,** *80*, 5794-5798.

82. Jeener, J.; Meier, B. H.; Bachmann, P.; Ernst, R. R., Investigation of exchange processes by 2-dimensional NMR spectroscopy. *J. Chem. Phys.* **1979,** *71*, 4546-4553.

83. Anwar, M. S.; Hilty, C.; Chu, C.; Bouchard, L. S.; Pierce, K. L.; Pines, A., Spin coherence transfer in chemical transformations monitored by remote detection NMR. *Anal. Chem.* **2007,** *79*, 2806-2811.

84. Smith, M.; March, J., *March's Advanced Organic Chemistry: Reactions, Mechanisms, and Structure*; 6th ed.; Wiley-Interscience: Hoboken, N.J., 2007.

85. Afeworki, M.; Vega, S.; Schaefer, J., Direct electron-to-carbon polarization transfer in homogeneously doped polycarbonates. *Macromolecules* **1992,** *25*, 4100-4105.

86. Silver, M. S.; Joseph, R. I.; Chen, C. N.; Sank, V. J.; Hoult, D. I., Selective population inversion in NMR. *Nature* **1984,** *310*, 681-683.

87. Shaka, A. J.; Keeler, J.; Freeman, R., Evaluation of a new broad band decoupling sequence - WALTZ-16. *J. Magn. Reson.* **1983,** *53*, 313-340.

88. Wolber, J.; Ellner, F.; Fridlund, B.; Gram, A.; Johannesson, H.; Hansson, G.; Hansson, L. H.; Lerche, M. H.; Mansson, S.; Servin, R.; Thaning, M.; Golman, K.; Ardenkjaer-Larsen, J. H., Generating highly polarized nuclear spins in solution using dynamic nuclear polarization. *Nucl. Instrum. Methods Phys. Res., Sect. A* **2004,** *526*, 173-181.

89. Wind, R. A.; Duijvestijn, M. J.; Vanderlugt, C.; Manenschijn, A.; Vriend, J., Applications of dynamic nuclear polarization in C-13 NMR in solids. *Prog. Nucl. Magn. Reson. Spectrosc.* **1985,** *17*, 33-67.

90. Lloyd-Jones, G. C.; Muñoz, M. P., Isotopic labelling in the study of organic and organometallic mechanism and structure: an account. *J. Labelled Compd. Radiopharm.* **2007,** *50*, 1072-1087.

91. Pan, Z. Z.; Raftery, D., Comparing and combining NMR spectroscopy and mass spectrometry in metabolomics. *Anal. Bioanal. Chem.* **2007,** *387*, 525-527.

92. Wittmann, C.; Heinzle, E., Mass spectrometry for metabolic flux analysis. *Biotechnol. Bioeng.* **1999,** *62*, 739-750.

93. Niittylae, T.; Chaudhuri, B.; Sauer, U.; Frommer, W. B., Comparison of Quantitative Metabolite Imaging Tools and Carbon-13 Techniques for Fluxomics. In *Plant Systems Biology*, Belostosky, D. A., Ed. Humana Press: 2009; Vol. 553, pp 355-372.

94. Neri, D.; Szyperski, T.; Otting, G.; Senn, H.; Wüthrich, K., Stereospecific nuclear magnetic resonance assignments of the methyl groups of valine and leucine in the DNA-binding domain of the 434 repressor by biosynthetically directed fractional ^{13}C labeling. *Biochemistry* **1989,** *28*, 7510-7516.

95. Szyperski, T., Biosynthetically directed fractional ^{13}C labeling of proteinogenic amino acids - an efficient analytical tool to investigate intermediary metabolism. *Eur. J. Biochem.* **1995,** *232*, 433-448.

96. Szyperski, T.; Bailey, J. E.; Wüthrich, K., Detecting and dissecting metabolic fluxes using biosynthetic fractional ^{13}C labeling and two-dimensional NMR spectroscopy. *Trends Biotechnol.* **1996,** *14*, 453-459.

97. Wiechert, W., ^{13}C metabolic flux analysis. *Metab. Eng.* **2001,** *3*, 195-206.

98. Sambrook, J.; Russell, W. D., *Molecular Cloning: A Laboratory Manual*; Cold Spring Harbor Press: Cold Spring Harbor, 2001.

99. Bligh, E. G.; Dyer, W. J., A rapid method of total lipid extraction and purification. *Can. J. Physiol. Pharmacol.* **1959,** *37*, 911-917.

100. Bowen, S.; Hilty, C., Temporal chemical shift correlations in reactions studied by hyperpolarized nuclear magnetic resonance. *Anal. Chem.* **2009,** *81*, 4543-4547.

101. Bowen, S.; Hilty, C., Rapid sample injection for hyperpolarized NMR spectroscopy. *Phys. Chem. Chem. Phys.* **2010,** *12*, 5766-5770.

102. Geen, H.; Freeman, R., Band-selective radiofrequency pulses. *J. Magn. Reson.* **1991,** *93*, 93-141.

103. Grogan, D. W.; Cronan, J. E., Cyclopropane ring formation in membrane lipids of bacteria. *Microbiol. Mol. Biol. R* **1997,** *61*, 429-441.

104. Henderson, B. S.; Larsen, B. S.; Schwab, J. M., Chemistry and photochemistry attending the inactivation of Escherichia coli β-hydroxydecanoyl thiol ester dehydrase by an acetylenic diazoketone. *J. Am. Chem. Soc.* **1994,** *116*, 5025-5034.

105. Ingram, L. O., Changes in lipid composition of Escherichia coli resulting from growth with organic solvents and with food additives. *Appl. Environ. Microbiol.* **1977,** *33*, 1233-1236.

106. Smirnova, N.; Reynolds, K. A., Branched-chain fatty acid biosynthesis in Escherichia coli. *J. Ind. Microbiol. Biotechnol.* **2001,** *27*, 246-251.

107. Cronan, J. E.; Waldrop, G. L., Multi-subunit acetyl-CoA carboxylases. *Prog. Lipid Res.* **2002,** *41*, 407-435.

108. Lai, C. Y.; Cronan, J. E., β-ketoacyl-acyl carrier protein synthase III (FabH) Is essential for bacterial fatty acid synthesis. *J. Biol. Chem.* **2003,** *278*, 51494-51503.

109. Rock, C. O.; Cronan, J. E., Escherichia coli as a model for the regulation of dissociable (type II) fatty acid biosynthesis. *BBA-Lipid Lipid Met.* **1996,** *1302*, 1-16.

110. Stryer, L., *Biochemistry*; Freeman: New York, 1995.

111. Brown, J. L.; Ross, T.; McMeekin, T. A.; Nichols, P. D., Acid habituation of Escherichia coli and the potential role of cyclopropane fatty acids in low pH tolerance. *Int. J. Food Microbiol.* **1997,** *37*, 163-173.

112. Banerjee, R. V.; Matthews, R. G., Cobalamin dependent methionine synthase. *FASEB J.* **1990,** *4*, 1450-1459.

113. Pluschke, G.; Overath, P., Function of phospholipids in Escherichia coli - influence of changes in polar head group composition on the lipid phase transition and characterization of a mutant containing only saturated phospholipid acyl chains. *J. Biol. Chem.* **1981,** *256*, 3207-3212.

114. Legendre, S.; Letellier, L.; Shechter, E., Influence of lipids with branched chain fatty acids on the physical, morphological and functional properties of Escherichia coli cytoplasmic membrane. *Biochim. Biophys. Acta* **1980,** *602*, 491-505.

115. On, S. L. W., Identification methods for Campylobacters, Helicobacters, and related organisms. *Clin. Microbiol. Rev.* **1996,** *9*, 405-422.

116. Ashwell, G.; Wahba, A. J.; Hickman, J., Uronic acid metabolism in bacteria.1. purification and properties of uronic acid isomerase in Escherichia Coli. *J. Biol. Chem.* **1960,** *235*, 1559-1565.

117. Nguyen, T. T.; Fedorov, A. A.; Williams, L.; Fedorov, E. V.; Li, Y. C.; Xu, C. F.; Almo, S. C.; Raushel, F. M., The mechanism of the reaction catalyzed by uronate isomerase illustrates how an isomerase may have evolved from a hydrolase within the amidohydrolase superfamily. *Biochemistry* **2009,** *48*, 8879-8890.

118. Williams, L.; Nguyen, T.; Li, Y.; Porter, T. N.; Raushel, F. M., Uronate isomerase: a nonhydrolytic member of the amidohydrolase superfamily with an ambivalent requirement for a divalent metal ion. *Biochemistry* **2006,** *45*, 7453-7462.

119. Purich, D. L.; Allison, R. D., *Handbook of Biochemical Kinetics*; Academic Press: San Diego, CA, 2000.

120. McClure, W. R., Kinetic analysis of coupled enzyme assays. *Biochemistry* **1969,** *8*, 2782-2786.

121. Storer, A. C.; Cornishb.A, Kinetics of coupled enzyme reactions - applications to assay of glucokinase, with glucose-6-phosphate dehydrogenase as coupling enzyme. *Biochem. J.* **1974,** *141*, 205-209.

122. Willem, R.; Biesemans, M.; Hallenga, K.; Lippens, G.; Malaisselagae, F.; Malaisse, W. J., Dual anomeric specificity and dual anomerase activity of phosphoglucoisomerase quantified by 2-dimensional phase-sensitive C-13 EXSY NMR. *J. Biol. Chem.* **1992,** *267*, 210-217.

123. Balaban, R. S.; Ferretti, J. A., Rates of enzyme-catalyzed exchange determined by two-dimensional NMR - a study of glucose-6-phosphate anomerization and isomerization. *Proc. Natl. Acad. Sci. U. S. A.* **1983,** *80*, 1241-1245.

124. Williams, L. Analysis of the mechanisms for uronate isomerase from E. coli, cobyrinic acid a,c-diamide synthetase from S. typhimurium, and cobyric acid synthetase from S. typhimurium. Ph.D. Thesis, Texas A&M University, College Station, TX, 2007.

125. Pelmore, H.; Symons, M. C. R., NMR studies of complexes formed by d-fructose and borate ions in aqueous solution. *Carbohydr. Res.* **1986,** *155*, 206-211.

126. Loomis, W. D.; Durst, R. W., Chemistry and biology of boron. *BioFactors* **1992,** *3*, 229-239.

127. Farmer, J. J., III; Eagon, R. G., Aldohexuronic acid catabolism by a soil Aeromonas. *J. Bacteriol.* **1969,** *97*, 97-106.

VITA

Name: Sean Michael Bowen

Address: Department of Chemistry
Texas A&M University
Corner of Spence and Ross
MS 3255
College Station, TX 77843-3255
c/o Christian Hilty

Email Address: sbowen@chem.tamu.edu

Education:

2011	Ph.D., Chemistry Texas A&M University, College Station, TX
2006	B.S., Chemistry Purdue University, West Lafayette, IN